UNIVERSITY OF
LINCOLN

Faculty: School of Science

Department: School of Life Sciences

Project Supervisors: Dr Alan Goddard and Dr Driton Vllasaliu

September 2015

Neurotensin: A Candidate For Peptide-Guided Drug Delivery

Joanna Bird

A Thesis Submitted in Fulfilment of the Degree of Masters By Research

Abstract

Modern pharmacotherapy, especially with regards to the treatment of cancer, has been faced with one major obstacle for many years: poor drug specificity. The use of many bio-therapeutic/chemotherapeutic drugs for the treatment of cancer is largely dose-limited due to their highly toxic nature and largely unspecific mode of action, causing 'off target' drug interactions, inadequate drug concentrations at 'on target' areas and poor patient compliance due to the necessity to receive large amounts of a drug that hinder quality of life. Currently available research into the development of recombinant biotherapeutic drugs, targeted to specific ligand receptors, has presented a new mode of drug delivery, which could potentially avoid these problems – drug delivery selective to the tissue of choice with minimal damage to physiologically normal cells. Neurotensin (NT) is a tridecapeptide known to exert a variety of effects on the human body; it has a dual role as both a neuromodulator in the central nervous system and as a local hormone in the periphery. The actions of neurotensin are mediated by specific interactions with one of three neurotensin receptors: NTS1, NTS2 and NTS3, all of which are known to internalise upon interaction with neurotensin. NTS1 in particular is thought to play the biggest role in eliciting the actions of neurotensin and is the main focus of this study; as NTS1 is known to be up regulated in a variety of different cancer types, including pancreatic and breast tumours, it could potentially serve as a target for neurotensin-mediated drug-delivery.

The data presented in this study characterises the extent of expression of NTS1 in both polarised and non-polarised Caco-2, and HEK293 cell lines. The uptake and transport of two NT-conjugated fluorophores (GFP and fluorescein) were compared to evaluate the affect of cargo size on cellular uptake. Investigation into uptake and transport of the two fluorophores, elicited by neurotensin, showed both to be internalised in a receptor mediated fashion with the smaller of the two (fluorescein) exhibiting internalisation and transport to a greater extent than the larger (GFP). Visualisation by confocal microscopy showed fluorophore localisation close to the nucleus of the cell.

From a more general perspective, this work aims to elucidate the potential for neurotensin to be employed to enhance the delivery of bio-therapeutics to treat 'difficult' cancers, such as pancreatic cancer, which is notorious for poor survival rates and is known to overexpress receptors for neurotensin. If successful, neurotensin-conjugation of bio-therapeutics could improve survival rates by lowering necessary dosages and increasing cancer cell specificity.

Certificate of Originality

This is to certify that this thesis submitted in fulfilment of MSc by Research in Life Sciences is my own independent work unless specified in either the acknowledgements or references section of this document. This document is an original works and has not been submitted to any institution.

Name: Joanna Bird

Signature:

Date: 21st September 2015

Acknowledgements

Firstly, I would like to thank my principal supervisor, Dr Alan Goddard, for his constant support, guidance and incomparably sage words of advice - words that will stay with me throughout every stage of my professional development. I would also like to extend thanks to my secondary supervisor, Dr Driton Vllasaliu, for his equally constant support and ability to roll with (and not judge) my sense of humour. They have both taught me a great deal, and importantly, have been friends to me. I would also like to thank my fellow molecular biology lab colleagues, you know who you are. Without whom, my first experience as a postgraduate student would have been far less entertaining.

I extend thanks to all academics in the schools of Life Sciences, Pharmacy and Chemistry that have assisted me any way over the course of the last year. Also, to the undergraduate students that endured my teaching.

Special thanks go out to my dear friends, and housemates (not forgetting Dave), who filled this last year with laughter and happiness. I have cherished my time at Lincoln, and the fond memories it has given me. But not the fire alarms, never the fire alarms.

I would like to thank Henry, who has been a constant source of inspiration throughout our marathon of living apart. He unknowingly motivates me every day to be the best that I can and is not only a role model for me, but also my best friend.

Finally, I would like to thank my close family, for their unconditional support and kind understanding, even though my heavy workload got in the way sometimes.

Table of Contents

List of Figures

Chapter 1

Chapter 2

Chapter 3

Chapter 4

Chapter 5

Chapter 6

List of Tables

List of Equations

List of Abbreviations

DMEM	Dulbeccos Modified Eagle Medium
DMSO	Dimethylsulphoxide
DOX	Doxorubicin
ECACC	European Collection of Cell Cultures
E.coli	*Escherichia coli*
EDTA	Ethylene Diamine Tetraacetic Acid
EGF	Epidermal Growth Factor
FBS	Foetal Bovine Serum
F-NT	Neurotensin-Conjugated Fluorescein
GFP	Green Fluorescent Protein
GFP-NT	Neurotensin-Conjugated Green Fluorescent Protein
GPCR	G Protein-Coupled Receptor
HBSS	Hank's Balanced Salt Soution
IMAC	Immobilised Metal Affinity Chromatography
MW	Molecular Weight
NETs	Neuroendocrine Tumours
NT	Neurotensin
NTS1	Neurotensin Receptor 1
NTS2	Neurotensin Receptor 2
NTS3	Neurotensin Receptor 3
PBS	Phosphate Buffered Saline
SDS-PAGE	Sodium Dodecylsulphate Polyacrylamide Gel Electrophoresis
TAE	Tris-Acetic Acid-EDTA
TE	Tris-EDTA
TGN	Trans-Golgi Network

Chapter 1
Introduction

1.1: Introduction To Peptide Guided-Drug Delivery

Modern pharmacotherapy, especially with regards to the treatment of cancer, has been faced with one major obstacle for many years: poor drug specificity. The use of many bio-therapeutic/chemotherapeutic drugs for the treatment of cancer is largely dose-limited due to their highly toxic nature and largely unspecific mode of action, causing 'off target' drug interactions, inadequate drug concentrations at 'on target' areas and poor patient compliance due to the necessity to receive large amounts of a drug that causes quality of life dampening effects (Kimchi-Sarfaty *et al*., 2013; Spadiut *et al*., 2014). Currently available research into the development of recombinant biotherapeutic drugs has presented a new mode of drug delivery, which could potentially avoid these problems – drug delivery selective of the tissue of choice with minimal damage to physiologically normal cells (Carter, 2011).

Over a century ago, Paul Ehrlich introduced the idea of a 'magic bullet' for the treatment of cancer. His discovery of the specificity of antigen-antibody interactions made a huge impact on chemical and biological research, but remained relatively unexplored for many decades from a pharmacological point of view. Ehrlich's vision called for a chemotherapeutic selective of a target cancerous cell, as an antibody is selective of its respective antigen. Based on the assumption that tumours express antigens specific to their own constitutive cells, he conceived the idea that chemotherapeutics could be delivered in a specific manner once bound to the appropriate monoclonal antibody (Ehrlich, 1956). Advances in monoclonal antibody research allowed the advent of monoclonal antibody therapies (Köhler and Milstein, 1975) which paved the way for further advances in targeted drug delivery (Baldwin, 1985), such as the employment of peptides and peptide receptors in place of antigens and antibodies. In theory, the use of monoclonal antibodies for targeted delivery of chemotherapeutics is ideal, but the seemingly simple principle has proven

difficult to transpose into reality due to their relatively large molecular mass of ~150kDa (Serafini, 1993).

Peptide-based therapies have been successfully employed to treat numerous diseases such as autoimmune diseases, fibrosis and asthma (Atamas, 2012; Boulet, 2004; Larché, 2005). They are particularly successful candidates for therapeutic exploitation due to their specificity, ease of production and importantly, relatively small size (Reubi, 2003). Peptide therapy, as a broad term for an emerging therapy, encompasses a large variety of drugs (including the peptides themselves acting as the therapeutic agent) with different modes of action.

Primary cancerous tissue of human origin is known to overexpress peptide receptors compared to physiologically normal cells (Reubi, 2003). For many years, researchers have been exploring the potential for *in vivo* cancer imaging via the targeting of peptide receptors for diagnostic and therapeutic purposes (Heppeler *et al*., 2000; Kwekkeboom *et al*., 2000). Due to the success of the first widely used receptor-targeted radiation therapies and medical imaging techniques in somatostatin receptor positive tumours, other receptors have been evaluated as potential candidates for conceptually identical treatment (Barbieri *et al*., 2013; Morgat *et al*., 2014).

Peptides can be employed in a variety of different manners to aid the detection, diagnosis and treatment of cancer. This includes using peptides alone to directly target the tumour; peptides conjugated to cytotoxic agents or radiolabelled peptides, which will be discussed in turn (Reubi, 2003).

1.2: Significance of Peptides and Peptide Receptors in Cancer

Due to the fact that peptide receptors are often overexpressed in primary cancer, focus has been drawn to the possibility of targeting them for the purposes of diagnosis and treatment. In the majority of cases, previous research has demonstrated that peptide receptor expression is significantly different to its corresponding normal tissue/tissue of origin. In terms of receptor targeting, it can be

done in one of two ways: binding sites for radioligands (only external cellular attachment is required in this case) or as a target to mediate a functional response; the desired response being ligand-bound receptor internalisation. Generally, literature suggests that little consideration has been given in the past for the peptide receptor's biological function; research relies on the presence of peptide receptors and the ability for its analogue to bind, and not on the physiological processes that the peptide itself mediates (Reubi, 2003).

Many different peptides/peptide receptor couples are being investigated for use in peptide receptor targeted therapies, including: somatostatin (the most widely studied), cholecystokinin/gastrin, substance P, bombesin and neurotensin. Compared to the other peptides listed, neurotensin specific therapies have been explored less (Reubi *et al*., 2005).

1.2.1: Peptide-Based Therapies

Peptides themselves are highly permeable and usually hydrophilic molecules that allow for rapid delivery to target tissues after systemic injection. As they are physiological compounds, they are non-toxic compared to currently marketed chemotherapeutic agents. Most peptide-conjugates are not able to cross the blood-brain barrier due to their size, to reach the majority of densely expressed neuropeptide receptor sites. This can be perceived as a limitation for the treatment of tumours located beyond this barrier, but in this case, presents an advantage for the treatment of peripheral tumours in the form of a physical barrier between the desired site of action and the site most likely to elicit negative side effects. However, blood-brain barrier structural disruption has been previously observed in undifferentiated neural tumours such as glioblastomas – where the peptide would have access to the target site and be able to remain there (Haldemann *et al*., 1995).

This approach to peptide therapy relies on the particular biological response elicited by activation of functional peptide receptors. This requires the peptide or peptide analogue in question to be non-toxic, unlabelled and remain at a therapeutic plasma concentration for an extended period of time. The structural conformation of

peptides makes them particularly susceptible to cleavage from peptidases present in most tissues – as such, metabolically stable peptide analogues must be synthesised prior to clinical applications, particularly for longer treatment periods. One example is the use of octreotide – an octapeptide somatostatin analogue with a much more potent inhibitory effect on the secretion of growth hormone, glucagon and insulin than somatostatin itself (Lamberts *et al*., 1996).

A number of peptides have been shown to positively contribute to the mechanisms of growth regulation of cancerous cells (Moody *et al*., 2003), suggesting that long-term exposure to appropriate antagonists or therapeutic-bound peptide analogues may have a negative influence on the growth rate of tumour cells *in vivo.* Previous research focussed on peptide-receptor expressing animal tumours shows that tumour growth inhibition is achieved with the use of corresponding radioactive, nontoxic peptide analogues (Moody *et al*., 2003; Schally, 1988).

Peptide therapies of this manner are understandably targeted towards neuroendocrine tumours (NETs) – a group of heterogeneous neoplasms originating from endocrine tissues with a shared ability to produce peptides/polypeptide hormones. From a clinical point of view, NETs are incredibly variable: ranging from slow to fast growing, hormonally active to inactive and highly aggressive to malignant (Gulenchyn *et al*., 2012). However, diagnosis of these tumour types is usually into the late stages of tumour growth with associated metastases, due to its slowly progressive nature (Yao *et al*., 2008). In advanced and metastasised NETs, methods of treatment such as surgery, chemotherapy and external radiotherapy are limited. However, use of somatostatin analogues such as octreotide have been shown to increase the time taken for tumour progression as well as provide symptomatic relief from a reduction in hormone overproduction in placebo-controlled studies.

1.2.2: Radio-Labelled Peptide Therapies

Radio-labelled peptide analogues (radioligands) have been successfully employed for the purposes of diagnostics and targeted radiotherapy *in vivo* on the basis of their specificity to peptide-receptor expressing tumour cells. Treatment of this variety exploits a key characteristic shared by many G protein-coupled peptide receptors (GPCRs) – internalisation of the peptide/analogue-receptor complex following interaction at the cell membrane (De Jong *et al*., 1998; Mazella *et al*., 1991; Nouel *et al*., 1997). A particular study of note, especially with regards to this work, is the observed internalisation of fluorescently labelled neurotensin in neurotensin receptor 1 (NTS1) transfected COS-7 cells conducted by Vandenbulcke *et al.,* (2000). Internalisation was able to be prevented by hypertonic sucrose, potassium depletion and cytosol acidification, demonstrating that not only is neurotensin (NT) internalised in a receptor-mediated fashion via clathrin-coated pits, it is trafficked to the trans-golgi network through a series of endosomes after delocalisation from NTS1 with acidic early endosomes (see figure 1.1). The ability for the peptide to enter the cell and avoid degradation suggests a promising candidate for targeted drug delivery.

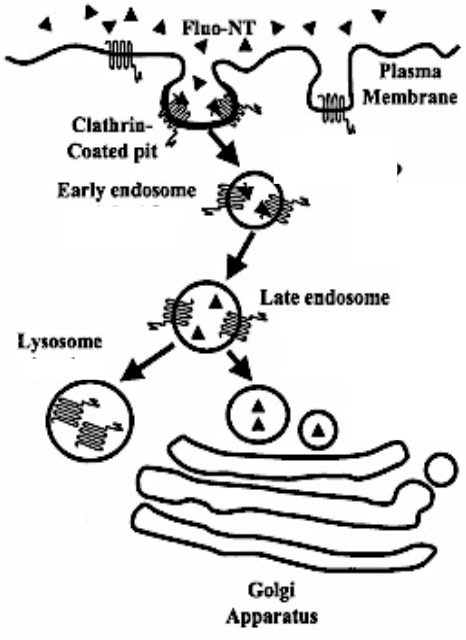

Figure. 1.1: Adapted from (Vandenbulcke *et al*., 2000). Receptor mediated internalisation of fluorescently labelled neurotensin (Fluo-NT). Fluo-NT binds to neurotensin receptor 1 at the plasma membrane, where it is internalised via clathrin-coated pits. It is then trafficked through early to late endosomes, dissociating from its receptor in late endosomes. Neurotensin receptor 1 is separately degraded in lysosomes and Fluo-NT arrives at the trans-golgi network.

The technique of peptide receptor scintigraphy in humans was first trialled with radioisotope-labelled somatostatin analogues to demonstrate the presence of somatostatin receptor-positive tumours (Krenning *et al*., 1989). The radioactive label, conjugated to peptide analogues, can be detected (once incubated long enough internally to bind to peptide receptors expressed by tumours) by external radiation detectors and analysed by medical experts (see figure 1.2). As the radioligand is administered by systemic injection, it must be noted that tumours that are poorly vascularised may not be as accessible to the radioligand and may not be able to collect in the tissue of interest in the same manner as tissues that are well vascularised. However, excessive recruitment of vasculature is considered a hallmark of cancer and so would most likely be highly vascularised (Hanahan and Weinberg, 2011). It is estimated that 80-90% of primary neuroendocrine tumours and metastases can be imaged and identified in this manner (Le Guludec *et al*., 1996).

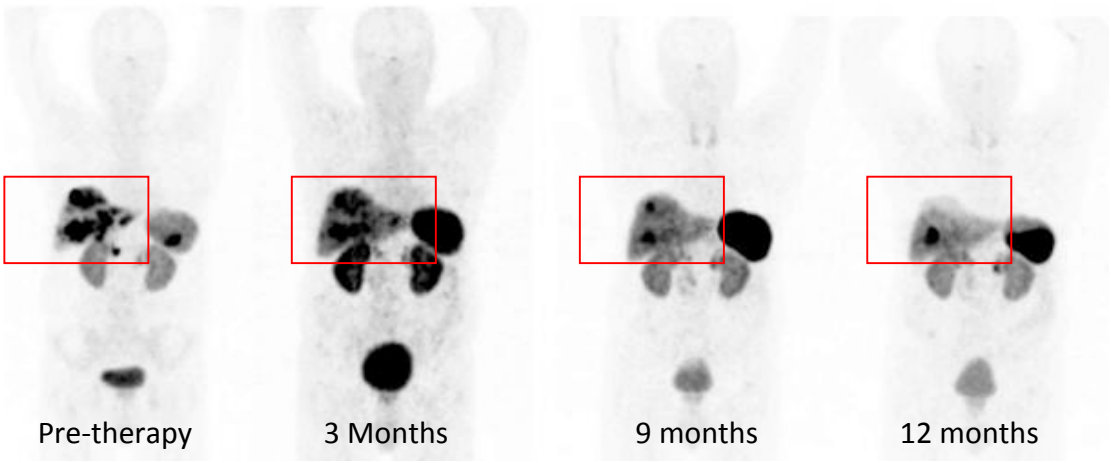

Figure 1.2: Adapted from (Baum and Kulkarni, 2012). Depicts somatostatin receptor targeted scintigraphy of a 56 year old woman. Displays tumour size and location before radiolabelled peptide therapy, 3 months after, 9 months after and 12 months after treatment.

Peptides have previously been conjugated to radioactive isotopes for therapeutic purposes also; they are reliant on the same specificity of peptide-to-peptide receptor that is employed for medical imaging techniques such as scintigraphy. Buchegger *et al*., 2003 produced the first radiolabelled neurotensin analogue, called ^{99m}Tc-NT-XI. However, many variants of neurotensin analogues have been synthesised since which have proven to be more successful in a medical application. NT-XI used in their study was a hexapeptide analogue of the carboxy-terminus of

neurotensin, covering the amino acids 8-13 in its sequence. The modifications made to neurotensin in this instance increased the stability of the peptide – for example, the link between residues 8 and 9 had been replaced with a pseudolink that is resistant to serum enzymes. ^{99m}Tc-NT-XI was created by connecting the N-terminus of NT-XI to a ^{99m}Tc moiety with an (NαHis)Ac group, allowing for stable labelling of the neurotensin analogue. The same technique allowed for coupling of other radioisotopes. ^{99m}Tc-NT-XI showed a similar receptor affinity compared to neurotensin alone and compared to other radioisotope analogues of neurotensin in production at the time, showed favourable tumour uptake. Unfortunately, the clinical trials following development of this analogue were disappointing but the development of the drug itself and the increased stability achieved from modification of the analogue provided a platform for future advances (Morgat *et al*., 2014).

1.2.3: Peptide-Chemotherapeutic Conjugates

Modern cancer therapy usually involves highly intrusive processes; insertion of catheters to deliver highly toxic, non-specific agents into the blood to initially shrink tumours, surgeries to remove them and a plethora of further chemotherapy and radiation. The fundamental concept of chemotherapeutic agents is simple: to selectively kill cells that are more metabolically active than others (this generally applies to cancerous cells, which have by definition, metabolic deregulation). This is the case in adults, but not in children that have a ubiquitously high proportion of quickly dividing cells attributing to their growth and development; extra considerations must be made when treating children. Vast improvements to patient survival have been made over the last 25 years but there is still a need to combat the negative side effects associated with chemotherapy and radiotherapy (Brannon-Peppas and Blanchette, 2012; Hanahan and Weinberg, 2011). Most of the early anti-cancer therapeutics had selectivity to cancer cells in this way, by inhibiting essential processes like DNA replication and cell division (Chabner and Roberts, 2005), but the critical limitation is their severe toxicity to physiologically normal cells (Hanahan and Weinberg, 2011). Due to this highly toxic effect, the therapeutic window (see figure 1.3) of most chemotherapeutic agents is relatively small compared to other

pharmaceutics (Luo *et al*., 2009). The term 'therapeutic window' refers to a range of plasma concentrations of a pharmaceutic drug in which it has a successful therapeutic effect – the treatment of illness with the intention of improving health. A plasma concentration below this 'window' will result in no therapeutic effect and anything above results in toxicity to the body (Das *et al*., 2011). As a result, the majority of chemotherapeutics cannot be administered in amounts high enough to completely eradicate all cancer cells present in the body – this is partially responsible for the occurrence of anti-cancer drug resistance and tumours that are therefore refractory to treatment (Luo *et al*., 2009).

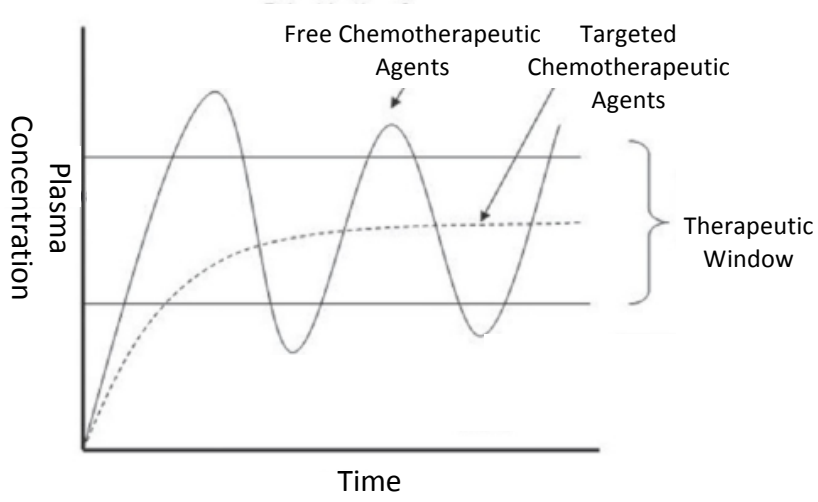

Figure 1.3: Adapted from (Das *et al*., 2011) displays a representation of a theoretical therapeutic window and pharmacokinetic profile of conventional chemotherapeutic drug formation vs that of targeted therapies

The technique of creating carriers for chemotherapeutic compounds by conjugating them to peptides has also been previously investigated for therapeutic purposes with a variety of peptides and neuropeptides with the intention of internalisation and subsequent cellular death of target cancerous cells. Continuing with the theme of somatostatin receptor targeting, which is certainly the most well documented receptor for peptide-targeted therapies, a variety of differing radiolabels conjugated to octreotide have been shown to induce neuroendocrine tumour shrinkage and partial remissions. Successful treatment/tumour response was positively correlated with octreotide uptake. Targeted treatment appears to differ from non-targeted

treatment with a reduced incidence of side effects such as nausea and vomiting (Kwekkeboom *et al*., 2003).

1.3: *In Vitro* Peptide Receptor Expression in Cancerous Tissues vs. Normal Tissue

With regards to non-cancerous, physiologically normal tissue, peptide receptor distribution is not fully understood; mainly due to a lack of access to normal human tissues. But, known locations are primarily the colon and the lungs (White *et al*., 2012). It is not a viable option to extrapolate data from animal tissues due obvious species differences in physiology and biochemical control mechanisms. However, with reference to somatostatin receptors – receptor binding studies, mRNA detection and receptor immunocytochemistry has placed somatostatin receptors in a relatively widely dispersed pattern throughout the human body. Including: the pituitary, kidney, gut, thyroid, pancreas, the brain and the immune system (germinal centres of the lymph nodes). Somatostatin receptor appears to be dispersed in a subtype specific manner throughout these tissues (Maurer and Reubi, 1986; Thoss *et al*., 1996; Schindler *et al*., 1998).

Reubi and Waser (2003) documented in a range of neuroendocrine tumours, many of the tumours concomitantly expressed more than one peptide receptor, speculating that a cocktail of peptides with their respectively bound therapeutic agent could be used to target several co-expressed peptide receptors on a single tumour for a more effective and powerful means of diagnosis and therapy. The same study found that the great majority of investigated tumour types expressed subtype receptors for vasoactive intestinal peptide receptor and somatostatin, far more frequently than other peptide hormone receptors such as bombesin receptor and neurotensin receptor. This selective receptor expression pattern allows for pathobiochemical contrast between neuroendocrine tumours of differing origin. Furthermore, allowing for a much more refined tumour-specific target, theoretically reducing any non-specific cell death mediated by peptide receptors expressed on physiologically normal cells. Ideally, any peptide receptors expressed on the cell surface of cancerous cells would be highly overexpressed on those cancerous cells and expressed at minimal levels elsewhere in the body.

1.4: Pitfalls of Targeting Peptide Receptors for Drug Delivery

The major limitation of peptide receptor targeted therapies is the heterogeneous nature of cancer, and with it, the variability of receptor expression between cells of the same tumour and between individuals. Ideally, all of the constituent cells of a tumour would express the targeted peptide receptor highly and homogenously, but this is unfortunately not likely to be the case. As variability of expression will undoubtedly be present in cells of the same tumour, it is expected that such variation will also be observed between tumours of the same classification in different individuals. Furthermore, studies using laboratory mice or cell lines cultured *in vitro* are not considered sufficient for determination of receptor expression *in vivo* in the related tissue type, as receptor expression may differ profoundly in the corresponding primary human tumour. For example, *in vitro* colonic cancerous cell lines express certain peptide receptors but gastric carcinomas *in vivo* are often devoid of expressing them themselves (Reubi *et al*., 1999). With regards to ascertaining receptor expression *in vivo* from patients presenting with neuroendocrine tissues, sample/biopsy collection, preparation and processing is difficult to standardise. For example, if the technique is immunostaining (the current standard is immunohistochemistry), many variations can affect the end result: the delay before delivery to a laboratory for receptor expression-determining staining, sample processing (fresh/frozen), method of fixation, non-standardised protocols, antibody specificity etc. Inadequate storage during transport and excessive freeze/thawing of tissue samples can lead to false-negatives. It must also be noted that there may be differences in receptor expression in different areas of the tumour, suggesting multiple biopsies from different positions would give the most detailed description of personalised *in vivo* receptor expression (Kaemmerer *et al*., 2014; Reubi, 2003). In terms of an optimal method of receptor detection, Kaemmerer *et al*, (2014) compared the effectiveness of manual evaluation of immunohistochemistry to automated evaluation with software-based analysis and positron emission tomography (PET) and computerised tomography of *in vivo* tumour as a whole in somatostatin receptor expressing NETs. The cohort found there to be no significant difference in determination of the relative quantity of expressed receptors.

Medical imaging techniques such as scintigraphy are limited by the minimum required quantity of radioactive peptide analogue collected in one area (by a tumour) to register any tumourous tissue present. Techniques such as this are not particularly effective at detecting tumours smaller than $1cm^3$. This principle also applies to radiotherapy – an adequate amount of radioligand is required to effectively administer a therapeutic dose of internal radiotherapy. As the absorbed amount of radioligand shows huge inter-patient variance, receptor expression *in vivo* limits the therapeutic value of this method of treatment (Bison *et al*., 2014).

1.5: Neurotensin

Neurotensin (NT) is a tridecapeptide (Glu-Leu-Tyr-Glu-Asn-Lys-Pro-Arg-Arg-Pro-Tyr-Ile-Leu) originally isolated from calf hypothalamus and characterised by Carraway and Leeman (1973). Structurally, neurotensin is very similar to a related peptide neuromedin N. Both peptides have been shown to originate from a common precursor, differentially processed at dibasic sites by proprotein convertases (Kislauskis *et al*., 1988). See figure 1.4 for detail of the peptides structure.

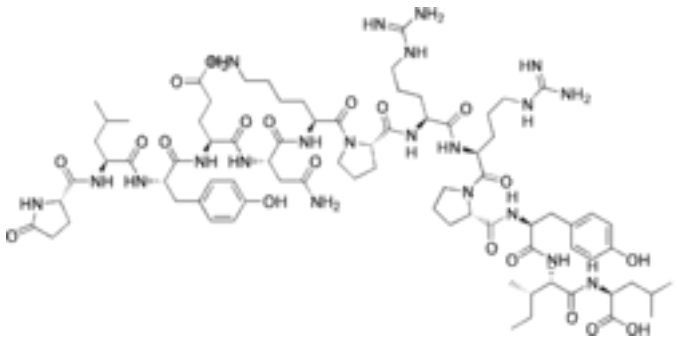

Figure 1.4: The structure of neurotensin

Neurotensin was named on the basis of its neural localisation and the vasodilation observed after local administration. Over the past 25 years, there has been a steady interest in understanding the locality, structure and function of NT. Neurotensin has a dual role as both a neurotransmitter and neuromodulator in the central nervous system, in addition to acting as a local hormone in the periphery (Ferris, 2010). In the central nervous system, neurotensin acts as a neuromodulator of dopamine transmission and anterior pituitary hormone secretion, as well as inducing potent hypothermic and analgesic effects on the brain (Vincent *et al*., 1999). With regards to the gastrointestinal tract, neurotensin is released from enteroendocrine N cells in response to interactions with lipids – where it stimulates the release of digestive acids from the pancreas, gall bladder and stomach, facilitates fatty acid absorption and regulates small bowel motility (White *et al*., 2012).

A large number of peptide hormones have been identified as growth factors in cancer (Heasley, 2001). NT has been associated with the differentiation and progression of tumours in the periphery, where is has been documented to increase the size of lung and colon tumours when exposed to the peptide (St-Gelais *et al*., 2006). In dividing human neuroblastoma cell line N1E-115, it has been documented that prolonged exposure to NTS1 agonists causes NTS1 to recycle back to the cell surface to allow for constant sensitisation (Toy-Miou-Leong *et al*., 2004). Literature also suggests that cancerous cells have the ability to perform autocrine signalling, as a method of enhanced self-propagation (Carraway and Plona, 2006).

1.6: Neurotensin Receptors

The actions of NT are mediated by specific interactions with neurotensin receptors (NT-R) presented on the surface membrane of cells. The C-terminal region of neurotensin (residues 8-13) is responsible for binding to NT-R (Gully *et al*., 1993). Neurotensin receptors are divided into three subtypes: neurotensin receptor 1 (NTS1), neurotensin receptor 2 (NTS2) and neurotensin receptor 3/sortilin (NTS3). NTS1 and NTS2 belong to the GPCR family and have a high and low affinity to neurotensin respectively, whilst NTS3 has only a single transmembrane domain which has a 100% homology with gp95/sortilin (Wu *et al*., 2013). The two G protein-

coupled receptors can be differentiated by NTS2's specific sensitivity to levocarbastine (Yamada *et al*., 1998).

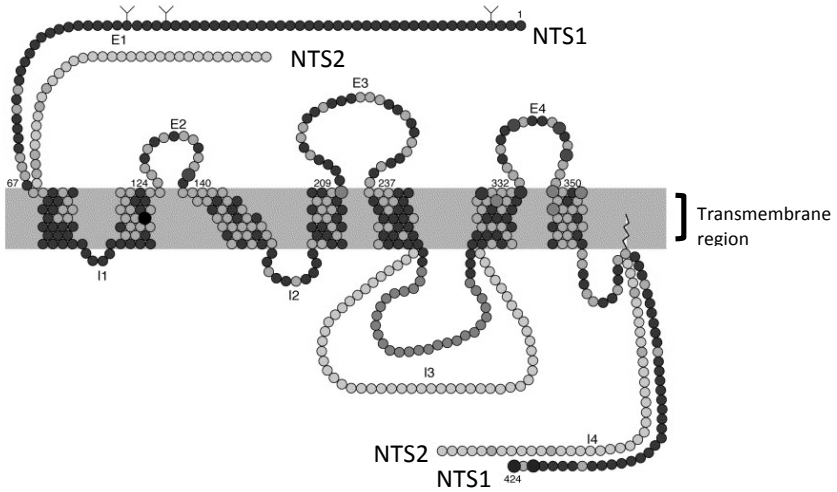

Figure 1.5: Adapted from Vincent *et al*., (1999). Visualisation of rat NTS1 and NTS2 – light grey residues within the transmembrane region are indicative of invariant residues between the two receptor subtypes. I1, I2, I3, I4 are intracellular loops 1-4 respectively and E1, E2, E3 and E4 are extracellular loops 1-4 respectively. E1, 13 and 14 are regions of the NTS2 receptor that strongly differ from NTS1 (dark grey). Residues involved in the binding of NT are located on E2 and E4.

Neurotensin receptors are unstable in detergent solution, which creates difficulties for assessing their structure – particularly in an agonist bound state (thought to be less stable than an antagonist bound state). White *et al*., (2012) used conformational thermostabilisation to overcome this issue and generated a thermostable mutant of NTS1 in the presence of NT as an agonist, as crystallisation of the receptor in its unbound state proved to be unsuitable (see figure 1.6). The cartoon structural representation is displayed in figure 1.5. Pharmacological characterisation of this mutant found the receptor affinity to be similar to that of the wild-type receptor.

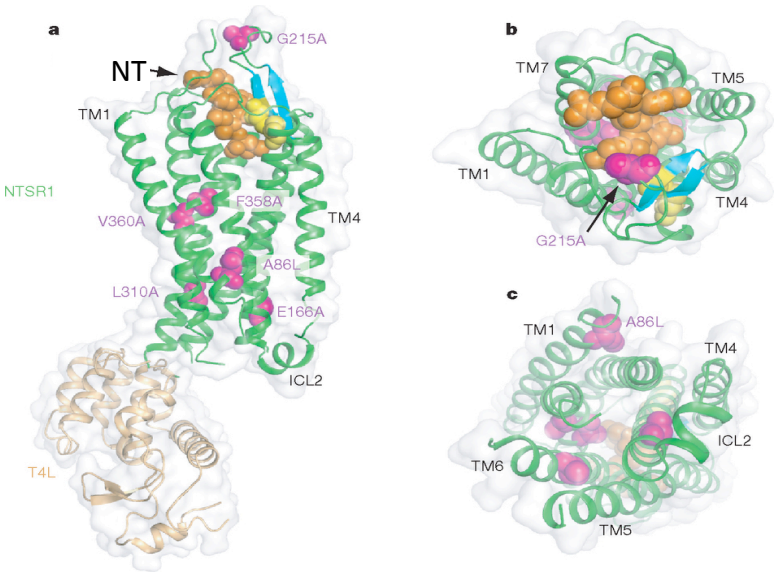

Figure 1.6: Adapted from White *et al*., (2012). Conformational structure of thermostable mutant of NTS1 bound to NT. (A) Side view, (B) extracellular view and (C) intracellular view. Mutations required for thermostabilisation are indicated along with additional T4 lysozyme that had been incorporated into the third intracellular loop. NT is coloured in orange. Thermostabilising mutations are coloured purple, and the disulphide bond is coloured yellow. The beta-hairpin in extracellular loop 2 of NTS1 is coloured blue. Each transmembrane region is coloured in green and annotated TM1, TM2 etc. for transmembrane region 1 and 2 respectively.

The effects of NT are primarily transmitted through its high affinity receptor NTS1, which has a sub-nanomolar affinity of ~0.3 nM. In comparison, the lower affinity G protein-coupled receptor (NTS2) has an affinity of 2-4 nM (Sarret *et al*., 2003). The signalling pathway of NTS1 is by far the most well documented – including Ca^{2+} release after inositol 1,4,5-triphosphate stimulation (Chabry *et al*., 1994) and activation of mitogen-activated protein kinases via protein kinase C, prompting its role in cell proliferation (Poinot-Chazel *et al*., 1996). All three neurotensin receptor subtypes have been shown to internalise upon interaction with NT (Mazella *et al*., 1991). For example, 60-70% of COS cells have been shown to internalise NT upon interaction with NT in a temperature dependent manner (Chabry *et al*., 1994).

1.7: Neurotensin Internalisation Mechanism

All three receptor subtypes are known to internalise upon interaction with neurotensin, but NTS1 has thus far proven to be the most functionally involved in the proliferative effects of neurotensin, and with the greatest affinity for the ligand

(see figure 1.7). Biochemical morphology studies in neuronal cell lines have demonstrated that the internalisation of NTS1 was time-dependent, temperature-dependent and sensitive to phenylarsine oxide (an endocytosis inhibitor) (Mazella *et al*., 1991). Chabry *et al*., (1993) observed the temperature-dependent nature of NTS1 internalisation in neurons. The study documents rapid internalisation at 37°C, but inhibition of internalisation at 4°C. The application of the NTS1 antagonist SR48692 virtually inhibits all NT-R specific binding in primary adenocarcinoma (see figure 1.9), suggesting that the majority, if not all binding of neurotensin is specific to NTS1 or only NTS1 is overexpressed in this cancer type; in turn suggesting the majority of NT internalisation is mediated by NTS1. Furthermore, Mazella *et al*., (1991) compared the internalisation of NT at 37°C and 10°C in primary neuronal cultures from the cerebral hemispheres of mouse embryos. Their study documented the binding capacity to be 3x higher at 37°C as opposed to the cooler temperature. Virtually all neurotensin molecules solely were membrane bound and readily washable by hypertonic acid solution at 10°C. Whereas, 70% of neurotensin was detected internally in the 37°C condition with a large proportion located in the perikarya.

The internalisation of GPCRs is a phenomenon elicited by ligand stimulation. The rapid internalisation of GPCRs once stimulated, known as sequestration, follows the ligand-mediated phosphorylation of the GPCR in question by specific GPCR kinases. It is this initial phosphorylation of the receptor that induces sequestration (Ferguson *et al*., 1995). Receptor phosphorylation also serves to increase the affinity of GPCRs to β-arrestins, which in addition to initiating uncoupling of GPCRs from the G-proteins themselves and preventing further stimulation, act as adaptor-like molecules for receptor trafficking. B-arrestins are proteins that bind to GPCRs once phosphorylated and contribute to the desensitisation of the receptor by uncoupling the signal transduction process (Ferguson *et al*., 1996). The phenomenon of GPCR desensitisation is observed as a response to continuous or repeated stimulation by agonists (Freedman and Lefkowitz, 1996). There is considerable evidence suggesting that GPCRs internalise in a clathrin-mediated manner (Delom and Fessart, 2011; Moore *et al*., 1995).

NTS1 is thought to not be recycled after ligand-mediated internalisation, whereas NTS2 largely is (Botto *et al*., 1998; Hermans and Maloteaux, 1998). Visualisation by confocal microscopy of NTS1 expressing neurons incubated with fluorescently labelled NT demonstrated internalisation together with the receptor towards the perinuclear region within small vesicles (Faure *et al*., 1995; Nouel *et al*., 1997). A similar internalisation locality was observed by Vandenbulcke *et al*., (2000), which monitored the migration of a fluorescently labelled analogue of NT, bound to NTS1, after internalisation into NTS1 transfected COS-7 cells. The study concluded that internalisation was mediated via clathrin coated-pits, to later accumulate with the receptor in acidic early endosomes where the ligand dissociates from its receptor due to the increased acidity. After the loss of co-localisation, neurotensin migrated in late endosomes to the Trans-Golgi network, whilst NTS1 was detected in lysosomes. Therefore, documenting a peptide/peptide receptor recycling cycle unique among GPCRs, mediating targeting of a peptide from the membrane, to endosomes, to the Trans-Golgi Network (see figure 1.1).

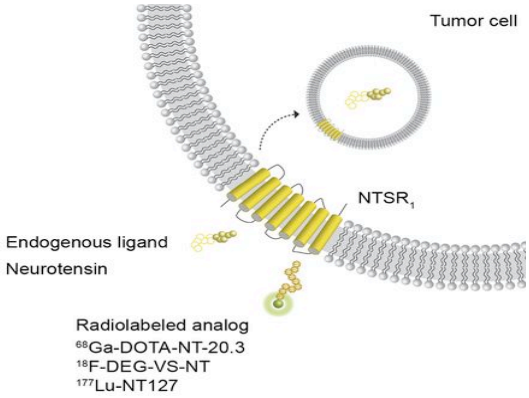

Figure 1.7: Adapted from (Morgat *et al*., 2014). Schematic representation of neurotensin receptor internalisation with its endogenous ligand and examples of radiopharmaceuticals conjugated to its endogenous ligand.

Most of what is known about intracellular trafficking mechanisms of peptides derives from studies concerning single transmembrane domain receptors. For example, Kalgaonkar and Lönnerdal (2009) documented the receptor-mediated uptake of ferritin-bound iron by the human intestinal epithelial cell line, Caco-2. After previous studies of theirs suggested that the cellular uptake of iron from

ferritin (a relatively large iron-binding protein) was different to cellular uptake of iron from $FeSO_4$ – suggesting a different method of internalisation of larger molecules such as ferritin. They investigated the internalisation mechanism of ferritin-bound iron with the use of radiolabelled iron, determining that internalisation is in fact receptor mediated at physiological concentrations. Additional macropinocytosis was observed at higher concentrations.

1.8: Neurotensin Receptors in Cancer

Over 20 years ago, neurotensin receptors were found to be highly expressed on ~75% of primary pancreatic adenocarcinomas (see figure 1.8) whilst not being expressed by non-neoplastic pancreatic ducts (Reubi *et al*., 1998). This almost ubiquitous expression on pancreatic carcinoma was later conformed by Ehlers et al., (2000) documenting an approximate 90% incidence of NT receptor expression by RT-PCR measurement – presenting a therapeutic target for a notoriously aggressive cancerous adversary (Oberstein and Olive, 2013). NT-R is known to also be expressed in other cancer types such as sarcomas, gastrointestinal and prostate tumours (Carraway and Plona, 2006; Reubi *et al*., 1998; Swift *et al*., 2010). A study by Körner *et al*., (2015) documents the expression of neurotensin receptors on aggressive primary pancreatic adenocarcinomas and metastases as a novel and specific marker, strongly suggesting that radioactive neurotensin analogues should be developed for diagnosis and therapy (see figure 1.8).

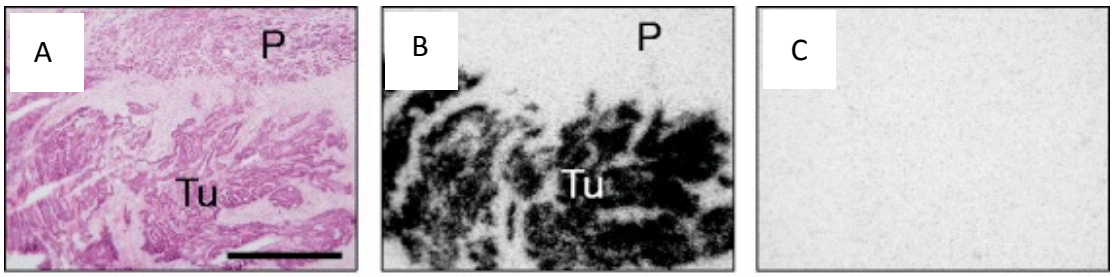

Figure 1.8: Adapted from Körner *et al*., (2015). Depicts NT-R expression in a biopsy from a primary pancreatic carcinoma. (A) Shows a haematoxylin and eosin stained section (B) Shows autoradiogram of radio-labelled NT bound to NT-R. (C) Shows an autoradiogram of non-specific binding of of radio-labelled NT to NT-R (in the presence of 100 nM free neurotensin). Bars =1 mm. Annotations Tu refers to tumorous tissue and P refers to normal pancreatic tissue.

The role and function of NT-R in cancer has come to light over the last decade, particularly that of NTS1. NT-R has been shown to mediate the proliferative effect of

NT in a variety of tumours (Olszewski and Hamilton, 2009; Thomas *et al*., 2003; Vincent, 1995). As such, the use of neurotensin analogues has been proposed as an anti-proliferative treatment for pancreatic tumours (Carraway and Plona, 2006). The functionality of neurotensin receptors in different tumour types has been tentatively documented; in prostate cancer, the receptor is observed to be up-regulated in the absence of androgens as an alternative growth pathway (Sehgal *et al*., 1994). Receptor expression was not observed in normal prostate epithelial cells however (Gugger and Reubi, 1999), but in cell cultures (PC-3M cell line), expression was found to increase in concordance with tumourigenic potential of the cells. It has also been speculated that NTS1 expression in this cancer type is involved in resistance to radiotherapy (Valerie *et al*., 2011). This pattern of receptor expression has also been documented in breast and lung cancer, with 91% of invasive ductal breast carcinomas (Souazé *et al*., 2006), 60% of stage 1 lung adenocarcinomas (Alifano *et al*., 2010a) and 90% of mesotheliomas (Alifano *et al*., 2010b) testing positively for NTS1 expression. As such, NT-R positivity was strongly correlated with decreased survival rates (Alifano *et al*., 2010a).

There is strong evidence suggesting that SR48692, an NTS1 selective antagonist, can inhibit tumour proliferation by inhibiting the binding of NT to NT-R (see figure 1.9). *In vitro,* SR48692 was shown to inhibit proliferation of lung adenocarcinoma (Moody *et al*., 2001). A study by Moody *et al*., (2001) documents the use of SR48692 and SR142948A (a non subtype-specific NT-R antagonist) on small cell lung cancer cell lines NCI-H209 and H345. SR48692 was found to inhibit proliferation and decrease colony sizes of both cell lines in a concentration dependant manner. The same study documents the growth rate of HCI-H209 xenographs in the presence of 10 μg of SR48692 compared to untreated – the untreated xenograph increased in volume from $0mm^3$ to ~$1600mm^3$ over a period of five weeks, whereas the treated xenograph expanded no more than ~$50mm^3$ over the same time period.

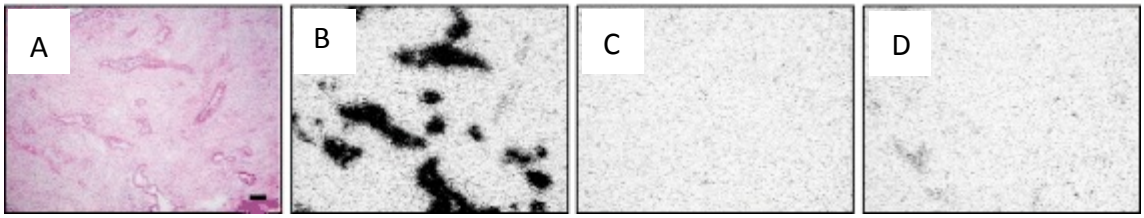

Figure 1.9: Adapted from Körner *et al*., (2015). Depicts NT-R expression in a biopsy from a primary adenocarcinoma. (A) Shows a haematoxylin and eosin stained section (B) Shows autoradiogram of radio-labelled NT bound to NT-R. (C) Shows an autoradiogram of non-specific binding of radio-labelled NT to NT-R (in the presence of 100nM neurotensin). (D) Shows an autoradiogram of non-specific binding of radio-labelled NT to NT-R (in the presence of 1μM SR48692 – confirming the detected NT-R receptors are NTS1) Bars =1mm.

1.9: Conclusion

Peptide receptors are an excellent target for drug delivery, especially with regards to cancer treatment as it presents an opportunity for eliminating the negative side effects associated with non-specific drug interactions. Compared to somatostatin, neurotensin is expressed less frequently on physiologically normal tissues and appears to be highly overexpressed on aggressive cancer types (such as pancreatic adenocarcinoma) that currently face poor survival rates and a limited arsenal of successful therapies. The uses of radio-labelled and chemotherapeutic neurotensin analogues for diagnostic and therapeutic purposes respectively have shown to be promising candidates for treatment of aggressive peripheral tumours and metastases. Especially as peptide-conjugation significantly lowers the dose needed to be administered due to neurotensins nM affinity for NTS1.

Inhibition of NTS1 in particular, as this is the receptor to show the greatest functional role in the proliferative effect of neurotensin, has shown to inhibit the growth of tumours and even show a reduction in cell counts in various cell lines. The internalisation of larger molecules, such as ferritin, is also known to be internalised in a receptor-mediated fashion, suggesting that it is also possible for larger chemotherapeutic molecules bound to an appropriate peptide to be internalised in a receptor mediated fashion.

1.10: Aims and Objectives

Overall, the aim of this study is to evaluate the potential for neurotensin to be employed to specifically deliver molecules (with a size comparable to that of GFP) to NTS1 overexpressing cells. Differentiated Caco-2 cells, grown in transwells, were used to model drug transport across an intestinal epithelial barrier. As these cells were found to overexpress NTS1 in this study once differentiated, they allow for modelling of NTS1 mediated trans-epithelial transport. Undifferentiated Caco-2 and HEK293 cells were used to represent and model fluorophore-conjugated NT uptake into tumoral cells. As each cell line expressed neurotensin receptors to differing degrees (Caco-2 minimally, HEK293 moderately and NTS1 transfected HEK293 highly), this presented the opportunity to speculate how NTS1 expression affects uptake of each NT-bound molecule.

The aims of this study are to express in bacteria, purify and quantify a recombinant model drug: histidine-tagged emerald green fluorescent protein (eGFP) conjugated to NT to be referred to hereon as GFP-NT. GFP-NT will be applied to two separate cell lines, Caco-2 and HEK293, to assess internalisation and transport of this model drug. GFP-NT will also be compared against another, smaller, fluorophore conjugated to NT: fluorescein. NT-conjugated fluorescein will heron be referred to as F-NT. The effect of extent of NTS1 expression will also be examined by comparing uptake of both NT-bound fluorophores in NTS1 transfected vs non-transfected HEK293 cells. Exogenous NTS1 expression will be determined in both cell lines and internalisation of NT-conjugated fluorophores will be visualised using confocal microscopy.

This study focuses on the potential for cytotoxic drug conjugation to a neuropeptide, with the use of a model drug (green fluorescent protein) as a preliminary experimental model. The aim is to differentially target overexpression of the focal neuropeptide's respective receptor on cancerous cells over physiologically normal cells.

Chapter 2
General Methods and Materials

2.1: Materials

2.1.1: Cell Culture – Cells, Media and Other Solutions

Caco-2 cells were obtained from the European Collection of Cell Cultures (ECACC) and were used between passages 60-80. HEK293 cells were obtained from the American Type Culture Collection (ATCC®) and were used between passages 25-40. Dulbeccos Modified Eagles Medium (DMEM) with 4500mg/L glucose, L-glutamine, sodium pyruvate and sodium bicarbonate was purchased from Sigma Aldrich®. Hank's Balanced Salt Solution (HBSS) with sodium bicarbonate and without phenol red were obtained from Sigma Aldrich®. Phosphate buffered saline tablets were obtained from Oxoid®. 0.25% Trypsin/EDTA solution (2.5g porcine trypsin and 0.2g EDTA per litre of HBSS) was obtained from Sigma Aldrich®. Antibiotic/antimycotic solution (penicillin, streptomycin and amphotericin), fetal bovine serum (FBS) non-USA origin, dimethylsulphoxide (DMSO), Trypan blue solution and poly-L-lysine (0.1% solution, mw = 70,000-15,000) were also all obtained from Sigma Aldrich®. DMEM was supplemented with 10% FBS and 1% complete antibiotic/antimycotic solution to produce complete DMEM solution. 100% Ethanol was supplied by Fisher Scientific®.

2.1.2: Glassware and Plasticware

Clear polystyrene 12 well plates (sterile, pyrogen-free), culture flasks (75 cm^2, canted neck with vented caps), Nalgene™ cryogenic tubes (1.5 ml), and opaque black 96 well plates were supplied by Sarstedt®. 1, 2, 5, 10 and 25 ml pipettes, and sterile 50 ml falcon tubes were also supplied by Sarstedt. 12-well Transwell® permeable supports of 12 mm diameter and 0.4 µm pore size polycarbonate membrane filters were obtained form Corning Life Sciences®. Haemocytometer was provided by Sigma Aldrich®.

2.1.3: Chemicals

Model drugs GFP-NT and GFP were synthesised internally as described in section 2.21-2.2.14. Human Neurotensin (>90% purity by HPLC) and paraformaldehyde was supplied by Sigma Aldrich®. SR142948 (non-peptide NTS1 and NTS2 receptor antagonist) was obtained from Tocris Bioscience©. Triton-X 100 was supplied by Fisher Scientific®. Tris and NaCl were supplied by Melford Laboratories Ltd®. Protease inhibitor tablets (cOmplete™ protease inhibitor cocktail tablets, EDTA-free) were supplied by Roche Diagnostics®, from which a 25x stock solution was made by adding 1 tablet to 2 ml of distilled water.

2.2: Methods

2.2.1: Production of the pJB1 Plasmid by Mutagenesis

pJB1 (pET vector containing the gene for recombinant His-GFP) was synthesised by mutagenesis of pAG3 (pET vector containing the gene for recombinant His-GFP-NT) using custom oligonucleotide primers to introduce a stop codon before the gene coding for NT in the plasmid. PCR reaction mixture was set up as follows (all reagents supplied by Novagen):

- 1x Buffer for KOD Hot Start DNA Polymerase (concentration as stated by the supplier)
- 0.2 mM dNTPs
- 1.5 mM $MgSO_4$
- 2 µM forward primer (AG6)
- 2 µM backward primer (AG7)
- 50 ng pAG3
- 0.5 µl of IU/µl KOD Hot Start Polymerase
- Make up to 50 µl with PCR grade water

Reaction mixture was cycled through optimised PCR programme as follows:

- 30 seconds – 90°C
- Repeat 18 times:
    - 30s – 95°C
    - 60s – 60°C
    - 5 min- 68°C
    - 7 min – 68°C

2.2.2: *DpnI* Digest

The PCR product (total of 50 µl) obtained from 2.2.1 was incubated with 0.25 µl of *DpnI* (20,000U/l, New England Biolabs) and 5µl of 10x CutSmart buffer at 37°C for 1hr to eliminate methylated DNA (bacterial DNA/pAG3) and ensure only PCR product is present in the sample.

2.2.3: *BamHI*/*NdeI* Restriction Digest

All reagents were supplied by New England Biolabs. Restriction digests were set up as follows:

- 1x NEBuffer 4
- 6 µl pf pAG3 (500 ng/µl)
- 1 µl *BamHI* (20,000 U/ml)
- 1 µl *NdeI* (20,000 U/ml)
- Make up to 30 ml with PCR grade water

The reaction mixture was incubated at 37°C for one hour prior to being analysed by gel electrophoresis (see section 2.2.4).

2.2.4: Gel Electrophoresis

A Fisher Scientific© horizontal electrophoresis tank was used for this procedure. A 1% agarose gel was made with 1x TAE buffer (40 mM Tris-HCl, 1 mM EDTA and 20 mM acetic acid at pH 8) and left to set in the tank for ~30 mins with a comb placed appropriately. Once set, the gel was submerged in 1x TAE buffer. 3 µl of DNA sample was combined with 3 µl PCR grade water and 3 µl of DNA loading buffer (30% glycerol, 0.025% bromophenol blue in TE buffer) and loaded into the wells of the gel. TE buffer comprised of 10 mM Tris-HCl pH 7.4, 1 mM EDTA at pH 8. The gel was then run at 150V until the dye front was ~80% of the way down the gel. At this stage, the gel was removed and placed into a separate plastic container, submerged in TAE buffer (just enough to cover the gel) and 5 µl of ethidium bromide (10 mg/ml) for ~30 mins. The gel as then imaged using a ChemiDoc™ MP imaging system (Bio-Rad).

2.2.5: Bacterial Transformation for Plasmid Expression

100 µl of XL-1 Blue competent *E.coli* (kindly supplied by Dr Enrico Ferrari, University of Lincoln) were transformed on ice with either a pET vector containing a gene coding for recombinant histidine tagged GFP-NT (pAG3) or a gene coding for

histidine tagged GFP (pJB1) for 20 mins in a 1.5 ml eppendorf tube. The Eppendorf tube was removed and heat shocked at a temperature of 42°C for 45s on a heated block. The tube was then replaced on ice for a further 2 minutes. 0.5ml of sterile LB broth (containing 100 µg/ml of ampicillin) was then added to the tube containing the transformed XL-1 Blue culture and incubated at a temperature of 37°C and 180 rpm for one hour to recover in a shaking incubator. Following recovery, 150 µl of the contents of the tube was plated onto LB agar (containing 100 ug/ml of ampicillin) and incubated for 18hrs at 37°C.

2.2.6: Bacterial Culture Expansion

LB agar plates (containing 100 ug/ml of ampicillin) with cultures of transformed XL-1 Blue or BL21 (DE3) bacteria were removed from the 37°C incubator following incubation for 18hrs as described in section 2.2.5 or 2.2.8. A single bacterial colony was isolated and used to inoculate 5ml of sterile LB broth (containing 100 ug/ml of ampicillin) in 50 ml Falcon tubes. Tubes were incubated for 18hrs at 37°C and 180 rpm in a shaking incubator.

2.2.7: Bacterial Plasmid Extraction

QIAprep® Spin Miniprep Kit was used for plasmid extraction (Qiagen, UK). Plasmid extraction was carried out as stated in the manufacturer's instructions. The collected sample was then stored at -20°C until required.

2.2.8: Bacterial Transformation for Protein Expression

100 µl of BL21 (DE3) competent *E.coli* (kindly supplied by Dr Enrico Ferrari, University of Lincoln) were transformed on ice with either a recombinant pET vector containing a gene coding for histidine tagged GFP-NT (pAG3) or a gene coding for histidine tagged GFP (pJB1) for 20 mins in a 1.5 ml eppendorf tube. This procedure was carried out from this point as stated in section 2.2.5.

2.2.9: Protein Expression and Induction with IPTG

200 ml of LB broth was made up in 2L Erlenmeyer flasks, autoclaved, left to cool and ampicillin was added to a final concentration of 100 µg/ml. The sterile broth was then inoculated with a 5 ml bacterial culture as described in 2.2.6 and left to

incubate at 37°C at 180 rpm until the optical density of the culture was 0.4 (roughly 2hrs). Culture was induced with 1 mM IPTG (Melford Laboratories Ltd) and left to incubate at 37°C at 180 rpm for a further 8hrs. Cultures were then removed from the incubator and processed prior to purification as stated in section 2.2.10.

2.2.10: Protein Extraction from Bacterial Cultures

The original 200 ml culture was separated into 4x50 ml samples in 50 ml Falcon tubes and immediately centrifuged at 8000g for 10 minutes at 4°C. Supernatant was discarded and bacterial pellets were resuspended in 5 ml of protein buffer with added DNase and protease inhibitors (50 mM Tris, 100 mM NaCl, 10 µl/ml DNase and 200 µl of protease inhibitor stock solution (see section 2.1.3) at pH 7.4). Samples were pulse sonicated on ice for a total of 5 mins (5s on, 5s off). Samples were centrifuged again at 8000g for 20 mins at 4°C. Supernatant was collected, filtered through 0.2 µm pore size syringe filter and stored at -80°C until purification (section 2.2.11).

2.2.11: Protein Purification (Immobilised Metal Affinity Chromatography)

Frozen samples from section 2.2.10 were thawed on ice prior to purification. 100 µl of raw protein sample was reserved for later comparison to the purified samples collected in this section. 1 ml HisTrap HP columns were used for purification (GE Healthcare Life Sciences). The column was initially washed with 5 column volumes (cv) of distilled water. Column was then equilibrated with 5cv of protein buffer described in 2.2.10 (minus DNase and protease inhibitors). Protein sample was then applied to the column and washed with 10 cv of protein buffer containing 50 mM imidazole, collecting the flow through in one batch (no protein should have been eluted in this step). Sample was then eluted from the column with 10cv of protein buffer containing 200 mM imidazole and collected in 1 ml aliquots (majority of the purified protein was observed to be collected in the 2^{nd} 1 ml aliquot). Column was then cleaned with 10 cv of 50 mM imidazole protein buffer, 5 cv of distilled water and 5 cv of 20% ethanol, leaving the final 1 cv of 20% ethanol in the column.

2.2.12: Protein Quantification

GFP-NT protein samples (from section 2.2.11) were quantified using a UV-Vis spectrophotometer and UV Probe™ software (Shimadzu Scientific Instruments®). Protein buffer (see section 2.2.10) was used as the appropriate blank and diluent for samples, if dilution was required. Both sample and blank were loaded into the spectrophotometer and absorbance was measured at 490 nm (appropriate for eGFP). The Beer-Lambert law was then applied to quantify GFP-NT present in the sample. Absorption coefficient of eGFP is known to be 57,500 $M^{-1}cm^{-1}$ - See section 4.2.4. F-NT was synthesised and provided by Alta Biosciences© in a known amount and samples subsequently made from this were made up to differing concentrations (as required) from this known value. Quantification of F-NT was not required for this reason.

2.2.13: SDS-PAGE

The Hoefer® small format vertical protein electrophoresis system was used for this procedure. 1 mm gels were made as stated in table 2.1. 10% APS was made on the day of use. Resolving gels were made as 10% acrylamide composites. 10 ml of resolving gel and 5 ml of stacking gel was enough to yield two complete gels.

Resolving Gel	Volume required to make 10 ml of 10% resolving gel
Deionised water	4.13 ml
30% Acrylamide/bisacrylamide	3.3 ml
1.5 M Tris-HCl containing 0.4% SDS (pH 8.8)	2.5 ml
10% APS	60 µl
TEMED	13 µl
Stacking Gel	**Volumes required to make 5 ml of stacking gel**
Deionised water	3 ml
30% Acrylamide/bisacrylamide	700 µl
0.5 M Tris-HCl containing 0.4% SDS (pH 6.8)	1.25 ml
10% APS	25 µl
TEMED	20 µl

Table 2.1: Composition of resolving gels (10%) and stacking gels as recommended by Thermo Scientific®.

Glass plates and spacers were assembled in the supplied gel-casting frame, ensuring the contact between the plates was adequate to prevent leaks; this was simply tested with water and removed with filter paper. Components of the resolving gel

were combined in 50 ml falcon tubes (adding APS and TEMED last), inserted into the apparatus (leaving space for the resolving gel) and left to polymerise for ~30 mins – surplus gel in the falcon tubes indicated when polymerisation had been achieved. A layer of distilled water was immediately placed on top of the gel line to prevent any differences in gel texture forming between the gel exposed to air and the main body of the gel as this could affect migration of the samples. Components of the stacking gel were then combined and added to the surface of the polymerised resolving gel and the comb was inserted after removal of the distilled water. This was left to polymerise for a further 30 mins. The set gel encased in glass plates was then transferred from the gel caster to the electrophoresis tank and submerged in running buffer (see table 2.2).

Buffer	Components
SDS running buffer (500 ml)	7.2 g Glycine 1.5 g Tris 5 ml of 10% SDS solution Make up to 500 ml with deionised water
SDS loading buffer (10 ml)	4.8 ml sterile distilled water 1.2 ml 0.5M Tris pH 6.8 1 ml glycerol 2 ml 10% SDS solution 0.5 ml 0.1% Bromophenol blue 0.5 ml β-mercaptoetanol
Coomassie Blue (1 L)	250 ml propan-2-ol 100 ml acetic acid 650 ml deionised water 2 g Coomassie Brilliant Blue
Destain (5 L)	250 ml propan-2-ol 350 ml acetic acid Made up to 5 L with deionised water

Table 2.2: Composition of buffers and imaging reagents used for SDS-PAGE

10 µl of each sample was paired with 10 µl of loading buffer (see table 2.2) in 1.5 ml eppendorf tubes and heated to 100°C for five minutes to denature protein in the sample. Samples was left to cool and centrifuged at ~17,900g (13,000rpm) on a bench top microcentrifuge for 60 seconds to ensure all contents of the tube were collected at the bottom of the tube prior to running the sample on the gel. The comb was removed from the gel (ensuring no air entered the wells). 15 µl of sample was loaded into each well of the gel. 10 µl of ColorPlus prestained protein ladder, broad

range 10-230 kDa (NEB, UK) was also loaded onto the gel for reference (if the protein ladder differs from this, it is stated in the appropriate figure legend). Once all samples were loaded, the gel was run at 150 V until the dye front had reached the bottom of the gel (approximately 45 mins). The power was disconnected from the tank, gels removed from the apparatus and separated from the stacking gel, and submerged in Coomassie Blue stain (see table 2) for 30 minutes on a platform rocker. The gel was then rinsed in deionised water and resubmerged in destain solution (see table 2 for composition) for 30 mins, followed by a second submersion in fresh destain until appropriately destained. The gel was then imaged in either a ChemiDoc™ MP system (Bio-Rad) or digital camera (mounted on a light box) dependant on the intensity of the bands present on the gel.

2.2.14: Preparation of Protein Samples

Model drugs GFP-NT and GFP (as a negative control to GFP-NT) were produced in house by recombinant expression in *E.coli,* purified and quantified before being aliquoted in 50µl fractions. The amount of protein expressed from each batch of the procedure conducted was variable; hence the final concentrations of the protein stocks were variable also (however, never less than 50 µM). Hence, the amount of protein used from each stock was variable dependant on the concentration. These aliquots were stored at -80°C. An aliquot of each protein was taken from the -80°C freezer and defrosted on ice to elongate the thawing process and protect structural integrity. Stock concentrations of human neurotensin (NT) and SR142948 were prepared from the anhydrous forms received from Sigma Aldrich and Tocris Bioscience respectively. Appropriate amounts of each stock solution were added into HBSS to yield the desired concentration of each protein sample. SR142948 was used at a final concentration 10x that of the concentration of conjugated fluorophore sample present in the same solution (e.g 10x more SR142948 than GFP-NT). NT was used at a final concentration 100x that of the protein present in the same sample. GFP-NT and GFP concentrations ranged from 10 nM - 1 µM during the proceedings of this study. NT-bound fluorescein (F-NT) was also used in this study, as synthesised and supplied by Alta Biosciences® in lyophilised form. Protein samples

containing F-NT were prepared as replicates in concentration and inhibitor content as the original GFP-NT samples.

2.2.15: Routine Cell Culture

Note: all methods referring to tissue culture were performed in sterile conditions within an appropriate laminar flow tissue culture hood, sterilising all materials used with 70% ethanol. Both Caco-2 and HEK293 cell lines were routinely cultured in 75 cm^2 flasks at 5% CO_2, 95% relative humidity and 37°C. Flasks were cultured until confluence was reached (~70% for HEK293, 70-90% for Caco-2). Both cell lines were cultured in 10-12 ml of complete culture medium (DMEM) as described in 2.1.1. During the time taken to reach confluence, complete culture medium was replaced every two days. Media was pre-warmed to 37°c before introduction to the cells. Cell growth was regularly monitored by observation under a light microscope. Cells were passaged by removing the culture medium by aspiration, washing the cells gently with PBS (~5 ml is sufficient to remove any dead cells and remaining media) and applying 3 ml of Trypsin/EDTA solution (See section 2.1.1) to the cells for 75 cm^2 flask. Flasks were then incubated at 5% CO_2, 95% relative humidity and 37°C for ~2 mins for HEK293 cells (as they are a weakly adherent cell line), and ~5 mins for Caco-2. Flasks were examined using a light microscope to evaluate detachment from the flask. If the cells were not adequately detached, they were replaced in the incubator for a further 2-3 mins and re-evaluated. Following detachment, the total flask volume was topped-up with complete culture medium to 10 ml and gently pipetted up and down to homogenise the cell mixture. This dilutes the cells and deactivates the trypsin. 1-3 ml of Caco-2 cells (dependent on when confluency was next required) or 1-2 ml of HEK293 cell added to a new 75 cm^2 flask containing the appropriate amount of pre-warmed complete culture medium to bring the total volume up to 12 ml.

2.2.16: Cryopreservation of Cells

Cells were cultured to confluence and detached from the culture flask as described in section 2.2.15. At the stage where the cells had been detached with trypsin/EDTA (see section 2.1.1) solution and diluted with complete media, the contents of the

flask were transferred to a 50 ml Flacon tube and centrifuged at 200g for five minutes. The supernatant was then removed and the cells were resuspended in 1 ml of complete media containing 10% DMSO. The cells were then added to sterile 1.5 ml Nalgene™ cryogenic tubes (clearly labelled with the date, cell line and passage number). Cryovials were transferred to a -20°C freezer for one hour, followed by incubation over night at -80°C before addition to liquid nitrogen dewars for storage. The freezing procedure was stepped in this way to ensure gradual, rather than fast, freezing.

2.2.17: Revival of Cells

Note: this procedure was conducted as quickly as possible to ensure maximum cell survival. All equipment and reagents required for this procedure were prepared prior to collection of the cells from liquid nitrogen. Cryovials were removed from liquid nitrogen and immediately placed in a 37°C waterbath for 5 mins to thaw. Vial contents were transferred to a sterile 15 ml Falcon tube containing 5 ml of pre-warmed complete media and centrifuged at 200g for 5 mins to remove DMSO-containing media. The supernatant was removed and cells were resuspended in 5 ml of culture media. This cell suspension was then added to a new 75 cm^2 flask containing 7 ml of pre-warmed culture media. The flask was then incubated at 5% CO_2, 95% relative humidity and 37°C.

2.2.18: Counting Cells

Cells were cultured to confluence and detached from the culture flask as described in section 2.2.15. At the stage where the cells have been detached with trypsin/EDTA solution and diluted with complete media, 10 µl of cell suspension was collected and combined with 10 µl of Trypan blue solution. 10 µl of this mixture was then applied to a haemocytometer and counted under a light microscope (x10 magnification) as follows: chamber and cover slip of the haemocytometer were cleaned with 70% ethanol, cells were loaded onto the haemocytometer and live cells were counted in all four of the 4x4 grids of the haemocytometer. Trypan blue allowed for differentiation between dead and live cells as dead cells take up the blue dye, live cells do not). The number obtained was then doubled (to account for the trypan blue

dilution) and divided by four to obtain the average number of cells per grid. This number $x10^4$ is equal to the number of cells per 1 ml of cell suspension.

2.2.19: Culture of Caco-2 Cells On Transwells®

Caco-2 only were detached from the culture flask as described in section 2.2.15 and counted as described in section 2.2.18. Each well was seeded with 0.5 ml of complete media containing $1x10^5$ cells on the apical side of the transwell® filter. 1.5 ml of complete media was added to the basal side of the filter. The day of seeding was considered to be day 0. Cells were routinely grown to 21-24 days, with media replaced every two days. The media was replaced as follows: media on the basal side of the transwell® was first aspirated for all 12 wells, followed by the apical side. Fresh media was then added to the apical first, followed by the basal side. Replacing the media in this manner ensures minimal drying out of the cellular monolayer. TEER measurements were used to assess cell growth (as described in section 2.2.20).

2.2.20: Measurement of TEER

Trans-Epithelial Electrical Resistance (TEER) was measured to monitor cellular growth of Caco-2 cells in Transwells®. This was a non-invasive method to evaluate the confluence of the cells and the integrity of intercellular tight junctions. TEER measurement apparatus is depicted in figure 2.1.

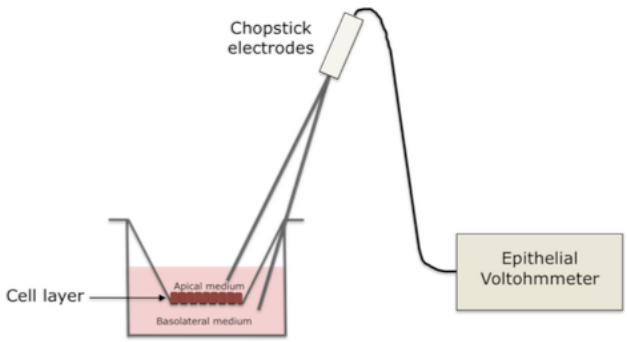

Figure 2.1: Apparatus used to determine TEER and arrangement of Transwell® supports.

The chopstick electrodes were first submerged in absolute ethanol for 30 mins to sterilise, and washed with sterile water to remove any residual ethanol. The chopsticks were then left to air dry (care was taken to not allow the ends of the

electrodes to touch any surfaces) before being inserted into the media bathing the cells in each well of the Transwell®. The short end of the electrode was submerged into the apical side of the filter (taking care not to disrupt the cell monolayer) and the longer end was submerged into the basal side. The electrode was held, submerged in the media for a few seconds until the resistance reading (in Ωcm^2) stabilised on a single figure. The electrode was then gently removed and the resistance of that well was recorded in a table. During initial culture of Caco-2 cells in this manner, the TEER of each Transwell® was measured every other day from day 2 to 21 (the final reading indicated cellular integrity prior to experimentation on the same day). Daily measurements were not taken to limit potential damage to the cells caused by the process. Experiments were conducted on day 21 on culture, resistance on this day was typically ~2000 Ω/cm^2.

2.2.21: Culture of Cells on 12 Well Plates

As HEK293 cells are weakly adherent, they were grown on poly-l-lysine coated coverslips in 12 well plates. Coating of the coverslips was performed manually as follows: one coverslip was placed inside each well of the plate and rinsed with sterile deionised water. The water was then aspirated and left to air dry. 0.5 ml of 0.1% poly-l-lysine solution was then added to each well and manually swirled for five minutes to ensure an even coating was achieved. The poly-l-lysine was then removed and the coverslips were thoroughly washed with sterile deionised water (5 times) and left to air dry for at least 3hrs. Caco-2/HEK293 cells were detached from their culture flasks as described in section 2.2.15 and counted as described in section 2.2.18. $1x10^5$ cells were seeded in each well in a total volume of 1 ml of complete media (this applied to both Caco-2 and HEK293). The plates were then incubated at 5% CO_2, 95% relative humidity and 37°C for 48 hours prior to experiments.

2.2.22: Light Microscopy

75 cm^2 culture flasks containing Caco-2 or HEK293 cells were grown as described in section 2.2.15. Flasks were placed on the stage of a light microscope and images were taken using a Nikon DN100 digital camera control unit and Nikon Eclipse TS100 light microscope. Images were magnified using a x10 objective lens. A specific

confluency of the cells was not required as this was purely for the purposes of qualitative evaluation of cellular health.

2.2.23: Transfection Procedure (HEK293 Only)

Only HEK293 cells grown in 12 well plates were transfected. Lipofectamine® 2000 Transfection reagent was used for this procedure, supplied by Thermo Fisher Scientific. The NTS1 containing plasmid (pcDNA3.1-NTS1, from cDNA.org) was supplied by Dr Alan Goddard and quantified using the NanoDrop 2000 (Thermo Scientific). This procedure was optimised as described in section 3.2.2 – resulting in the use of 4 µl of Lipofectamine per well of cells. 1 µg of DNA was used per well of cells. The procedure was conducted as follows and is sufficient to transfect *one* 12 well plate of cells: ~12 µl (dependant on amount needed for 12 µg of DNA) of DNA was pipetted into 240 µl of serum and antibiotic/antifungal solution-free DMEM. The mixture was homogenised by vortexing. 48 µl of Lipofectamine was then added to the DNA/DMEM mixture and left to incubate at room temperature for 60 mins to form DNA-containing liposomes. This mixture totalled 300 µl in volume. The media in each well of the plate was replaced with reduced serum media (5% FBS) and 25 µl of the transfection mixture was then pipetted into each well of the plate. The plate was then incubated at 5% CO_2, 95% relative humidity and 37°C for 24 hrs before use in experiments.

2.2.24: Immunostaining of Transwells® (Caco-2 Only)

Caco-2 cells were grown for 21 days as described in section 2.2.19 and evaluated for monolayer integrity as described in section 2.2.6. The contents of each well were then aspirated, followed by two washes with PBS. The cell monolayer (on the apical side of the Transwell® filter) was then fixed with 200 µl of 4% paraformaldehyde in PBS for 30 mins at room temperature. After 30 mins of fixation, the monolayer was washed 3 times with PBS and incubated for one hour with 0.5 ml of 1% bovine serum albumin (BSA) at room temperature as a non-specific binding blocking step. A 1:5000 dilution of the primary antibody (Rabbit Anti-Human NTS1) was prepared in 1% BSA in PBS as recommended by the supplier (Thermo Scientific). Optimisation of primary antibody dilution was carried out and 1:5000 was found to be sufficient. After incubation with blocking solution, the contents of the well were aspirated and each

monolayer was incubated with 300 µl of primary antibody solution for one hour at room temperature. Primary antibody solution was omitted for the negative controls and replaced with antibody diluent solution. Each monolayer was then washed thoroughly with PBS 3 times, and incubated for one hour with 0.5 ml of goat anti-rabbit AlexaFluor®488 at a dilution of 1:800 in 1% BSA in PBS. The secondary antibody solution was then removed and each monolayer was washed thoroughly with PBS five times. The filters from each Transwell® (containing the immunostained cellular monolayer) was then excised from the attached plastic insert with a scalpel and mounted on a glass slide, taking care to mount the membrane as flat as possible, monolayer side facing up. The monolayer was then covered with two drops of Fluoroshield™ with DAPI mounting medium and covered with glass cover slips. The slides were then left to dry overnight and assessed by confocal microscopy.

2.2.25: Immunostaining of 12 Well Plates

Caco-2 and HEK293 cells were grown until ~70% confluency as described in section 2.2.21. The contents of each well were then aspirated, followed by two washes with PBS. The cell monolayer was then fixed with 0.5 ml of 4% paraformaldehyde in PBS for 30 minutes at room temperature. After 30 minutes of fixation, the well was washed 3 times with PBS and incubated for one hour with 0.5 ml of 1% bovine serum albumin (BSA) at room temperature as a non-specific binding blocking step. A 1:5000 dilution of the primary antibody (Rabbit Anti-Human NTS1) was prepared in 1% BSA in PBS as recommended by the supplier (Thermo Scientific). Optimisation of primary antibody dilution was carried out and 1:5000 was found to be sufficient. After incubation with blocking solution, the contents of the well were aspirated and each well was incubated with 0.5 ml of primary antibody solution for one hour at room temperature. Primary antibody solution was omitted for the negative controls and replaced with antibody diluent solution. Each well was then washed thoroughly with PBS 3 times, and incubated for one hour with 0.5 ml of goat anti-rabbit AlexaFluor®488 at a dilution of 1:800 in 1% BSA in PBS. The secondary antibody solution was then removed and each monolayer was washed thoroughly with PBS five times. The coverslip from each well was then removed from the well with a scalpel and placed on a glass slide, cell-covered side facing up. The coverslip was

then coated with two drops of Fluoroshield™ with DAPI mounting medium and topped with a square glass cover slip. The slides were then left to dry overnight and imaged by confocal microscopy.

2.2.26: Confocal Microscopy

The Leica TCS SP8 confocal microscope was used for qualitative assessment of NTS1 expression in HEK293 cells, transfected HEK293 cells and Caco-2 cells. Pre-programmed settings in the LAS-AF programme for DAPI (at gain 600) and AlexaFluor®488 (at gain 750) were used to detect fluorescence of both components of the immunostain. DAPI stains for nucleic acids and so showed the position of the nucleus and AlexaFluor®488 indicated the presence of human-NTS1 receptors on the cell membrane. The gain of the lasers was kept constant for DAPI and AlexaFluor®488 in all immunostained sections imaged by confocal microscopy in this study unless stated otherwise in the accompanying figure legend. The Z stack function was used to obtain any 3D images displayed in this study

2.2.27: Evaluation of Cellular Growth in Transwells®

Transwells® were seeded as described in section 2.2.19 with Caco-2 cells. TEER readings (see section 2.2.20) were taken every two days for the full duration of their growth (21 days) and plotted on a line graph to assess their growth rate. TEER measurements were taken prior to any experimentation with the Transwell® to ensure structural integrity of the cell monolayer. TEER was measured immediately after being taken out of the incubator (as incubation periods at room temperature affect the TEER reading). This continuity allowed for reliable comparison of data to track the growth of the cells and integrity of intercellular tight junctions.

2.2.28: Evaluation of Cellular Growth in 12 Well Plates

Cells were grown in 12-well plates as described in section 2.2.21. Caco-2, HEK293 and transfected HEK293 were assessed in this procedure. Transfected HEK293 cells were transfected 24 hrs before this procedure. 48 hrs after seeding, growth media was removed and cells were washed and detached from the coverslips in each well with 200 µl of trypsin, incubated at 5% CO_2, 95% relative humidity and 37°C until detached (2 mins for HEK293/5 mins Caco-2). Each well was then topped up to 1 ml

by adding 800 µl of complete media. This mixture was not centrifuged to remove trypsin as the centrifugation process may have compromised cellular integrity. 10 µl of each cell line (transfected and non-transfected for HEK293) was then mixed with 10 µl of trypan blue and counted using a haemocytometer (see section 2.2.18). The number of viable cells was compared against the number of dead cells to assess cell viability after 48 hours of growth.

2.2.29: Protein Transport Studies in Transwells®

TEER was measured in each well prior to experimentation to ensure structural integrity of the cell monolayer, this was typically ~2000 Ω/cm^2 (see section 2.2.20). If the resistance measured in any of the wells were significantly different, that well was not used for experimentation. Each well of the transwell® was then incubated at 5% CO_2, 95% relative humidity and 37°C in pre-warmed HBSS for at least 30 mins to acclimatise to the change in media. Samples of GFP-NT of GFP (with or without inhibitors NT and SR142948) as described in section 2.2.14, were prepared at variable concentrations in HBSS. Contents of the wells were gently aspirated and 0.5 ml of an appropriate protein sample was then applied to the apical side of the cell monolayer and 1.5 ml of fresh HBSS was added to the basal side. A 100 µl sample of HBSS from the basal side of the transwell® was taken immediately after introduction of the protein samples (to the apical side) as a measure of protein transport through the monolayer at time 0 mins. This was done to ensure there were no leaks in the polycarbonate filter or cellular monolayer affecting the data obtained. 100 µl of fresh HBSS was then added to the basal side to replace that taken for the previous sample. 100 µl samples were then taken every 30 mins for three hours, replacing the volume of sample taken with fresh HBSS each time. Between samples, the Transwell® was returned to the incubator each time and covered with aluminium foil to protect the fluorescent protein samples from light. Care was taken to ensure the external environment was as dark as possible. Each sample was loaded into an appropriate well of a black 96 well plate and stored in the dark at 4°C between sampling times. After three hours, the plate was read for fluorescence (Fluorescein - ex: 490 nm, em: 525 nm/GFP – ex: 488 nm, em: 509 nm) using the Tecan Infinite® Pro 200 microplate reader at gain 100.

2.2.30: Protein Uptake Studies in Transwells®

TEER was measured in each well prior to experimentation to ensure structural integrity of the cell monolayer, this was typically ~2000 Ω/cm^2 (see section 2.2.20). If the resistance measured in any of the wells were significantly different, that well was not used for experimentation. Each well of the transwell® was then incubated at 5% CO_2, 95% relative humidity and 37°C in pre-warmed HBSS for at least 30 mins to acclimatise to the change in media. Samples of GFP-NT of GFP (with or without inhibitors NT and SR142948) as described in section 2.2.14, were prepared at variable concentrations in HBSS. The HBSS was then gently aspirated from the wells (both apical and basal sides) and 0.5 ml of an appropriate protein sample (GFP-NT) etc. in HBSS) was then applied to the apical side of the cell monolayer and 1.5 ml of fresh HBSS was added to the basal side. One filter of each protein sample condition tested was immediately transferred to a fresh 12 well plate (to represent cellular uptake at time 0) and the remaining wells in the original transwell® were covered in aluminium foil and replaced in the incubator. The samples transferred were then aspirated of previous contents and washed 3 times by swirling with cold (4°C) PBS. The temperature of the PBS halted any cellular transport of the protein sample. 200µl of 0.1% Triton-X 100 in protein buffer (200 mM Tris, 50 mM NaCl with 200 µl of 25x complete protease inhibitor stock solution (see section 2.1.3)) was then added to the apical side of the cell monolayer (to permeabilise the cells) and left to incubate at room temperature for 30 minutes (taking care to not expose samples to light). After incubation, the contents of each well were pipetted up and down to detach cells from the filter and homogenise contents, before being transferred to a 1.5 ml eppendorf and stored at 4°C in the dark until required for quantification. This was repeated for each protein sample condition every 30 minutes for 2.5 hours to represent protein uptake at times: 0.5, 1, 1.5, 2 and 2.5 hrs. Care was taken to ensure the external environment was as dark as possible. Once all samples had been collected, samples were centrifuged at 17,900g (13,000 rpm) in a bench top centrifuge to extrude cellular debris. The supernatant (100 µl) was then loaded into appropriate wells of a black 96 well plate and read for fluorescence (Fluorescein -ex: 490 nm, em: 525 nm/GFP – ex: 488 nm, em: 509 nm) using the Tecan Infinite® Pro 200 microplate reader at gain 100.

2.2.31: Protein Uptake Studies in 12 Well Plates

Cells were seeded in the 12 well plate as described in section 2.2.21. After 48 hrs, the contents of the wells were aspirated and the wells were incubated with 1 ml of pre-warmed HBSS to acclimatise to new media and remove any dead cells. Note: the previous step was required to be performed gently with HEK293 cells, as they are a weakly adherent cell line. Samples of GFP-NT or GFP (with or without inhibitors NT and SR142948) as described in section 2.2.14, were prepared at variable concentrations in HBSS. 1 ml of the appropriate protein sample was added to each of the wells and incubated at 5% CO_2, 95% relative humidity and 37°C for 1 hr, taking care to protect the plate from light. Following incubation, contents of the wells were aspirated and the wells were washed with cold (4°C) PBS 3 times. Each wash was performed for five minutes whilst being gently rocked to ensure complete coverage of the cells. After washing the cells, they were incubated with 200 µl of 0.1% Triton-X 100 in protein buffer (200 mM Tris, 50 mM NaCl with 200 µl of 25x complete protease inhibitor stock solution) for 30 mins at room temperature whilst being protected from light. Following this, the contents of the well were pipetted up and down to ensure detachment of the cells from the wells and homogenise the contents of the well. Each sample was then transferred to a 1.5 ml eppendorf tube and centrifuged at 17,900g (13,000rpm) for 5 miNs to extrude cellular debris. The supernatant (100 µl) was then loaded into appropriate wells of a black 96 well plate and read for fluorescence (Fluorescein -ex: 490 nm, em: 525 nm/GFP – ex: 488 nm, em: 509 nm) using the Tecan Infinite® Pro 200 microplate reader at gain 100.

2.2.32: Statistical Analysis

Statistical analysis was performed using GraphPad Prism© software. The parametric unpaired Student's t-test was used to determine the significance of NT-conjugated fluorophore uptake into cells under different conditions (e.g inhibited by free NT/SR142948 or non-inhibited) compared to uptake of unconjugated fluorophore. Statistical analysis was performed for uptake of conjugated fluorophore for NTS1 non-transfected/transfected HEK293 and undifferentiated/differentiated Caco-2 cells. Welsh's correction was applied to each test, as the SD for each data point was not identical. See section 5 for graphical representation of the data sets used for this.

Chapter 3
Characterisation of Cell Lines

3.1: Introduction

3.1.1: Caco-2 Cell Line

The production of model mucosal membranes is widely employed to predict mucosal absorption of drugs intended for oral delivery (Antunes *et al*., 2013). One such cell line used for this purpose is Caco-2. The Caco-2 cell line, derived from a moderately differentiated human colon carcinoma, has been widely used over the last couple of decades as a model of the intestinal barrier (Sambuy *et al*., 2005). When grown on polycarbonate or nitrocellulose filters, Caco-2 cells undergo differentiation into enterocyte-like membrane monolayers, expressing several morphological and functional characteristics of the mature enterocyte. Morphological assessment of the differentiation of Caco-2 monolayers confirms an increase in cellular height (of ~500%), decrease in cell width (of ~50%) and presence of microvilli (Pinto *et al*., 1983). Past research into the use of differentiated (sometimes referred to as 'polarised') Caco-2 monolayers concludes that the use of such monolayers as a model transport system to mimic the small intestinal epithelium is valid (Hidalgo *et al*., 1989; Pinto *et al*., 1983).

3.1.2: HEK293 Cell Line

The HEK293 cell line was created following transformation of human embryonic kidney (HEK) cells following exposure to fragments of adenovirus type 5 (Ad5) DNA by Graham *et al*., (1977), and numbered due to Graham's habit of numbering his experiments. The cells were extracted from an embryo legally terminated in the Netherlands. Viral transformation resulted in incorporation ~4.5 kb of viral DNA into chromosome 19 of the cell line (Louis *et al*., 1997). This allows for hijacking of the cells internal control mechanisms and counteraction of apoptosis and created an effective tool for recombinant protein production (Lin *et al*., 2014). The HEK293T cell line used in this study (referred to here-on as 'HEK293') is a derivative of the original HEK293 cell line, which is the transformation product of HEK293 with the large T antigen of the SV40 virus. The HEK293T variant is documented to have a higher

transfection efficiency than the original, hence the reason for their use in this study. Graham *et al*., (1977) documented the pre-cursor transformation of HEK cells with adenoviral DNA to be difficult, suggesting that the cell line may not be of kidney origin at all. Although the name of the cell line suggests the origin of the cell line as kidney, Shaw *et al*., (2002), (a post-doc of Grahams') have provided evidence suggesting that all variants of the HEK293 cell line show similar characteristics to immature neuronal cell lines. As such, it was speculated that the adenovirus preferentially transform into cells of neuronal lineage, which would have been abundance in embryonic tissue.

3.1.3: Transfection

Eukaryotic cells are able to take up exogenous DNA under certain conditions. There are many methods of inducing this phenomenon for scientific gain, known as transfection, including: the calcium phosphate method, electroporation, liposome fusion, microinjection and with the use of retroviruses (Kim and Eberwine, 2010). However, chemical methods of transfection have been documented to elicit toxicity to certain cell types. Transfection is a procedure that inserts foreign nucleic acids into a host cell – this DNA can exist in one of two forms, stably or transiently. Stable transfections incorporate the foreign DNA into the hosts own DNA and is expressed sustainably, whereas transient transfection deliver foreign DNA to the nucleus without incorporating itself into host DNA (Kim and Eberwine, 2010).

Lipofectamine is a cationic lipid, synthesised by Felgner *et al*., (1987), which is known to spontaneously interact with DNA and form liposomes, fuse with mammalian cell lines and facilitate the delivery of DNA to the host cell. Non-viral delivery systems, such as lipofectamine, have been shown to have an advantage over viral methods as they are non-immunogenic, easy to produce and not oncogenic (Zhang *et al*., 2010). However, they do not have as great a transfection efficiency. The method of endocytosis with lipofectamine is not completely understood, however, Cui *et al*., (2012) have documented a correlation between clathrin-dependant endocytosis and transfection efficiency in HEp-2 cells.

3.1.4: Methods of Determining Cell Viability

There is a diverse array of methods for determining cellular viability, which is variable between studies. Understandably, this can influence the interpretation of experimental results from paper to paper. Commonly used methods of determining cellular viability include colorimetric assays such as the MTS/MTT assays, Alamar Blue assay, LDH assay, and crystal violet assay (Vega-Avila and Pugsley, 2011). The term viability can refer to variety of terms such as cell survival, cellular integrity and cytotoxicity; it is the interpretation of what constitutes viable, and the choice of assay used that causes these differences (Cook and Mitchell, 1989). Trypan Blue is a diazo dye commonly used to selectively colour dead cells, as the dye cannot penetrate intact cell membranes. One limitation associated with the method is the need to perform any cell count including the dye immediately as cells may non-selectively intake the blue-stain after ~5 minutes (Altman *et al*., 1993).

3.2: Results

3.2.1: Light Microscopy of Caco-2 and HEK293

Figure 3.1 depicts the morphology of HEK293 and Caco-2 cells respectively. The images were taken using the Nikon DN100 digital camera control unit and Nikon Eclipse TS100 light microscope (see section 2.2.22). Images were taken at x40 magnification.

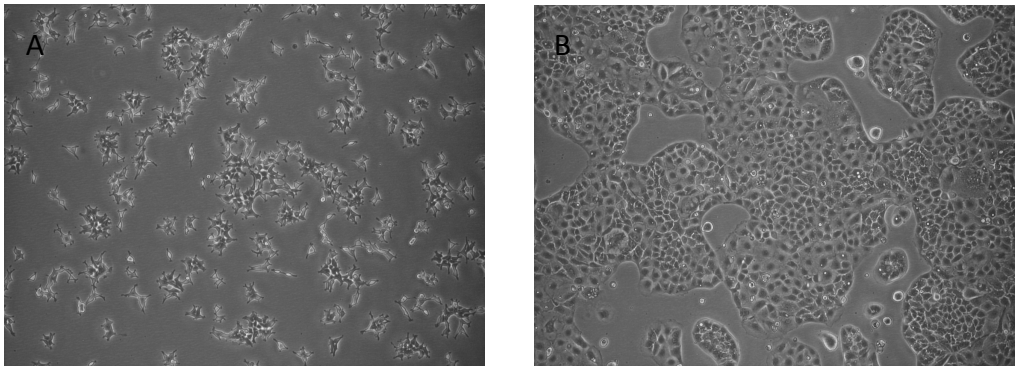

Figure 3.1: A – HEK293 cells at a confluency of 40-50%. B – image of undifferentiated Caco-2 cells at a confluency of ~70%. These images were taken at a 40x magnification.

3.2.2: Optimisation of Transfection of HEK293

Figures 3.2-3.4 show confocal microscope images detailing NTS1 expression following transfection of HEK293 cells with an NTS1 containing plasmid (with the intention of producing NTS1 overexpressing HEK293 cells) using differing concentrations of lipofectamine to perform the transfection. This was done to optimise the procedure and result in the highest level of NTS1 expresison possible. The amount of plasmid remained constant at 1µg per well (see section 2.2.23 for further details).

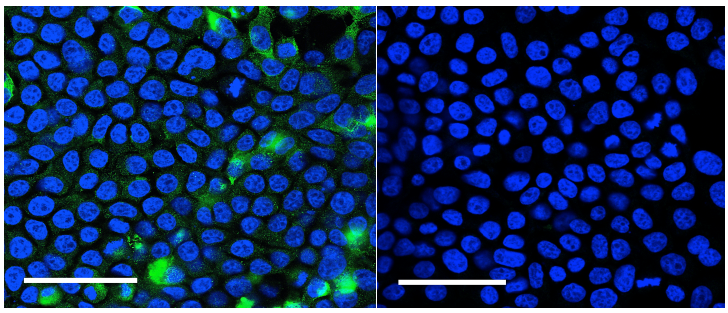

Figure 3.2: Qualitative evaluation of NTS1 expression in transfected HEK293 with **2 µl** of Lipofectamine per well (left) with negative control (right). Blue staining represents nucleic acids (stained by DAPI) and green staining represents NTS1. The white bar represents 50 µm.

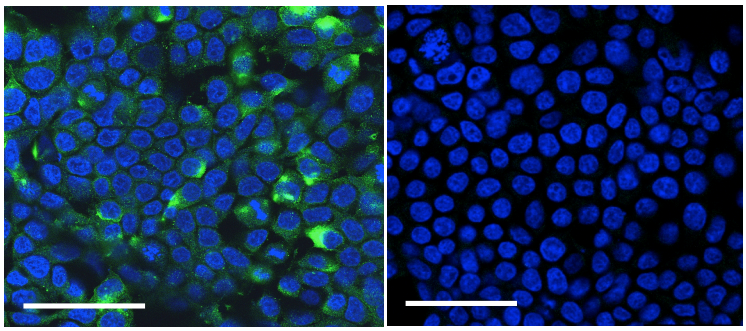

Figure 3.3: Qualitative evaluation of NTS1 expression in transfected HEK293 with **3 µl** of Lipofectamine per well (left) with negative control (right). Blue staining represents nucleic acids (stained by DAPI) and green staining represents NTS1. The white bar represents 50 µm.

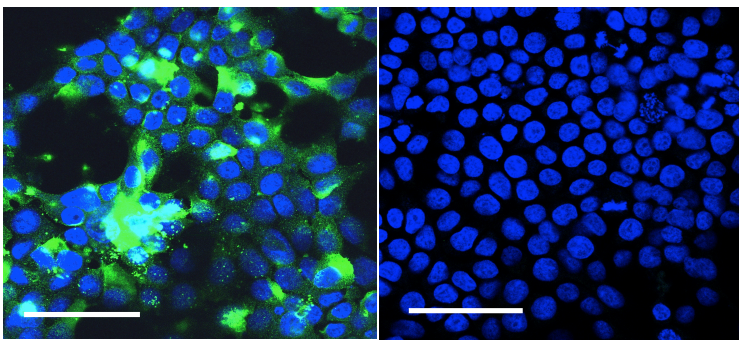

Figure 3.4: Confocal images of NTS1 expression in transfected HEK293 with **4 µl** of Lipofectamine per well (left) with negative control (right). Blue staining represents nucleic acids (stained by DAPI) and green staining represents NTS1. The white line is representative of 50 µm.

Figures 3.2-3.4 above are images of transfected HEK293 cells with differing amounts of lipofectamine used for the transfection procedure, coupled with their respective negative controls. Immunofluorescence staining of NTS1 was carried out as described in section 2.2.25. Images were taken using confocal microscopy as described in section 2.2.26. Figure 3.4 (representing a transfection protocol including 4 µl of lipofectamine per well) shows the highest level of NTS1 expression. As such this volume of lipofectamine was used for the transfection procedure described in section 2.2.23 henceforth.

3.2.3: Evaluation of NTS1 Expression in Caco-2 and HEK293 by Immunostaining

Figures 3.5 and 3.6 depict NTS1 expression on polarised (grown on a transwell® filter for 21 days) Caco-2 cells, non-permeabilised and permeabilised before immunofluorescence (section 2.2.24) respectively to display the locality of the receptor. Permeabilisation of the cellular membrane disrupts its integrity and therefore any membrane proteins present. NTS1 is strongly detected in figure 3.5 (non-permeabilised) and not figure 3.6 (permeabilised). Some fluorescence is noticeable located around the nucleus of cells in figure 3.6. Negative controls confirm that fluorescence on the test samples was not due to non-specific staining. Images were taken using confocal microscopy as described in section 2.2.26.

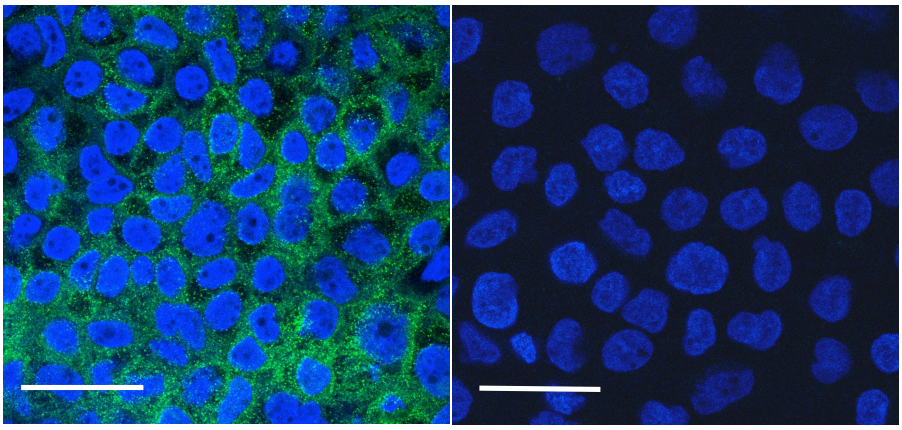

Figure 3.5: Confocal images of NTS1 expression in non-permeabilised polarised Caco-2 cells (left) with negative control (right). Blue staining represents nucleic acids (stained by DAPI) and green represents NTS1. The white bar is representative of 50 µm.

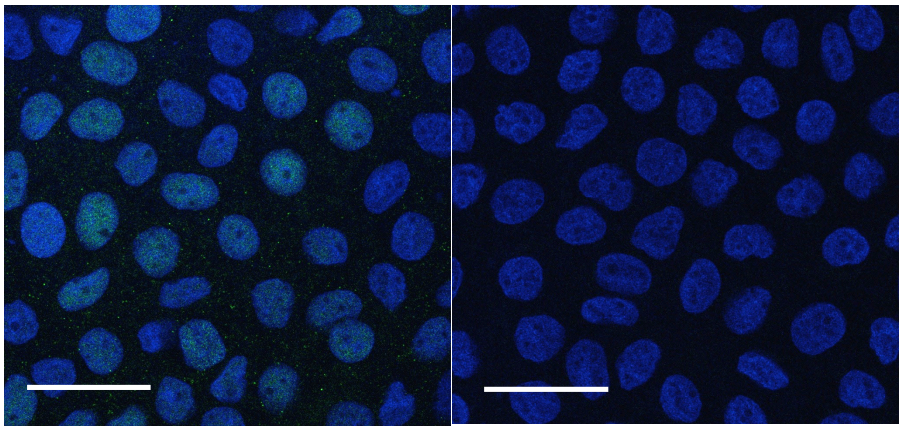

Figure 3.6: Confocal images of NTS1 expression in permeabilised polarised Caco-2 cells (left) with negative control (right). Samples were permeabilised with 0.1% Triton X 100 in PBS. Gain of the laser detecting DAPI was reduced in this image compared to other confocal images displayed in order make fluorescence of AlexaFluor®488 clearer. Blue staining represents nucleic acids (stained by DAPI) and green staining represents NTS1. The white bar is representative of 50 µm.

Figure 3.7 depicts NTS1 expression on non-polarised Caco-2 cells grown as described in section 2.2.21. NTS1 immunostaining was performed as stated in section 2.2.25. Images were taken using confocal microscopy as described in section 2.2.26. Suggested by a lack of fluorescence, NTS1 is not expressed in undifferentiated Caco-2 cells.

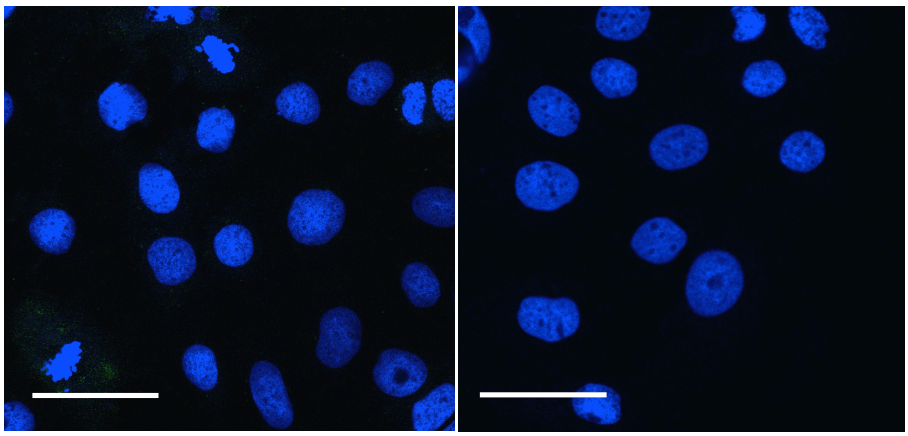

Figure 3.7: Confocal images of NTS1 expression in undifferentiated Caco-2 cells (left) with negative control (right). Blue staining represents nucleic acids (stained by DAPI) and green staining represents NTS1. The white bar is representative of 50 µm.

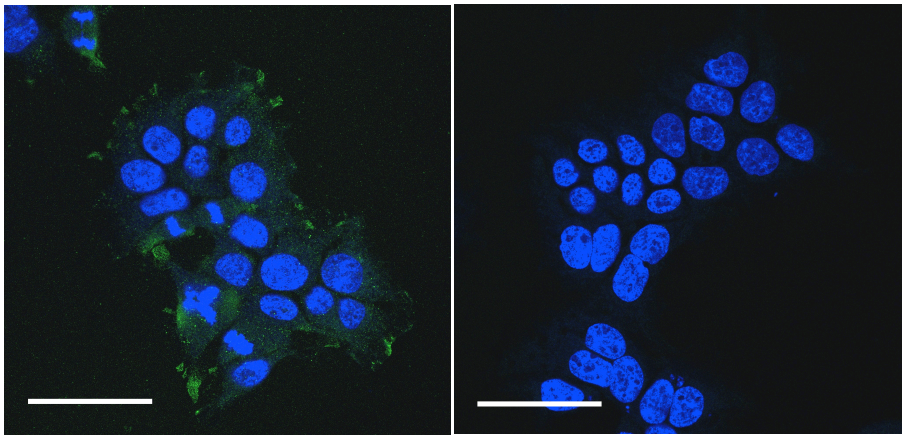

Figure 3.8: Qualitative evaluation of NTS1 expression in untransfected HEK293 cells (left) with negative control (right). Blue staining represents nucleic acids (stained by DAPI) and green staining represents NTS1. The white bar is representative of 50 µm.

Figure 3.8 depicts NTS1 expression on non-transfected HEK293 cells grown as described in section 2.2.21. Images were taken using confocal microscopy as described in section 2.2.26. HEK293 are shown to express NTS1 as suggested by observable fluorescence in figure 3.8. Negative controls confirm that fluorescence on the test samples was not due to non-specific staining.

3.2.4: TEER Profile of Caco-2 Cells Grown in Transwells®

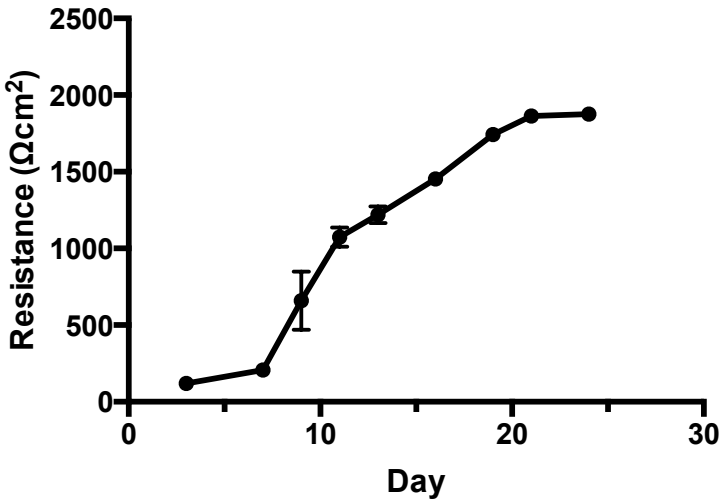

Figure 3.9: TEER profile of Caco-2 cells, grown for a total of 24 days in Transwells®. Error bars are representative of ±SD. Data points plotted are representative of n=12.

Figure 3.9 shows the TEER (Ω/cm^2) of Caco-2 cells grown in Transwells® for a total of 24 days (see section 2.2.19). TEER was recorded (as described in section 2.2.27) every two days from seeding. Each value plotted is the mean of 12 wells. Error bars plotted are representative of one standard deviation. An almost linear increase in TEER is observable, followed by a plateau of resistance at day 21.

3.2.5: Evaluation of Cellular Growth in 12 Well Plates

Figure 3.10: Displays cellular growth over 48 hours when grown in 12 well plates (see section 2.2.28). Cells were counted and healthy cells were identified using Trypan blue as described in section 2.2.18. Data is representative of N=4 wells per cell line. Each well was counted three times and averaged. Error bars are equal to one standard deviation. Wells were seeded at $10x10^4$ cells per cm^3.

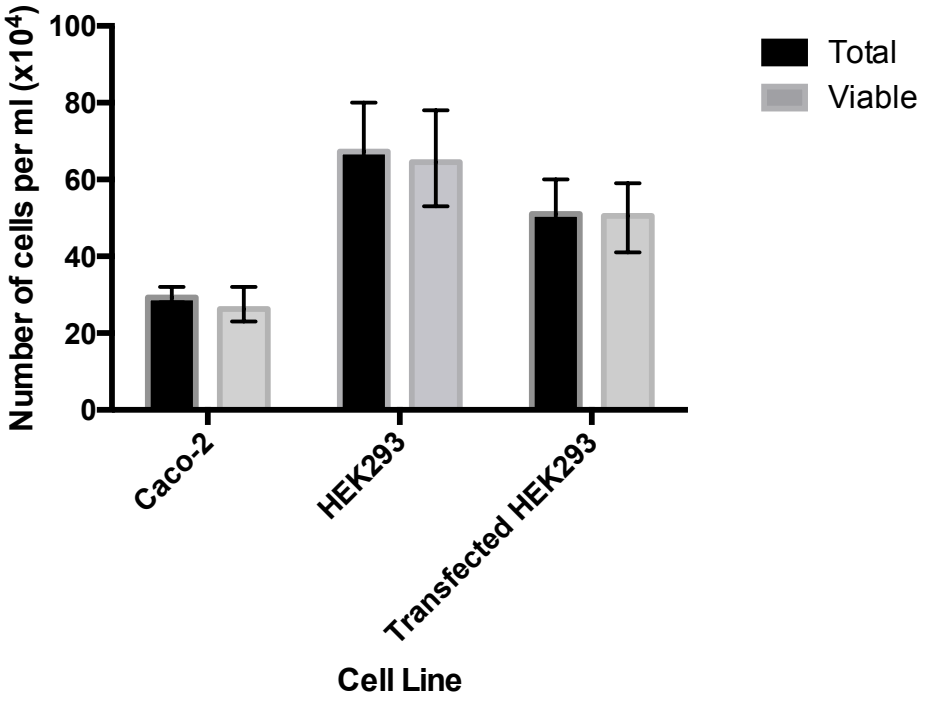

Figure 3.10: Cellular growth of Caco-2, HEK293 and HEK293 transfected with NTS1 when grown in 12 well plates for 48 hours. Black bars represent the total number of cells (n=3) and grey bars represent the total number of viable cells (n=3). Error bars are representative of ± SD.

Figure 3.11: Displays % cellular viability of each cell line after 48 hours when grown in 12 well plates (see section 2.2.21). Cells were counted and healthy cells were identified using Trypan Blue as described in section 2.2.18. Data is representative of

N=4 wells per cell line. Each well was counted three times and averaged for that well. Caco-2 = 92.07%, HEK293 = 95.91%, Transfected HEK293 = 99.02%.

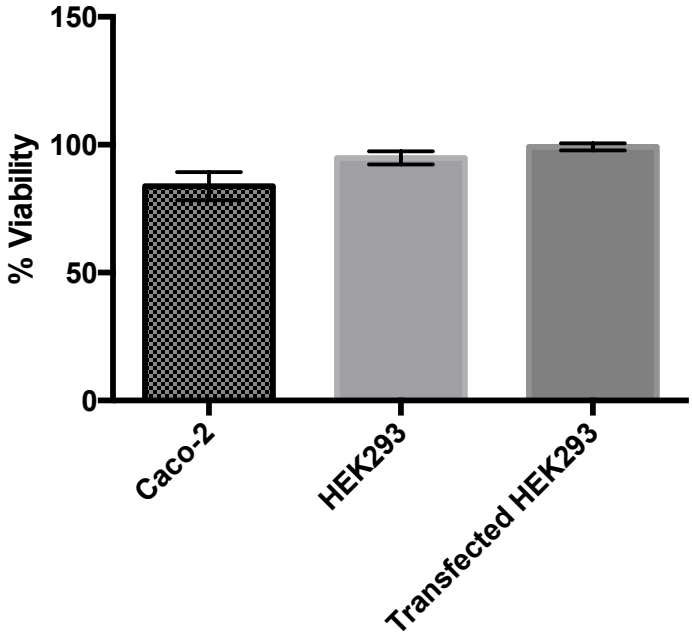

Figure 3.11: % cellular viability of Caco-2, HEK293 and HEK293 transfected with NTS1 when grown in 12 well plates for 48 hours. The data displayed in each bar is representative of n=4.

3.3: Discussion

3.3.1: Caco-2 Cells

NTS1 is documented to be expressed in foetal colonic epithelial cells, but not mature, differentiated enterocytes in physiologically normal conditions. Expression in the gastrointestinal system is thought to be localised to the distal small intestine, with little or no expression in the healthy colon (NTS1 is transiently expressed during colon development, however). Expression is known to be unregulated in a progressive manner during neoplastic transformation of colonic adenocarcinomas (Evers *et al*., 1993; Gui *et al*., 2008). A comparison of figures 3.5 and 3.7 indicates a clear absence of NTS1 expression in undifferentiated Caco-2 cells compared to an almost homogenously high level of expression in differentiated cells. The differentiation process itself following a progressively neoplastic transformation or NTS1 having a direct role in the differentiation process of Caco-2 cells could explain this. However, no previous research has been done into NTS1 expression in Caco-2

cells during the differentiation process. As Caco-2 cells are sourced from a moderately differentiated adenocarcinoma as opposed to a poorly differentiated one, undifferentiated Caco-2 cells might be exhibiting similar characteristics to the healthy colon with regards to NTS1 expression. The comparison of internalisation of NT-bound fluorophores between undifferentiated and differentiated Caco-2 cells (later described in chapters 5 and 6) will therefore serve as an experimental model for internalization of NT in invasive adenocarcinoma/other NTS1 expressing cancerous cells vs physiologically normal cells.

Gui *et al*., (2008) found NTS1 expression to be predominantly localised in the basal cells of the crypts, known to contain the self-renewing epithelial stem cell populations and rapidly dividing cells, compared to superficial colonic epithelial cells. However, they also noted there to be low levels of NTS1 mRNA present in around 40% of normal colonic mucosa samples examined. This supports the idea that NTS1 plays a role in cellular propagation and division, as well as its role as a hormone receptor in the gut. Interestingly, although undifferentiated Caco-2 cells showed next to no expression of NTS1, cells that were visually determined to be in the process of cellular division appeared to up regulate expression of the receptor (see figure 3.12). This applied to both undifferentiated Caco-2 cells and HEK293 cells. The image of the dividing Caco-2 cell in figure 3.12 is an enlargement of the dividing cell visible in figure 3.7.

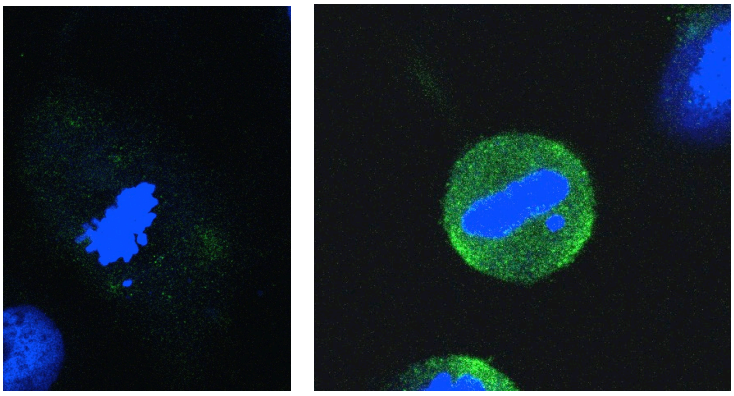

Figure 3.12: Shows Caco-2 cells (left) and HEK293 cells (right) in the progress of cellular division. NTS1 is noticeably up regulated compared to cells in interphase (Figures 3.7 and 3.8 respectively). This further supports the idea that NTS1 is involved in cellular division and propagation.

Expression levels of differentiation markers such as the GLUT-5 transporter and sucrose-isomaltase have been shown to increase in later passages of Caco-2s compared to earlier ones (Sambuy *et al*., 2005). Due to observable shifts in phenotype, it is safe to assume that the passage number may also affect NTS1 expression in both differentiated and undifferentiated Caco-2 cells. As such, further studies into how the passage number of Caco-2s affects NTS1 expression is recommend. As this study has continuously utilised and assessed NTS1 expression in Caco-2 cells of passage 60-80, it should be representative of that range of passages only until the effect of passage number on NTS1 expression has been determined.

The most obvious limitation in this study is the lack of quantification of NTS1 expression (in both Caco-2 and HEK293). All confocal images in the results section of this chapter are representative of replicate slides and multiple fields of view, however, a lack of quantification presents a inability to definitively compare expression levels between both cell lines and undifferentiated vs differentiated conditions for Caco-2 cells. Therefore, it is recommended that NTS1 expression be quantified by RT-PCR, flow cytometry or by employing software for the quantification of NTS1 expression obtained by immunofluorescence.

Several studies have suggested that the passage number of the cell line also increases the proliferation rate and elicits higher TEER readings in later passages (Briske-Anderson *et al*., 1997; Lu *et al*., 1996). However, Anderle *et al*., (2003)

evaluated changes in transport properties of Caco-2 from earlier to later passages, including transcellular (mannitol), paracellular (hydrocortisone) and carrier-mediated (dipeptide) methods. All of which were shown to be unchanged in earlier compared to later passages. The cells used for this study fell in between the ranges for early and late passaged cells stated from the describe studies, 35-47 and 82-95 respectively.

The density of cell seeding has also been put under scrutiny in previous studies. A common problem with the production of monolayers when grown on polycarbonate filters is a tendency to form multilayers. This tendency is also dependent on the cell line used. Tavelin *et al*., (2002) speculates that this is due to high seeding densities. Their study suggests that any seeding density above $0.6x10^4$ cells/cm^2 will require a washout of cells three hours after seeding to avoid this problem. However, Caco-2 cells were seeded at a density of $2x10^5$ cells/cm^2 for this study, without washing after three hours, and no multilayer formation was observed as determined by a combination of confocal microscopy and light microscopy (see figure 3.13). Higher seeding densities, such as that used in this study, decrease the time taken for cells to reach confluency and thus allow for the development of tight junctions and maturation of the monolayer to proceed for longer (Ranaldi *et al*., 2003).

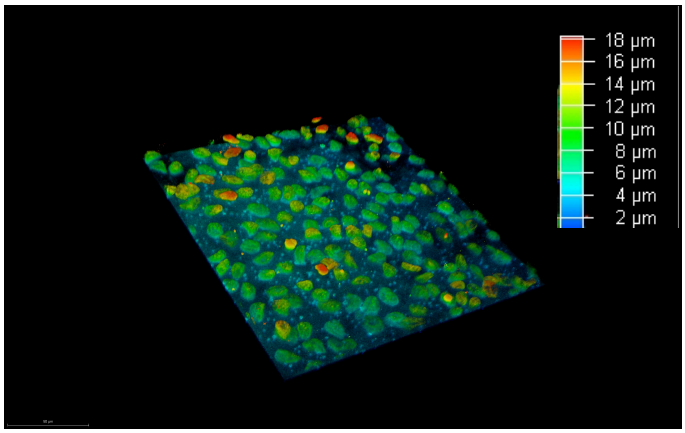

Figure 3.13: Confocal image taken of cell nuclei only (as stained by DAPI). This figure shows the relatively flat arrangement of cells with no overlapping. This image is coloured in relation to depth so areas with the same colour are the same height above the polycarbonate membrane. Relatively few cell nuclei appear to be positioned above

Caco-2 cells follow a well-documented, time-dependent pattern of differentiation into expressing the morphological characteristics of mature enterocytes. Expression of these characteristics happens through three phases of monolayer development; homogeneously undifferentiated (days 0-3), heterogeneously polarized and differentiated (days 3-20) and homogeneously polarized and differentiated (days 21+). Plateaus in TEER readings are documented to occur at 21 days (as seen in figure 3.9), in concordance with the generally accepted 21 days of culture for Caco-2 monolayers before experiments; but this does not affirm maximum homogeneous expression of NTS1 at day 21 of culture (Vachon *et al*., 1996). Bravo *et al*., (2004) evaluated expression of the PepT1 transporter in polarized Caco-2s, achieving maximum expression at day 25 of culture. It is recommended that NTS1 expression be evaluated at different time periods of monolayer culture as further work as it has not been previously evaluated.

3.3.2: HEK293 Cells

HEK293 cells were included in this study to provide a model for GFP-NT internalisation that does not mimic the intestinal membrane like Caco-2. To instead mimic internalisation of GFP-NT in NTS1 overexpressing solid-state tumours. HEK293 cells are known to exhibit some neuronal characteristics (as described in section 2.1.2), including the expression of neuroreceptors like NTS1 (Thomas and Smart, 2005).

As expression of NTS1 was transient in HEK293 cells, transfections were performed the day before and not stored past the day of experimentation. Transfection of NTS1 using the lipofectamine method appears to have been successful (see figure 3.4), but has not yielded homogeneous expression throughout observed immunostained sections. This may be due to the need for further optimization, the plasmid vector used not being highly efficient or the method of transfection itself. The 293T variant of HEK293 used for this study enables the amplification of plasmid vectors containing the SV40 ori (Lin *et al*., 2014) as previously described to increase transfection efficiency – the plasmid vector used for this study did not contain this. However, cationic lipids such as lipofectamine have generally yielded the highest

transfection efficiencies of all the chemical-based methods of transfection (de los Milagros Bassani Molinas *et al*., 2014).

Like Caco-2 cells, the passage number is known to affect the functionality of HEK293 cells. Lower passages of cells (<30) have been documented to have greater transfection efficiencies for DNA and RNA (Elbashir *et al*., 2002). The passage number of HEK293 ranged from 25-40 for this study – during which time the morphology and growth rate was observed to be consistent with that described in related literature. Figure 3.10 shows the growth rate of HEK293 to be almost double that of undifferentiated Caco-2, with a reduction in growth rate when transfected. This is to be expected as recombinant protein production of NTS1 will increase cellular demand and as a result, decrease growth rate. The influence of growth rate on internalisation of GFP-NT between the cell lines will be discussed in chapter 5.

3.4: Conclusion

Expression of NTS1 on differentiated Caco-2, undifferentiated Caco-2, wild type HEK293 and transfected HEK293 was qualitatively assessed along with optimization of the transfection procedure. 4µl of lipofectamine with 1µg of DNA was found to have the greatest transfection efficiency in reduced serum media. NTS1 expression was found to change from not present to highly present during the differentiation process of Caco-2 cells. As such, undifferentiated and differentiated Caco-2s can be used as a model for the comparison of GFP-NT internalization in the healthy colon vs NTS1 expressing adenocarcinoma. Similarly, the comparison of internalisation of HEK293 and transfected HEK293 can be used to compare internalisation of GFP-NT in cells moderately expressing vs highly expressing NTS1. However, the methods used for evaluation of NTS1 expression are purely qualitative in this instance and further quantitative evaluation is recommended for definitive comparison of how NTS1 expression influences internalization and transport of NT-bound fluorophores.

Chapter 4

Production of Neurotensin-Conjugated GFP

4.1: Introduction

4.1.1: Recombinant Therapeutics

The production of recombinant proteins has been increasingly utilised as a tool for molecular biologists as a result in demand for commercially available recombinant biotherapeutics. The technique is employed in a variety of areas for the production of large amounts of recombinant proteins from genetically manipulated bacteria, yeast, mammalian cells, plants and transgenic animals (Palomares *et al*., 2004). For example, Goeddel *et al.*, (1979) produced one of the first human recombinant proteins, insulin, by DNA manipulation in the bacterium *Escherichia coli* (*E.coli*), where it was originally synthesised separately as A and B chains. Later, the process was modified to produce proinsulin to be later modified by enzymatic cleavage (Johnson, 1983). As diabetes is one of the most prevalent diseases to date, the production of insulin maintains a large influence on the pharmaceutical today. The production of recombinant proteins also expands into the production of bioinsecticides, diagnostic kits and enzymes for numerous applications (Palomares *et al*., 2004).

There are over 200 recombinant biotherapeutics approved for human use on the market today, with over 30% of those produced using *E.coli* (Ferrer-Miralles *et al*., 2009).

4.1.2: Plasmid-Based Systems

Plasmids are extrachromosomal cytoplasmic DNA elements with the ability to self-replicate, found in eukaryotes and prokaryotes. They have been utilised as vehicles for recombinant genes since the advent of genetic engineering, and have been a favoured method of expression in prokaryotes due the ease of genetically manipulating plasmids (Margaritis and Bassi, 1991).

The number of plasmid copies held within each prokaryotic cell is variable, dependant on the prokaryote, the plasmid in question and the size of the protein to be expressed. As such, the number of copies for the plasmid within the cell determines the metabolic load on the host. As cellular resources must be utilised for recombinant protein expression (not just cellular replication) the greater the number of plasmids, the greater the metabolic load. The load also increases with the size of the insert, expression rate, protein yield, temperature of expression and toxicity of the expressed protein toward the host (Corchero and Villaverde, 1998; Summers, 1998). Increased metabolic load results in a decrease in growth-rate of plasmid containing cells. The main contributing factors for decreases in efficiency of recombinant protein expression lie with plasmid loss from host cells and the toxicity of the recombinant protein. Generally, this is caused by poor dispersion of plasmids during division to daughter cells, resulting in plasmid-free cells. However, production of plasmid-free daughter cells is unlikely with high plasmid copy numbers. As previously mentioned, plasmid-containing cells experience an increased metabolic load; the emergence of plasmid-free prokaryotes will therefore exhibit an increased growth-rate and begin to overtake the culture (Paulsson and Ehrenberg, 2001).

Various natural mechanisms exist to ensure plasmid survival in cell populations, which have been incorporated into recombinant plasmids to increase their stability. These mechanisms prevent plasmid instability if they present an advantage over plasmid-free cells, such as the introduction of antibiotic resistance genes to cultures grown with that particular antibiotic (Baneyx, 1999).

4.1.3: The pET Expression System

The pET expression system is commonly used for recombinant protein production, based on the T7 RNA polymerase (Studier, 1991). This system relies upon an *E.coli* host that contains a copy of the gene encoding for the RNA polymerase of bacteriophage T7, which is regulated by an isopropyl β-D-1-thiogalactopyranoside (IPTG) inducible promoter. An example is *lacUV5* – the construct is incorporated into the bacterial chromosome at the DE3 locus (Reznikoff, 1992). The locality of this construct is what gives rise to the name of competent *E.coli* strain commonly used in

conjunction with the pET system: BL21 (DE3). In the absence of IPTG, transcription of this promoter region (located in the bacterial chromosome) is inhibited by the *lac* repressor LacI, inhibiting synthesis of T7 RNA polymerase. Upon addition of IPTG and following subsequent transcription of T7 RNA polymerase, the T7 promoter located in the pET expression system is able to become active and enable transcription of the recombinant gene of interest, downstream (see figure 4.1). The pET expression system is commercially available from Novagen.

Due to the diversity of recombinant proteins, no specific promoter system can suit all recombinant proteins or bacterial strains used for protein expression. Optimally, the chosen system should demonstrate minimal faults in expression, high protein yield and be sensitive to inducer concentration (Brautaset *et al*., 2009).

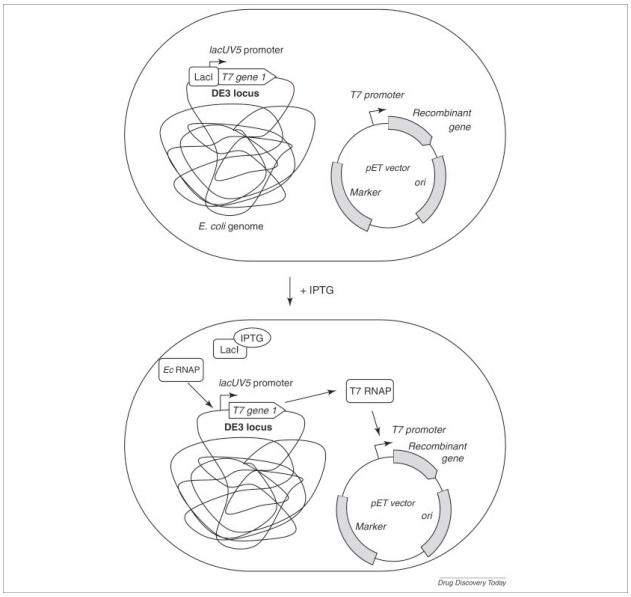

Figure 4.1: Taken from Overton, (2013). The pET system control mechanism. Diagrammatical representation of the activation of the *lacUV5* at the DE3 locus of the bacterial chromosome, and subsequent activation of the T7 promoter region in the pET system.

4.1.4: Green Fluorescent Protein

Green fluorescent protein (GFP) was originally cloned from the jellyfish species *Aequorea victoria.* The fluorophore absorbs blue light and emits fluorescence as green light – hence its name. It is a popular tool for molecular biologists due its stable nature and independence from substrates and cofactors (Cody *et al*., 1993). The fluorophore retains fluorescence when fused to other proteins or peptides on

both the N and C terminus, making it an attractive tool for intracellular targeting as a fluorescent tag (Leffel *et al*., 1997). With regards to the stability of the protein, it has been shown to maintain fluorescence even after incubation with strongly denaturing agents such as urea and sodium dodecyl sulphate (SDS). GFP has also been documented to continue to exert fluorescence for 5hrs when continuously exposed to UV light irradiation, with fluorescence lasting 6 days when stored at 4°c and 4 days when stored at room temperature (Liu *et al*., 1999). Mutants of GFP have been made and employed as a fluorophore since the original discovery of GFP, for the purpose of enhanced fluorescence. For example, emerald GFP or eGFP produced by Clontech (the variant used in this study) has an increased level fluorescence and decreased susceptibility to photo bleaching compared to GFP due to two amino acid substitutions. This shifts the emission wavelength from green (509 nm) to yellowish green (525 nm), with an excitation wavelength of 488 nm (Cubitt *et al*., 1995).

4.2: Results

4.2.1: Analysis of pAG3 by Restriction Digest

Figure 4.2 displays the success of bacterial plasmid transformation and subsequent plasmid extraction of pAG3 as described in sections 2.2.5-2.2.7. The pAG3 plasmid contains a recombinant DNA insert coding for GFP-NT. Gels were made as stated in section 2.2.4. A combination of the restriction enzymes *BamHI* and *NdeI* were incubated with the extraction samples as follows: *BamHI* and *NdeI* (2), *BamHI* alone (3) and without restriction enzymes (4) (see section 2.2.3). The restriction enzyme sites are displayed in figure 4.3. Lane 2 contains bands corresponding to the size of the insert (~0.75 kb) and the plasmid vector (3.3 kb). Lane 3 contains a band corresponding to the size of the plasmid cut at one site, and therefore linear in shape. Lane 4 contains a band corresponding to the uncut size of the plasmid vector plus insert. The lack of other bands on the gel eliminates the possibility of contamination. The sequence of the insert was confirmed as correct by genetic sequencing.

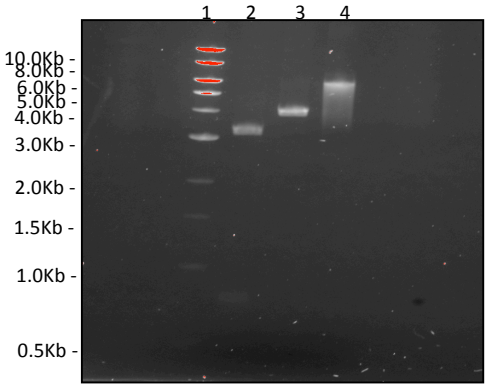

Figure 4.2: DNA electrophoresis of pAG3 Expression by restriction digest. Lane 1 contains DNA ladder, annotated to the left of this figure. Lane 2 contains a restriction digest of pAG3 with both *BamHI* and *NdeI.* Lane 3 contains a restriction digest of pAG3 with *BamHI* and lane 4 shows the undigested plasmid. A total volume of 10 µl was run in each lane (including the ladder), the composition of which is stated in section 2.2.3.

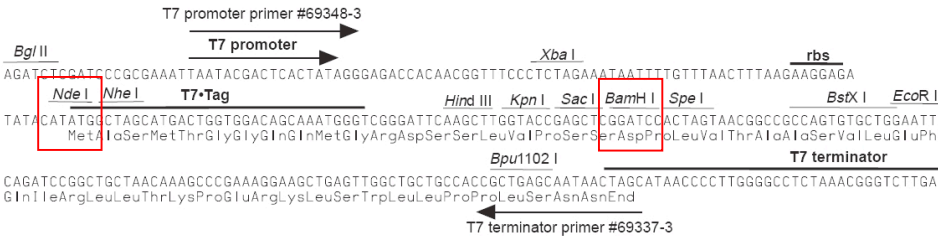

Figure 4.3: pET17b expression/cloning regions. The red boxes indicate the positions of *NdeI* (left) and *BamHI* (right) restriction sites.

4.2.2 Quikchange of pAG3 to Insert a Stop Codon

Quikchange mutagenesis was conducted (as described in section 2.2.1) to insert a stop codon before the coding sequence for NT. pAG3 was produced as described in section 2.2.5-2.2.7). The product of this procedure is referred to as pJB1. An optimised protocol has been produced and is listed in section 2.2.1. pJB1 underwent a *DpnI* restriction digest to remove the methylated template DNA before bacterial transformation of the Quikchange product (see section 2.2.2).

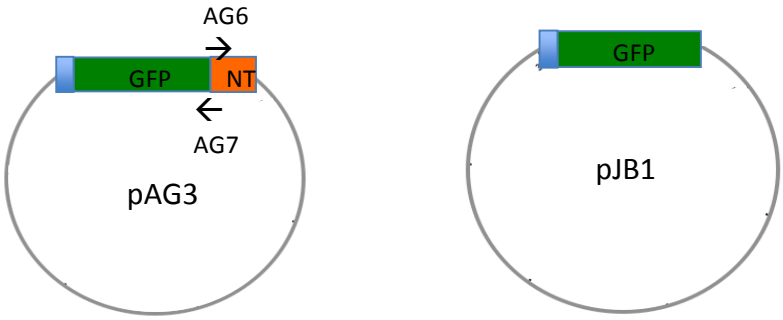

Figure 4.4: Schematic representation of the pAG3 and pJB1 plasmids. AG6 and AG7 represent the sense and antisense primers used for quikchange mutagenesis respectively (see table 3).

Primer	Sequence
AG6 (sense)	AGGACGAGCTGTACAAGTAAgaactgtatgaaaacaaacc
AG7 (antisense)	ggtttgttttcatacagttcTTACTTGTACAGCTCGTCC

Table 4.1: Sequences of the sense and antisense primers used for quikchange mutagenesis of pAG3. The antisense codon is coloured black with areas corresponding to the genes coding for GFP and NT in green and yellow respectively.

The His-tagged GFP-NT coding portion of the plasmid was fully sequenced, confirming the correct introduction of a stop codon (TAA) before the NT coding region (see figure 4.5).

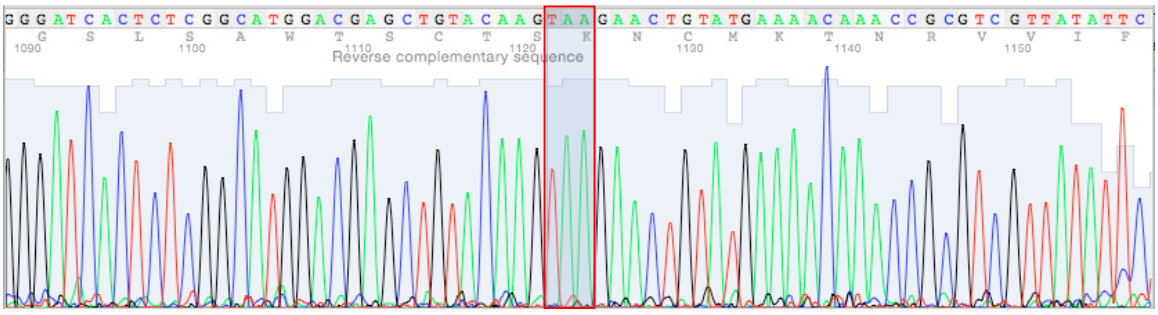

Figure 4.5: Chromatogram of sequenced pJB1 displaying the inserted stop codon from mutagenesis (indicated by the red box). GFP and NT encoding regions are located to the left and right of the stop codon respectively. 4Peaks software was used to visualise the sequence. Samples of pJB1 were sequenced by Source Biosciences (Nottingham) using the Sanger sequencing method.

4.2.3: Optimisation of Protein Expression

Figures 4.6 and 4.7 detail quantified protein expression over time after induction with 1 mM IPTG (see sections 2.2.8-2.2.10). GFP-NT expressed from the pAG3 plasmid and GFP was expressed from the pJB1 plasmid. Samples were quantified as cell lysates (filtered but not purified) as detailed in section 2.2.10. Expression at 37°C yields higher concentrations of both proteins quicker compared to 20°C. Greatest concentration of protein produced at both temperatures (~40-50 uM), regardless of the time taken to do so, was similar for both temperatures. Maximum protein expression took longer at 20°C but yielded the highest concentration of protein at 16hrs. Whereas, protein expression declined at 16hrs in the 37°C condition.

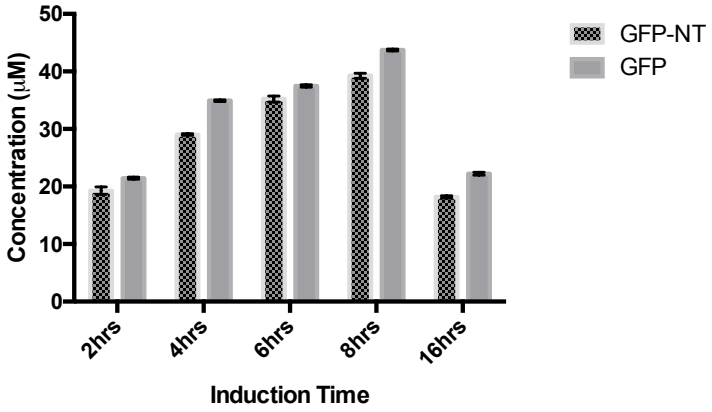

Figure 4.6: Quantified protein expression in BL21 (DE3) (as described in 2.2.12) over time at 37°C, quantified by UV-Vis spectrophotometry measured at an excitation 490 nm.

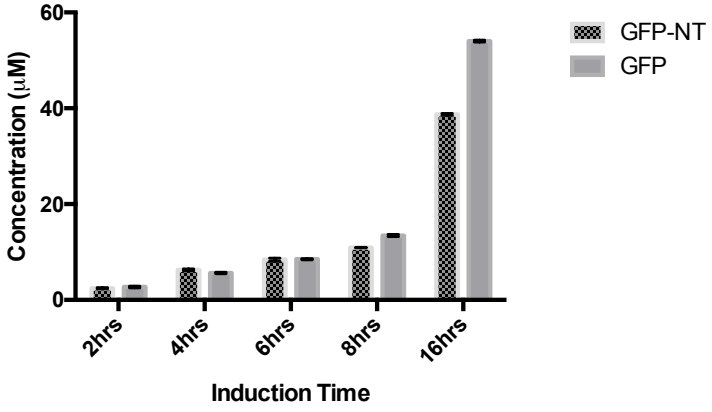

Figure 4.7: Quantified protein expression in BL21 (DE3) (as described in 2.2.12) over time at 20°C, quantified by UV-Vis spectrophotometry at an excitation wavelength of 490 nm.

Figures 4.8 and 4.9 show images of SDS-PAGE ran to visualise relative expression amounts of target protein produced at each optimisation condition. The gels vary in stain intensities slightly from one another - this is due to the amount of time spent in Coomassie Blue stain. Gels representative of the 37 °c expression series spent longer in the stain, therefore display a deeper blue colouration. As these gels are only used for comparison against the samples in the same gel and expression temperature, this is not an issue.

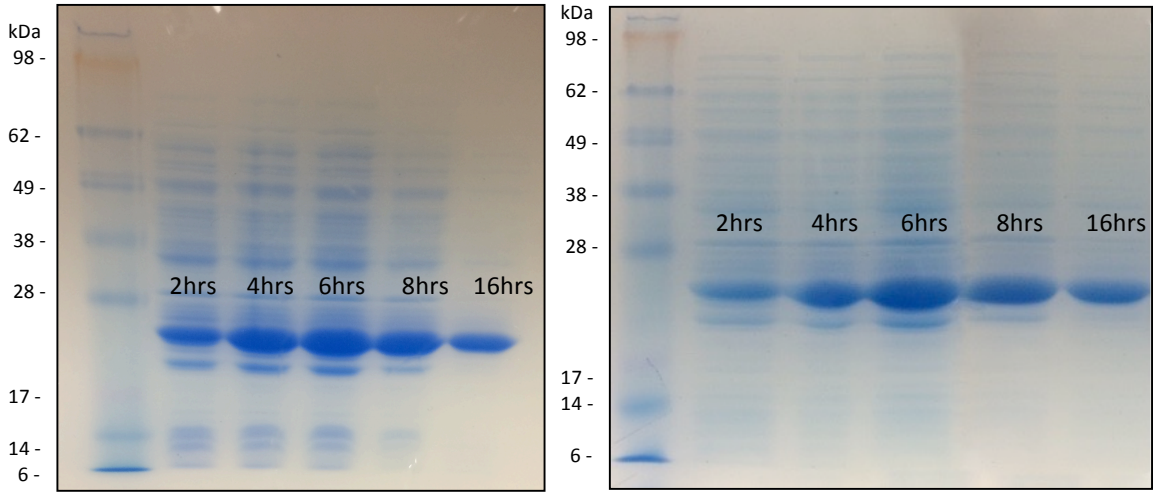

Figure 4.8: SDS-PAGE gels of GFP-NT (left) and GFP (right) samples taken at stated time intervals of expression. 10 µl of sample (that had been lysed, centrifuged, resuspended in protein buffer and filtered) was combined with 10 µl of loading buffer (see section 2.2.13), 15µl of this was run in each well of the gel. The ladder used for this gel was the SeeBlue® Plus2 protein standard (Life Technologies). The gels above are representative of the expression documented in figure 4.6.

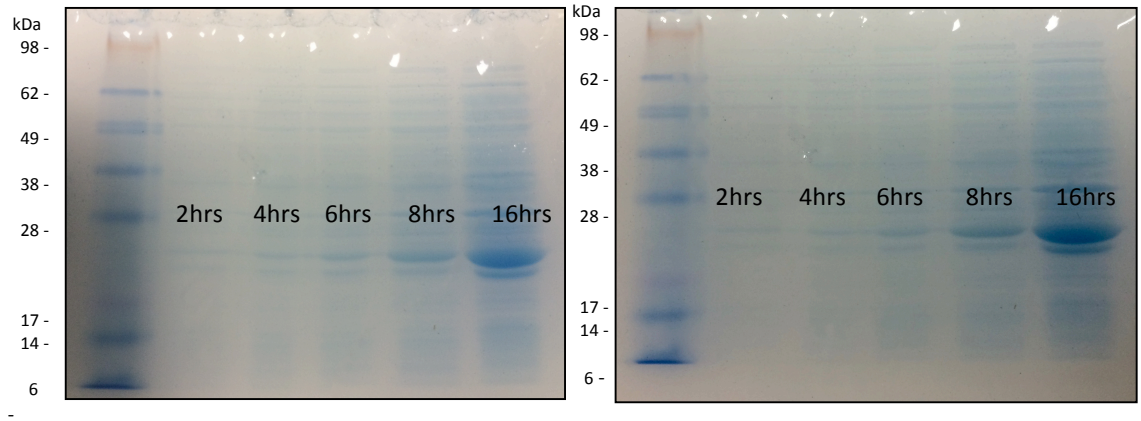

Figure 4.9: SDS-PAGE gels of GFP-NT (left) and GFP (right) samples taken at stated time intervals of expression. 10 µl of sample (that had been lysed, centrifuged, resuspended in protein buffer and filtered) was combined with 10 µl of loading buffer (see section 2.2.13), 15 µl of this was run in each well of the gel. The ladder used for this gel was the SeeBlue® Plus2 protein standard (Life Technologies). The gels above are representative of the expression documented in figure 4.7.

4.2.4: Quantitative Analysis of GFP-NT/GFP Purification

Protein samples were prepared from bacterial cultures after IPTG induction of transformed (with either pAG3 or pJB1) BL21 *E.coli.* Metal affinity chromatography was used to purify the samples using 1 ml nickel affinity HisTrap HP columns as described in section 2.2.11. With 200 mM imidazole, the second collected elution (in a series of 10 1 ml samples) was visibly determined to contain the highest concentration of eluted protein (see figure 4.10) and was selected to be aliquoted and stored. An aliquot was reserved for quantification of the sample. Care was taken to avoid air bubbles entering the purification columns including filtering and degassing of the protein buffers and other wash solutions with the use of a Merck Millipore™ chemical duty pump and filtration system.

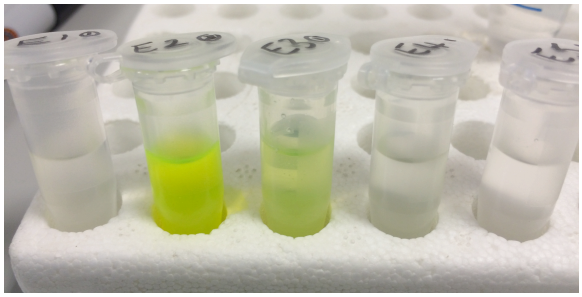

Figure 4.10: First five 1 ml samples eluted from the HisTrap column with 200 mM imidazole

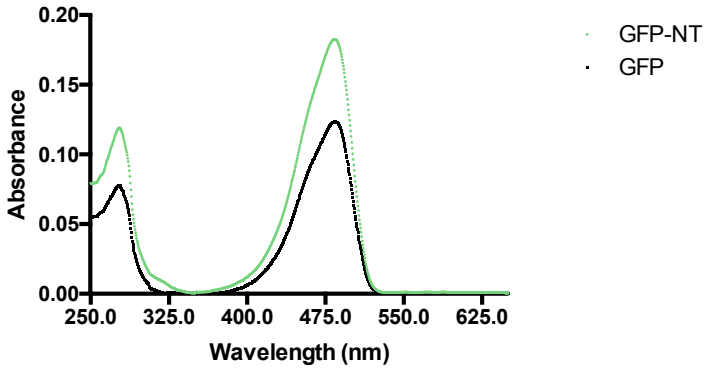

Figure 4.11: UV-Vis spectrophotometry of GFP-NT and GFP at a dilution of 1 in 20. Peak at 490 nm represents eGFP present in both samples.

Figure 4.11 shows the data obtained from quantification of GFP-NT (green curve) and GFP (black curve) as described in 2.2.12. This graph is representative of multiple quantifications of protein expression from pAG3 (GFP-NT) and pJB1 (GFP). The Beer-Lambert Law was used to quantify protein present in each sample (see equation 4.1).

The absorption coefficient for eGFP (specific GFP variant used in this study) is 24,995 $M^{-1}cm^{-1}$ at 280 nm, 57,500$M^{-1}cm^{-1}$ at 490 nm and the path length of light is 1cm. Extinction coefficients were calculated using ProtParam (this resource can be accessed here: http://web.expasy.org/protparam/) and the known amino acid sequence of eGFP.

$$A = \varepsilon c l$$

Equation 4.1: Beer-Lambert Law equation. A = absorbance at a specific wavelength. ε = absorption coefficient of eGFP at 490 nm. *c* = concentration of protein. *l* = path length of light.

Calculation of protein concentration of each sample was performed using the equation in figure 4.6. Known values were: absorption coefficient of eGFP at 490 nm, path length of light and the absorbance of the sample at 490 nm. The equation was rearranged to determine the unknown value (concentration) and corrected for any dilutions. Using the absorption coefficient of eGFP at 280 nm, the purity of the samples in figure 4.11 was calculated by comparing the amount of eGFP to the total amount of protein in the sample (using equation 4.1 and absorbance values at 280 and 490 nm) to be 64.5% and 67.8% respectively. These values are likely to be lower than the actual purity of the samples as small concentrations of imidazole and are present in the protein samples. As imidazole absorbs light at 280 nm, it will be forming the false blank plateau observable at ~260 nm seen in figure 4.11. The protein samples run on the SDS-PAGE gels in figures 4.12 and 4.13 indicate that the samples are at a much higher purity.

4.2.5: Qualitative Analysis of GFP-NT/GFP Purification

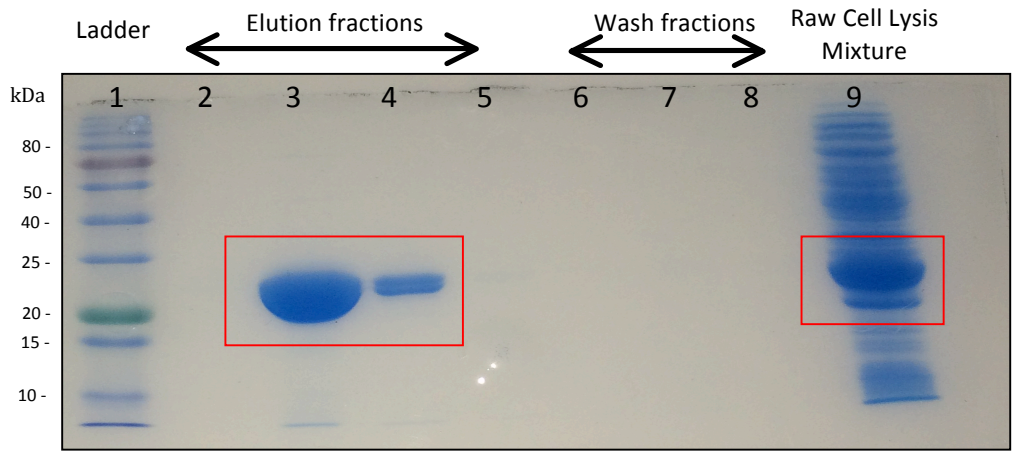

Figure 4.12: SDS-PAGE to display purity of purified His-GFP-NT. Each well contains 10 µl of each respective sample. This Image is representative of multiple purifications of His-GFP-NT. The, broad range 11-245 kDa colour pre-stained protein standard was used for reference in this gel (New England Biolabs).

Figures 4.12 and 4.13 show the qualitative success of protein purification from BL21 *E.coli* as described in 2.2.11. Wells 2-5 contain samples from the first four protein elution aliquots with 200mM imidazole. The lack of bands other than that corresponding to the size of GFP-NT confirms the purity of the elution product. Elution fraction in well 3 represents the aliquot with the greatest amount of protein eluted. This aliquot was later quantified and used in future experiments. Wells 6-8 represent wash fractions prior to addition of the protein sample, confirming that no protein was present in the column before use. Well 9 represents the 100ul sample taken from the bacterial lysis product described in section 2.2.10. The bands corresponding to the size of GFP-NT are labelled with red boxes.

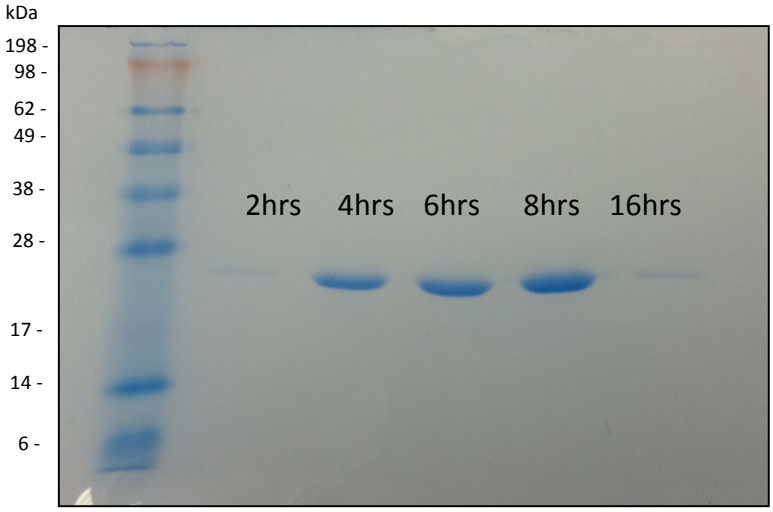

Figure 4.13: Displays purified samples of His-GFP following expression over time at 37°C. 10 µl of each sample (that had been purified) was combined with 10µl of loading buffer (see section 2.2.13), 15 µl of this was run in each well of the gel. The ladder used for this gel was the SeeBlue® Plus2 protein standard (Life Technologies). The presence of only one band corresponding to the size of GFP indicates purity of the samples qualitatively.

4.3: Discussion

Although the pET system is a popular vector of choice for recombinant protein expression, it is associated with several drawbacks. For example, the levels of T7 RNA polymerase generated within the bacterial cell may be higher than required, leading to excessive expression of the recombinant gene of interest. As previously mentioned, this could lead to a decrease in cellular growth, or potentially reach protein concentrations that are toxic to the cell. For this reason, and for the interest of obtaining protein samples as efficiently as possible, optimisation of the expression procedure was carried out (as documented in 4.2.3). Leaky control in gene expression, perhaps due to bacterial RNA polymerase, has also been observed in this vector – allowing for low levels of gene expression in the absence of IPTG (Overton, 2014). This was observed during protein expression of both small bacterial expansion cultures and large batch protein production cultures, which can be a problem if the recombinant protein in question is toxic to the cells. Some research speculates that eGFP is toxic to living cells, which could explain the decrease in protein quantified after sample collection at 16hrs from the 37°C expression condition. However, the only documented GFP-induced cell death in living cells

comes from constant intense excitation of the fluorophore over long periods of time, which is speculated to produce free radicals (Liu *et al*., 1999). As protein expression was performed in a relatively dark environment, this is unlikely to be the case. The decrease in protein expression observed at the 37°C seen at 16hrs is likely to be the result of cell lysis during culture due to a build up of toxic by-products of growth or excessive intracellular demand due to previously high throughputs of protein production (Shiloach and Fass, 2005). The doubling time of *E.coli* in LB broth has been extensively documented at 20 minutes during the steady-state/exponential growth phase, which lasts until an optical density of around 0.3 (but is slightly variable between strains of *E.coli*). After this time, a decrease in growth rate and cell size is observed (Sezonov *et al*., 2007). Recombinant protein production can be induced at either a high or low biomass phase of growth, to either induce production when cells are naturally slowing in growth or be produced concurrently with growth. Both methods have found success, but inducing at a high biomass when the expressed protein is toxic to cells will limit any growth inhibition caused (Overton, 2014). IPTG addition was synchronised with the end of the exponential growth phase in this study (see section 2.2.9). To minimise any loss in protein before purification, sample processing (section 2.2.10) was conducted immediately after collection from the original culture volume. If whole culture samples were frozen immediately after collection, a visually noticeable amount of cells had lysed during the freeze-thaw process, releasing protein into the supernatant, which would ultimately be discarded (see figure 4.14).

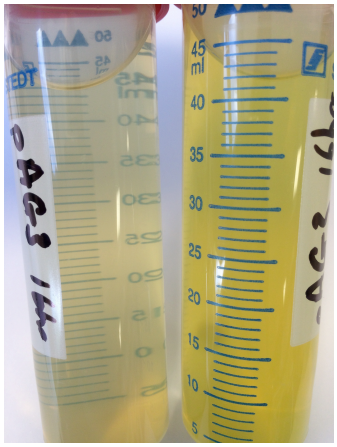

Figure 4.14: Comparison of supernatant colour after centrifugation of bacterial culture sample immediately after collection (left) or after a freeze-thaw cycle (right). Both samples were expressed at 20°C.

The concept of immobilised metal affinity chromatography (IMAC) was first developed by Porath (1975) and is based on the affinity of transition metal ions (Zn^{2+}, Cu^{2+} and Ni^{2+}) towards histidine, cysteine and tryptophan. A HisTrap HP column (GE Healthcare) was employed for this study, based on the affinity of Ni^{2+} to the histidine residues recombinantly expressed with GFP-NT and GFP. Imidazole acts by competing for binding sites in the column and displacing His-GFP-NT. Compared to other methods of protein purification, (such as size exclusion chromatography, high performance liquid chromatography and ultracentrifugation) IMAC compares well with biospecific affinity chromatography with respect to separation efficiency but without the limitation of degradation of antibodies or enzymes present in the column. Metal ions are much more likely to withstand the wear and tear of repeated use (Porath, 1992). Coupled with the ease of bioengineering Histidine tags into recombinant DNA, this makes IMAC an ideal candidate for protein purification of His-GFP-NT.

To ensure 100% purity of the protein sample, gel filtration chromatography could be utilised after initial purification by metal affinity chromatography. This is a form of partition chromatography used to separate molecules of different molecular sizes (O'Fágáin *et al*., 2011).

With regards to protein structural integrity post-expression – compared to the vast array of proteins that have been produced by recombinant expression, eGFP is relatively stable (as described in 4.1.4). However, to ensure protein structural integrity - protein samples (1 ml) once purified were separated into 50 ul aliquots and only thawed once on ice (when required for experiments) per aliquot, then discarded.

4.4: Conclusion

Generally, the pET system for recombinant expression worked very well for expression of the model drug His-tagged GFP-NT and for His-tagged GFP (created for the purposes of acting as a negative control in future experiments). No issues were encountered during the protein expression, purification and quantification procures that have not already been discussed. Expression for 8hrs and 37°c was found to be optimal and therefore employed for expression of all His-tagged GFP-NT and His-tagged GFP samples used in this study. Purification was assessed qualitatively and shown to be acceptable for further use. Considerations for the future use of the recombinant proteins in this study were made and enforced strictly to ensure no unnecessary degradation to the protein was incurred as discussed in section 4.3.

Chapter 5

Internalisation of Neurotensin-Conjugated Fluorophores

5.1: Introduction

5.1.1: Variability in Receptor Mediated Endocytosis

Endocytosis, a mechanism common to all cells in the human body, internalises molecules for retention within an endosomal scaffold and delivery to specific sub-cellular organelles. Internalisation mechanisms and the constructs associated with them (such as clathrin and caveolin) are specific to certain molecules and cell types; hence, researchers have been presented the opportunity to bioengineer molecular complexes for targeted delivery. One such target is membrane specific peptide receptors such as NTS1. The majority of targeted delivery systems aim to avoid lysosomal trafficking of the attached therapeutic molecule and subsequent enzymatic degradation (Bareford and Swaan, 2007).

Most of what is currently understood about internalisation of trafficked ligand-receptor complexes originates from studies focused on receptors with single transmembrane domains, such as the internalisation of transferrin via clathrin-coated pits. Following internalisation of many different ligand-receptors complexes, dissociation of ligand from receptor appears to be common in early endosomes due to their slightly acidic nature – from this point, variability in whether the ligand or receptor is degraded or recycled back to the cell surface is evident (Pearse, 1982).

In most cell types, receptor-mediated peptide internalisation results in fusion with lysosomes and degradation (Backer *et al*., 1990). However, internalisation of NT is thought to follow a different route. Vandenbulcke *et al*., (2000) investigated the method of internalisation of fluorescently labelled NT (Fluo-NT) in COS-7 cells transfected with NTS1; the team demonstrated, by methods of inhibition (hypertonic sucrose, potassium depletion and cytosol acidification) that NT internalisation is mediated by clathrin coated pits (see Figure 1.1). Within 30 minutes, NT-NTS1 complexes accumulated within early endosomes, characterised by

positively staining with Acridine Orange and for rab 5A. Between 30 and 45 minutes, NT was shown to have delocalised from its receptor and was later identified to be present in the non-acidic juxtanuclear compartment of the trans-golgi network (TGN). This suggested recruitment of the peptide from late endosomes. The receptor itself was determined to be trafficked to Lamp-1 positive lysosomes, suggesting degradation (see figure 5.1).

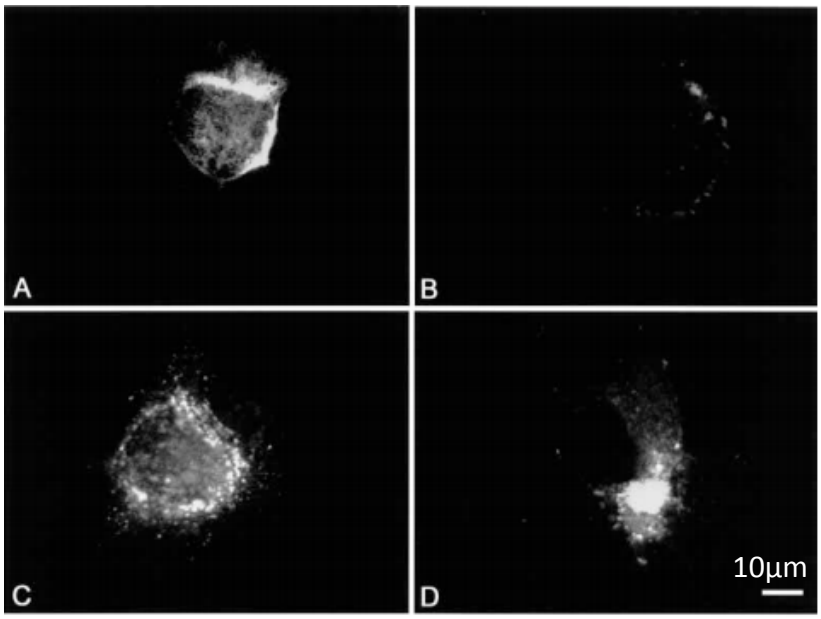

Figure 5.1 taken from (Vandenbulcke *et al*., 2000) shows the localisation of fluorescently labelled NT during internalisation over time in transfected COS-7 cells. (A) The majority of NT localised at the cell membrane after 5 minutes (B) After hypertonic acid stripping of NT after 5 minutes of incubation with NT (C) Localisation after 20 minutes of incubation with Fluo-NT in endosome-like particles within the cytoplasm. (D) Localisation after 45 minutes clustered near the nucleus.

The trafficking of GPCRs through endosomes is critical in determining cellular response to external agonists. Ligand-stimulated receptor endocytosis generally depletes GPCRs from the membrane in an attempt to prevent overstimulation of the cell from the ligand (as previously mentioned in section 1.7) – this can be reversed by receptor recycling and receptor dephosphorylation following internalisation (Ferguson, 2001; Garland *et al*., 1996). NTS1 has been shown to exhibit high affinity interactions with β-arrestins during receptor endocytosis (Oakley *et al*., 2000), which has been shown to be important for NTS1 internalisation in many cell types. However, the subject of whether NTS1 is recycled back to the cell surface or degraded is a controversial subject (Law *et al*., 2012). This characteristic appears to

be dependant on the cell type as NTS1 is recycled in human neuroblastoma cells CHP212 (Toy-Miou-Leong *et al*., 2004) but degraded in COS-7 cells (Vandenbulcke *et al*., 2000). Little is known about NT internalisation in Caco-2 and HEK293, although, Neuropeptide Y (also a neuropeptide) is thought to be internalised into HEK293 in a similar manner to NT is COS-7 (Pheng *et al*., 2003). Other GPCRs such as the β2-adernergic receptor, neurokinin 1 receptor and gastrin-releasing peptide receptor are all recycled following ligand-induced internalisation (Grady *et al*., 1996; Tarasova *et al*., 1997; Zastrow and Kobilka, 1992).

Studies into the internalisation of NT in cells of neuronal lineage, endogenously expressing NTS1, show that the ligand is internalised with the receptor and subsequently trafficked from the perikarya and dendrites to the perinuclear region within vesicular organelle-like structures. Interestingly, NT was only observed to be internalised with incubations at 37°c, as opposed to being almost completely membrane-bound with incubations at 4°c. Suggesting that the receptor-mediated internalisation of NT is temperature dependant (Nouel *et al*., 1997).

5.1.2: Clathrin-Mediated Endocytosis

Of all methods of endocytosis, clathrin-mediated is by far the most extensively studied. Other mechanisms of endocytosis include caveolin-mediated, macropinocytosis and phagocytosis. Many clathrin-dependant endocytosis events mediate the transport of large molecules needed for essential cell maintenance such as lipoproteins, iron-saturated transferrin and an array of growth factors (Conner and Schmid, 2003). The process of internalisation is a multi-step mechanism, starting with the formation of clathrin-coated vesicles, which requires the cooperative efforts of more than 50 different proteins. The formation of vesicles begins with the recruitment of clathrin, adaptor proteins and endocytic accessory proteins to the plasma membrane, where it forms lattices of clathrin around the internalised portions of membrane ranging in diameter from 10 to ~500 nm. Clathrin forms a cag-like spherical structure once vesicle formation is complete. Adaptor proteins mediate clathrin binding to transmembrane receptors shortly after ligand binding (and required conformational changes to the transmembrane receptor induced by

ligand binding). The cage-like clathrin structure is later disassembled by accessory proteins once internalisation of extracellular cargo has been achieved, releasing the contained vesicle into the cell for continued intracellular trafficking (Heuser, 1980).

Clathrin-mediated membrane vesicle formation is not limited to the cell membrane – it can also occur in the TGN, contributing to the transport of cargo from the TGN to endosomes, as well as transporting cargo from the cell membrane to the TGN (Robinson, 2004).

5.1.3: How Do Modifications To The Peptide Affect Internalisation?

As GPCRs are a popular target for therapeutic purposes, it is beneficial to modify their respective peptides or ligands to better avoid degradation prior to delivery to its receptor. This applies to the production if peptide analogues that have previously been described to be modified to withstand degradation by *in vivo* pH and temperature changes. Chemical modifications such as PEGylation and lipidation are employed to prolong the half-lives of peptides and have been shown to confer additional benefits. For example, modification of pancreatic polypeptides has shown to enhance the preference of the polypeptides to certain receptors over others. In this case, lipidation of the polypeptide encourages arrestin recruitment and internalisation, whereas PEGylation encourages the complete opposite (Mäde *et al*., 2014). This observation suggests that selective modifications to peptides may make them preferentially select certain receptor sub-types if it is a ligand to more than one receptor.

Jia *et al*., (2015) investigated the rates of internalisation of NT conjugated to a large molecule (DOTA), used for radiotherapy. The study found that the use of a spacer (β-Alanine) between NT and the large molecule increase internalisation rates of NT analogues mediated by NTS1 compared to conjugation of the molecule without a spacer. This reflects the work of Antunes *et al*., (2007) that documents the effect of spacers between somatostatin analogues and radiolabelled DOTA. The study found that the introduction of a β-Alanine spacer did not affect hydrophilicity (although other spacers did increase this), whilst maintaining the peptide analogue's structural

modifications and slightly decreasing the affinity of the analogue to its receptors. The main benefit of introducing of spacers was the noticeable increase in internalisation rate; somatostatin-DOTA uptake went from 0.48% IA/g in four hours to 4.17% IA/g in pancreatic tumour cells.

5.1.4: Small Molecule Fluorophores

Fluorescent compounds based on synthetic small molecules are useful tools for the visualisation of events inside living cells. Since the discovery of quinine sulphate in 1845, and the realisation that the molecule emitted blue fluorescence when exposed to UV light, fluorescent molecules have been continually modified and improved for use as labelling agents and biosensors (Terai and Nagano, 2013). Fluorescein has become *the* ubiquitous small-molecule fluorophore for countless scientific and industrial applications, including being the first label for immunofluorescence microscopy (Coons and Kaplan, 1950). The florescent properties of fluorescein are formed from an equilibrium of the 'open', fluorescent form of the structure and the 'closed' non-fluorescent structure – an equilibrium that can be modulated with the use of blocking groups to preserve its open structure (Tian *et al*., 2012). Fluorescein (F) is one of the most commonly used fluorescent probes, with a large fluorescence quantum yield and high photostability, it has proven to be an effective tool. Derivatives of fluorescein exist that are lipophilic in nature, but fluorescein itself is hydrophilic and can exist in many forms in aqueous solution: occurring in cationic, neutral, anionic and dianionic forms, making its fluorescent properties pH dependent (Sjöback *et al*., 1995).

5.2: Results

5.2.1: Converting Fluorescence Readings Into Concentrations

Calibration curves were made with serial dilutions of solutions of known concentrations for both F-NT and GFP-NT, originally quantified by UV-Vis spectrophotometry as described in section 4.2.4. The fluorescence of each dilution was read with the Tecan Infinite Microplate reader at an excitation wavelength appropriate for the fluorophore in question (see figure 5.2). Calibration curves were produced in triplicate and the graph plotted (figure 5.2) shows the average of those. The number of cells estimated to be present in each test well after 48 hours of growth in a 12 well plate (see Figure 3.10) was lysed in lysis buffer, removed of any cellular debris by centrifugation, and used as the diluent for each fluorophore dilution to ensure that cellular auto-fluorescence did not affect the data collected from each experiment.

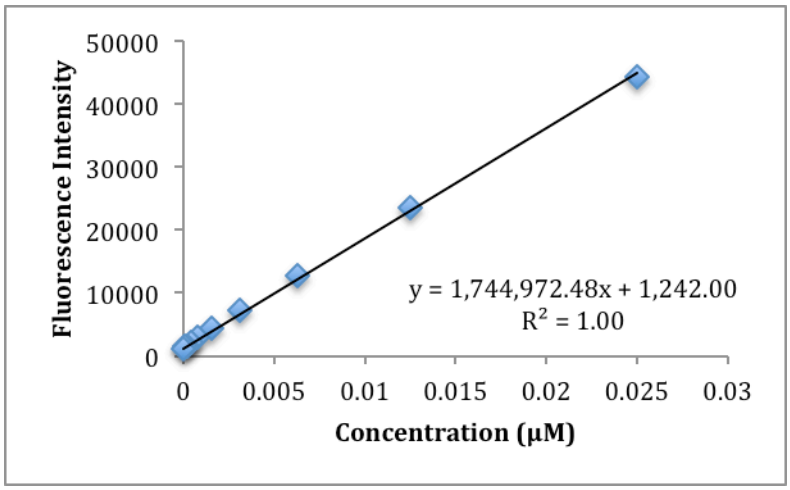

Figure 5.2: Calibration curve for the quantification of GFP-NT protein samples collected from undifferentiated Caco-2 cells.

The calibration curve shown is made from a serial dilution of GFP-NT. This curve has been constructed to exclude autofluorescence from experimental samples by including the intracellular contents of an appropriate number of undifferentiated Caco-2 cells. Calibration curves had also been made from serial dilutions of F-NT. Calibrations for each respective cell line were made using intracellular contents of HEK293 cells, undifferentiated Caco-2 cells and differentiated Caco-2 cells for both GFP-NT and F-NT. The appropriate calibration curve was used for converting fluorescence intensity into fluorophore concentration for each cell line and

fluorophore used in each assay to ensure the most accurate acquisition of quantitative uptake or transport of GFP-NT/F-NT into or through cells.

5.2.2: Fluorophore Internalisation into Undifferentiated Caco-2

See section 2.2.31 for the full description of methods employed in this section. Undifferentiated Caco-2 cells, grown for 48 hours (detailed in 2.2.21) were incubated with solutions of NT-conjugated fluorophores (GFP-NT or F-NT) containing either NT-fluorophore alone, NT-fluorophore with a 100x excess of free NT, NT-fluorophore with a 10x excess of SR142948 or fluorophore alone. This was done to compare internalisation of NT-fluorophore in receptor uninhibited and receptor inhibited conditions. Free NT competitively inhibits all NT receptors, and SR142948 selectively inhibits NTS1 and NTS2. All solutions were made in HBSS.

Figure 5.3 shows GFP-NT and F-NT internalisation into undifferentiated Caco-2 cells, which have been previously characterised to minimally express NTS1. The extent of internalisation seen for each condition is comparable to uptake of fluorophore alone, and therefore due to non-specific transport. Figure 5.4 provides a visual comparison of GFP-NT (A) and F-NT (B) internalisation into undifferentiated Caco-2 cells. The images show minimal amounts of both GFP-NT and F-NT within the cells.

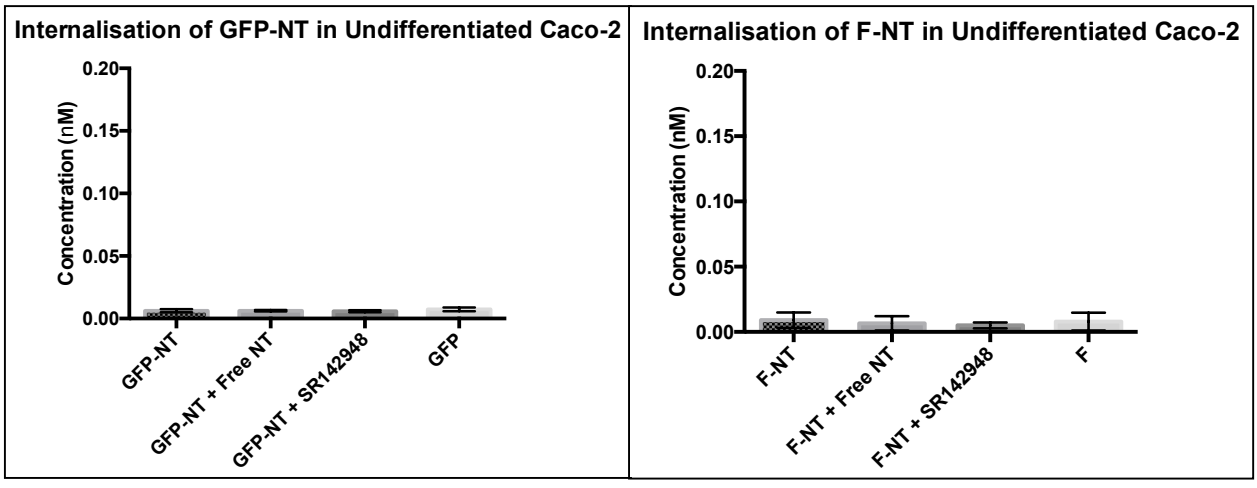

Figure 5.3: Quantification of internalised GFP-NT (left) or F-NT (right) in undifferentiated Caco-2 cells. The samples applied to each well (as annotated in this figure) are as follows: (GFP-NT/F-NT) = 20 nM GFP-NT in HBSS, (GFP-NT + Free NT/F-NT + Free NT) = 20 nM GFP-NT/F-NT + 2μM free NT, (GFP-NT + 2R142948) = 20 nM GFP-NT/F-NT + 200 nM SR142948, (GFP/F) = 20 nM GFP/F. Error bars are representative of ±SD and each data point is the mean of n=3.

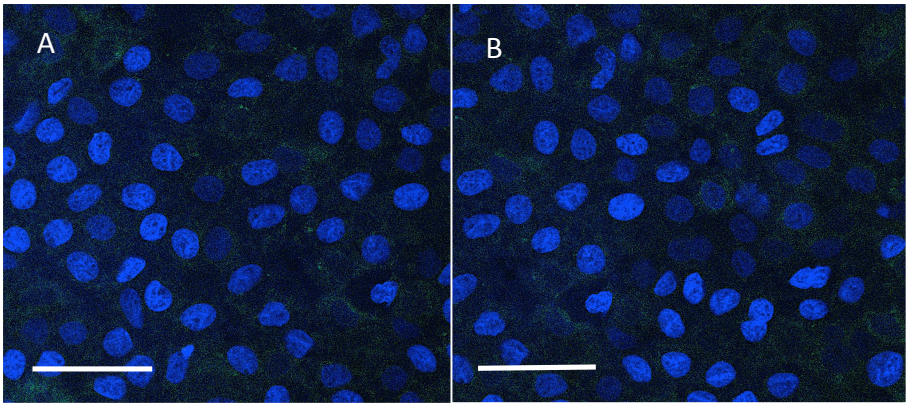

Figure 5.4: (A) GFP-NT internalisation in undifferentiated Caco-2 after incubation for 1hr with 20 nM GFP-NT. (B) F-NT internalisation in undifferentiated Caco-2 after incubation for 1hr with 20 nM F-NT. The white bar is representative of 50 µm.

5.2.3: GFP-NT Internalisation into HEK293

See section 2.2.31 for the full description of methods employed in this section.

HEK293 cells, grown for 48 hours (detailed in 2.2.21) were incubated with solutions of GFP-NT containing either GFP-NT alone, GFP-NT with a 100x excess of free NT, GFP-NT with a 10x excess of SR142948 or GFP alone. This was done to compare internalisation of GFP-NT in receptor uninhibited and receptor inhibited conditions. This was assessed in both non-transfected and transfected HEK293 cells. Free NT competitively inhibits all NT receptors, and SR142948 selectively inhibits NTS1 and NTS2. All solutions were made in HBSS.

Figure 5.5 shows GFP-NT internalisation to be receptor mediated as uptake is greatly reduced in conditions containing competitive inhibitors of NT-receptors (free NT and SR142948). The maximum uptake of GFP-NT alone is also greater in transfected HEK293 cells compared to non-transfected cells, suggesting uptake correlates with relative NTS1 expression (as transfected HEK293 express higher levels of NTS1). Table 5.1 states the p values of each data point in figure 5.5 when compared to the others in the same figure by (Student's T-test) to determine any significant differences in internalisation of each fluorophore. This table is separated into transfected and non-transfected cells.

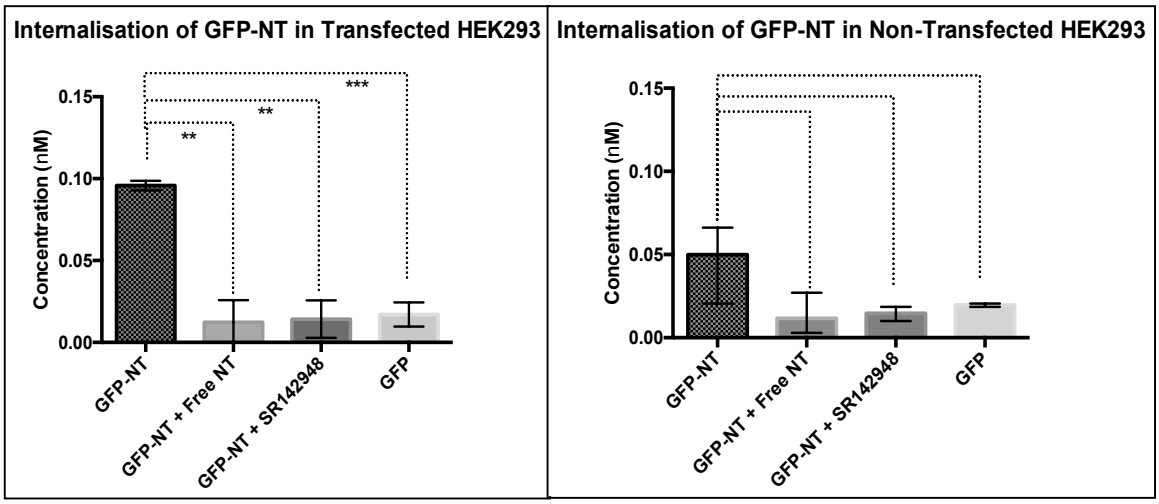

Figure 5.5: Quantification of internalised GFP-NT in non-transfected (left) and transfected (right) HEK293 cells. The samples applied to each well (as annotated in this figure) are as follows: (GFP-NT) = 20 nM GFP-NT, (GFP-NT + Free NT) = 20 nM GFP-NT + 2 µM free NT, (GFP-NT + SR142948) = 20 nM GFP-NT + 200 nM SR142948, (GFP) = 20 nM GFP. Error bars are representative of ±SD and each data point is the mean of n=3. Data sets were analysed using an unpaired t-test and P-values are stated in table 5.1.

Non-transfected	**P value**
GFP-NT vs GFP-NT + Free NT	0.1039 (ns)
GFP-NT vs GFP-NT + SR142948	0.0.1353 (ns)
GFP-NT vs GFP	0.1760 (ns)
Transfected	**P value**
GFP-NT vs GFP-NT + Free NT	0.0066 (**)
GFP-NT vs GFP-NT + SR142948	0.0044 (**)
GFP-NT vs GFP	0.0009 (***)

Table 5.1: Statistical significance of internalisation in each condition shown in Figure 5.5 as determined by an unpaired Students t-test with Welsh's correction. All P values are two-tailed.

Figure 5.6 provides a visual comparison of GFP-NT (A) and GFP-NT with a 100x excess of NT (B) internalisation into transfected HEK293 cells. Relatively large amounts of GFP-NT are observable in areas localised around the nucleus in (A), compared to minimal amounts seen in (B), confirming inhibition of uptake with the introduction of an excess of NT and transport being mediated via neurotensin receptors. The separated channels of (A), seen as DAPI (C) and GFP-NT (D) show main bodies of fluorescence originating from regions surrounding the nucleus of the cell.

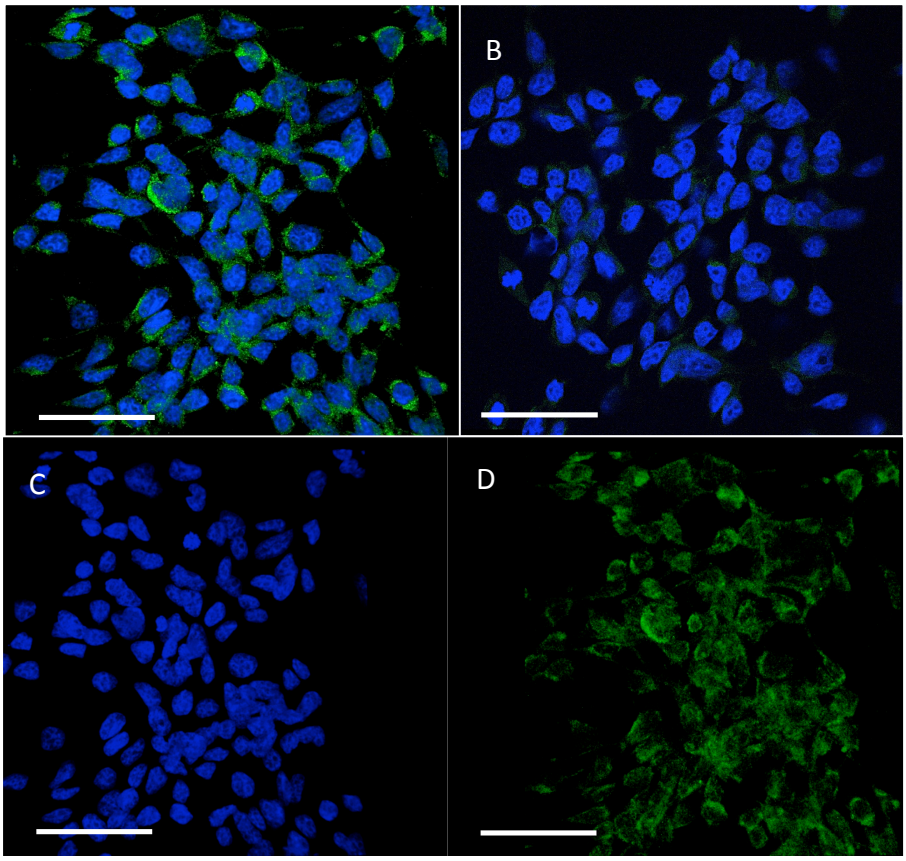

Figure 5.6: Confocal microscope images of transfected HEK293 after (A) incubation with 20 nM GFP-NT for 1hr and (B) incubation with 20 nM GFP-NT and 2 µM NT for 1 hr. (C) and (D) shows a breakdown of image (A) to show the locality of the fluorophore within the cell. The white bar is representative of 50 µm.

5.2.4: F-NT Internalisation into HEK293

See section 2.2.31 for the full description of methods employed in this section.

HEK293 cells, grown for 48 hours (detailed in 2.2.21) were incubated with solutions of F-NT containing either F-NT alone, F-NT with a 100x excess of free NT, F-NT with a 10x excess of SR142948 or F alone. This was done to compare internalisation of F-NT in receptor uninhibited and receptor inhibited conditions. This was assessed in both non-transfected and transfected HEK293 cells (refer to section 2.2.23 for the

transfection process). Free NT competitively inhibits all NT receptors, and SR142948 selectively inhibits NTS1 and NTS2. All solutions were made in HBSS.

Figure 5.7 shows F-NT internalisation to also be receptor mediated as uptake is greatly reduced in conditions containing competitive inhibitors of NT-receptors (free NT and SR142948). Similarly to GFP-NT uptake, maximum uptake of F-NT alone is also greater in transfected HEK293 cells compared to non-transfected cells, suggesting that uptake correlates with relative NTS1 expression (as transfected HEK293 express higher levels of NTS1). Maximum uptake is also greater with F-NT compared to GFP-NT in the same condition and cell transfection status (non-transfected or transfected). Table 5.2 states the p values of each data point in figure 5.7 when compared to the others in the same figure by (Student's T-test) to determine any significant differences in internalisation of each fluorophore. This table is separated into transfected and non-transfected cells.

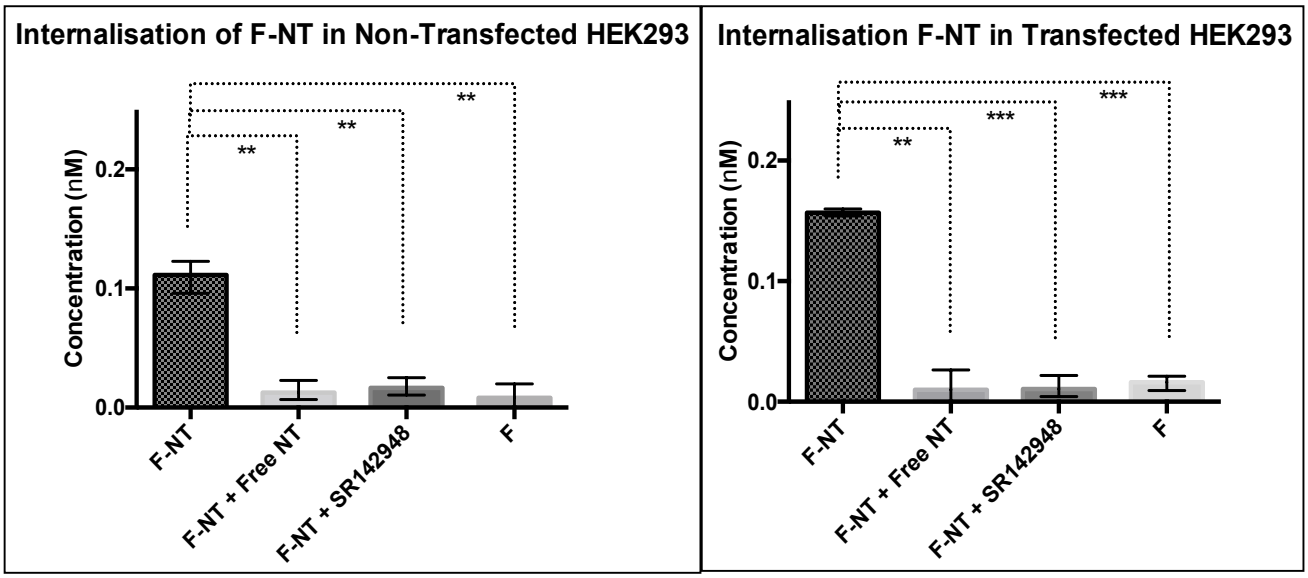

Figure 5.7: Quantification of internalised F-NT in non-transfected (left) transfected HEK293 cells (right). The samples applied to each well (as annotated in this figure) are as follows: (F-NT) = 20nMF-NT, (F-NT + Free NT) = 20 nM F-NT + 2 µM free NT, (F-NT + SR142948) = 20 nM F-NT + 200 nM SR142948, (F) = 20 nM F. Error bars are representative of ±SD and each data point is the mean of n=3. Data sets were analysed using an unpaired t-test and P-values are stated in table 5.2.

Non-transfected	**P value**
F-NT vs F-NT + Free NT	0.0011 (**)
F-NT vs F-NT + SR142948	0.0017 (**)
F-NT vs F	0.0012 (**)
Transfected	**P value**
F-NT vs F-NT + Free NT	0.0031 (**)
F-NT vs F-NT + SR142948	0.0007 (***)
GFP-NT vs F	0.0001 (***)

Table 5.2: Statistical significance of internalisation in each condition shown in figure 5.7 as determined by an unpaired Student's t-test with Welsh's correction. All P values are two-tailed.

Figure 5.8 provides a visual comparison of F-NT (A) and F-NT with a 100x excess of NT (B) internalisation into transfected HEK293 cells. Relatively large amounts of F-NT are observable in areas localised in 'C' shapes around the nucleus in (A), compared to a smaller in (B). Uptake inhibition was achieved with the introduction of an excess of NT, suggesting transport is mediated via neurotensin receptors. The separated channels of (A), representing as nucleic acids stained by DAPI (C) and F-NT (D) show main bodies of fluorescence originating from regions surrounding the nucleus of the cell with scattering of fluorescence observable throughout the cell cytoplasm.

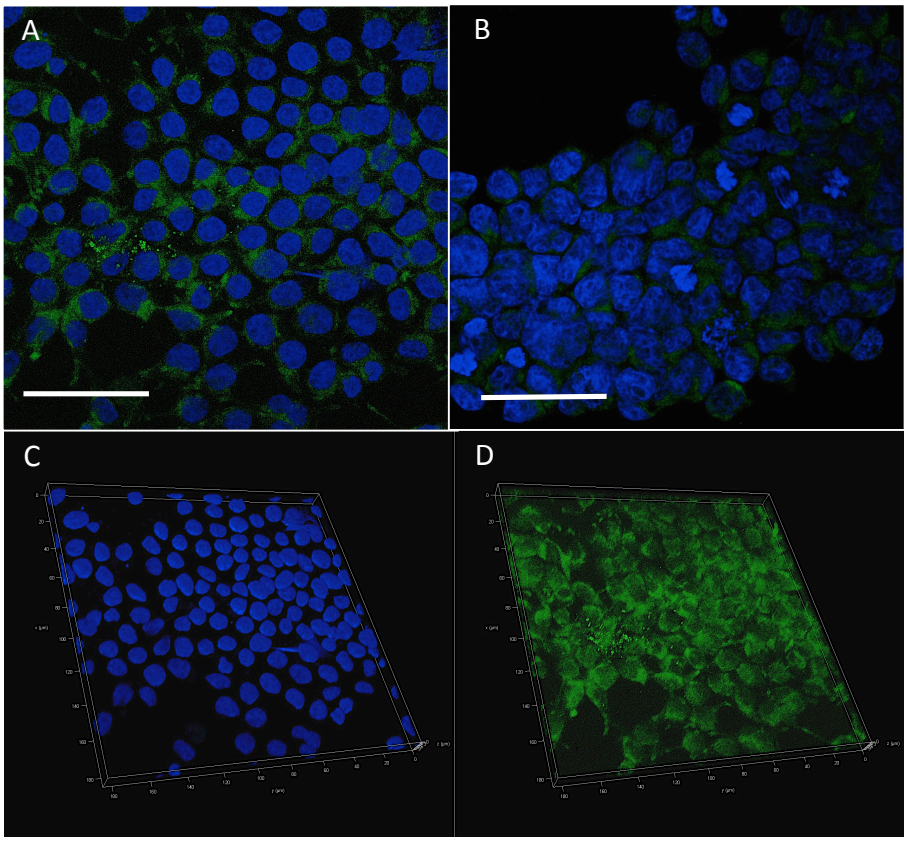

Figure 5.8: Confocal microscope images of transfected HEK293 after (A) incubation with 20 nM F-NT for 1hr and (B) incubation with 20 nM F-NT and 2 µM NT for 1 hr. (C) and (D) shows a breakdown of image (A) to show the locality of the fluorophore within the cell. The white bar is representative of 50 µm.

5.3: Discussion

Delivery of chemotherapeutic agents to overcome drug resistance is a major topic of interest and is currently being investigated for the potential to improve drug delivery of chemotherapeutics. For example Fan *et al*., (2015) recently investigated the influence of conjugating doxorubicin (DOX) to epidermal growth factor (EGF) for targeted delivery to EGF over-expressing tumours. Their study consisted of internalisation assays of EGF-DOX against internalisation of free DOX, and internalisation of EGF-DOX under inhibitory conditions, concluding that EGF-DOX uptake is far greater than uptake of DOX alone, which was documented to be receptor mediated. Uptake of NT-bound fluorophores in this study followed the same pattern in correlation with relative intensity of NTS1 expression (see chapter 3): transfected HEK293 cells internalised the most NT-bound fluorophores (see figures 5.5 and 5.7) and are also the cell line which appear to express the most NTS1

(see figure 3.4). Whereas, undifferentiated Caco-2 cells were characterised to express NTS1 very minimally, if at all (see figure 3.7) – these cells did not show any difference in cellular uptake of GFP-NT or F-NT compared to the fluorophore alone or in the documented inhibited conditions (see figure 5.3).

Referring to figures 5.5 and 5.7, the maximum uptake of GFP-NT appears to be lower than the maximum uptake of F-NT in both non-transfected and transfected HEK293. This could be attributable to the size of the fluorophore affecting the extent of uptake. It is estimated that about 2500 clathrin-coated vesicles leave the plasma membrane of cultured fibroblast cells every minute. Extracellular fluid is trapped in each clathrin-coated vesicle once internalised, bringing molecules in the surrounding area with it (Liu *et al*., 2001). It is possible that the greater extent of uptake seen for F-NT could be attributable to its small size, allowing for more molecules to become trapped during the internalisation process. Although they can enter the cell slowly by other non-specific means, clathrin-mediated endocytosis of receptor-ligand complexes is thought to be a rapid and more efficient method of gaining entry into the host cell in most cases. Whilst receptor complexes can be internalised in just 10 seconds, a select few can take several hours, such as the α-2-bungaratoxin receptor (August, 2013; Weigel *et al*., 2013). Little is known about the specific internalisation dynamics of neurotensin in the cell-lines used in this study, and as endocytotic rates can be variable, no conclusions can be drawn from the data presented in the study about how the size of the molecule affects internalisation rate. For further study, it is suggested that more frequent samples be taken between time 0 minutes and time 30 minutes to evaluate the dynamics of initial uptake when the rate is greatest. One possible means of further elucidating any possible relationship between fluorophore size and transport in this model would be to employ other quantitative techniques such as flow cytometry.

One topic that this chapter aimed to address is whether the size of the molecule conjugated to NT inhibits its internalisation. This would elucidate whether larger chemotherapeutic/biotherapeutic molecules have the potential to be delivered in this way. GFP has a relatively large structure of ~27kDa (Niwa *et al*., 1996) making it

larger in size or comparable to the size of most commonly used chemotherapeutics. Fluorescein is much smaller at ~330 Da (Tian *et al*., 2012). Data displayed in figures 5.5 (GFP-NT) and 5.7 (F-NT) determined that size does affect internalisation, but does not inhibit it. Quantified values for GFP-NT uptake were found to be ~50% lower than that of F-NT. Comparing the values obtained for uptake of GFP-NT vs F-NT in non-transfected HEK293, uptake of GFP-NT was not found to be significant compared to the fluorophore alone ($p=0.1760$). Whereas, uptake of F-NT was significant compared to uptake of the fluorophore alone ($p=0.0012$). This may suggest that a larger cargo is internalised less efficiently in cells that only moderately express NTS1. Although, other factors such as stability of the fluorophore in the cell cannot be ruled out. Either fluorophore may be more structurally integral within the cell compared to the other, affecting the fluorescence reading. This idea could be extrapolated to hypothesise that physiologically normal tissues, that only moderately expresses NTS1, such as cells within the gastrointestinal tract and the brain (Zhao and Pothoulakis, 2006), would uptake minimal amounts of NT-conjugates compared to NTS1 overexpressing tumours during peptide receptor targeted bio-therapeutic treatments.

Confocal images of HEK293 cells following 1hr incubation with 20 nM GFP-NT (figure 5.6) and F-NT (figure 5.8) show the localisation of the fluorophore within the cell. In concordance with the quantified amount of GFP-NT and F-NT within the cell (as described in figures 5.5 and 5.7 respectively), the visible amount GFP-NT in HEK293 appears to be less than that observed from F-NT. In terms of the locality of each fluorophore, the majority of both appear to be localised in areas surrounding the nucleus of the cell. However, neither fluorophore appears to be surrounding the nucleus as tightly as that documented by Vandenbulcke *et al*., (2000), see figure 5.1. This may be due to break-down of NT following internalisation as the peptide is very susceptible to enzymatic degradation by peptidases (Lamberts *et al*., 1996). As GFP is relatively stable and resistant to slight changes in pH (Liu *et al*., 1999), it may have avoided degradation itself and begun to diffuse throughout the cell, if not continuing its set internalisation route with intact NT. As both fluorophores appear to congregate around the nucleus of the cell, this suggests that internalisation of NT in

transfected HEK293 follows a similar (if not the same) route of uptake as that documented in COS-7 cells by Vandenbulcke *et al*., (2000). Further investigation would be needed to ascertain the exact internalisation mechanism of NT into transfected HEK293 cells, but the data presented in this study, with HEK293 acting as a model for NTS1 overexpressing solid-state tumours, suggests that conjugation of bio-therapeutics to NT for targeted delivery has potential for success. The data in this chapter was obtained flowing incubations with 20 nM solutions of NT-conjugates, and was able to elicit an observable response at this relatively small concentration. When this is brought into context with relative amounts of chemotherapeutic vs NT-conjugate needed to elicit a therapeutic effect, the difference is very clear. For example, for the treatment of metastatic breast cancer, 40-60 mg/m^2 of doxorubicin is administered intravenously and is known to cause a variety of adverse side effects, such as hair loss, skin reactions and diarrhoea (Ai *et al*., 2013; Misset *et al*., 1999). This amount could be greatly decreased if conjugated to a high affinity peptide such as neurotensin. The concentration of neurotensin in peripheral plasma is dependent on levels of fat ingestion, but rises to no more than 30 pM concentrations in the blood (Theodorsson-Norheim and Rosell, 1983). Theoretically, the targeted-delivery of therapies will have the ability to reach a therapeutic effect with a lower dose. Hopefully, this will reduce adverse side effects seen with chemotherapeutic therapies (Majumdar and Siahaan, 2012).

A limitation of this study is the lack of differentiation between NT receptor subtypes and therefore how each one influences internalisation in Caco-2 and HEK293. The antagonist SR142948, which is selective of both NTS1 and NTS2, was used in this study. To differentiate further, the NTS1 specific agonist, SR48692 could be used. Therefore the data obtained is representative of the inhibition of these receptor subtypes, and not NTS3 inhibition. However, the majority of data concerning neurotensin internalisation in multiple cell lines and tissues types suggests that NTS1 is responsible for the vast majority of NT uptake. This is shown by neurotensin binding/uptake being almost completely inhibited by the NTS1 specific antagonist SR48692 (Körner *et al*., 2015; Moody *et al*., 2001). However, this may not be the case for the cell lines used in this study. Further experimentation would be needed to

determine whether NTS1 is responsible for the internalisation documented in this study, and to also characterise NTS2 and NTS3 expression.

5.4: Conclusion

A relationship between the size of the molecule conjugated to NT and the amount internalised was suggested with the data presented in this chapter. Internalisation was shown to be receptor mediated, due to its inhibition with an excess of free neurotensin or SR142948 (as competitive inhibitors) and qualitatively correlated to relative expression of NTS1. However, no differentiation was made between which neurotensin receptor subtype was responsible for uptake of the conjugated fluorophores. It is also unable to compare quantitative values for internalisation against values for NTS1 expression as this was assessed qualitatively (see chapter 3). As a response is observed in concentrations as small as 20 nM, peptide-targeted delivery has been shown to be a promising candidate for the delivery of chemotherapeutics to NT receptor overexpressing tumours. Further work is needed to elucidate whether NT is degraded within the cell following internalisation and the precise mechanism of uptake.

Chapter 6

Internalisation and Transport of NT-Conjugated Fluorophores in Polarised Caco-2 Monolayers

6.1: Introduction

The use of intestinal epithelial cells such as Caco-2 has increased drastically in the field of pharmaceutical science over the last 20 years. A large proportion of these studies include cultivation as monolayers on permeable filters for studies into the transport, permeability or absorption of drugs (Artursson *et al*., 2012). Generally, the aim of cultivating these monolayers is to determine the bioavailability of new drug compounds, investigate the mechanism of drug uptake or transport across the epithelium (passive or active) identifying any relevant carriers that may be involved. For example, P-glycoprotein, an ATP binding cassette transporter responsible for the efflux of xenobiotics and drugs, is known to be localised on the apical side of several barrier epithelia including: the intestinal epithelia, brain endothelial cells and renal epithelial cells (Endres *et al*., 2006).

The transport of drugs across the epithelium of the intestine can occur in one of four ways, two passive and two active: passive transcellular/paracellular routes and active carrier mediated/transcytosis (see figure 6.1). However, there are other factors that need to be considered that influence the transport of drugs through epithelial membranes; P-glycoprotein has been related to the occurrence of multidrug resistance in a variety of CNS diseases and cancer (Hoosain *et al*., 2015). It is thought to be a contributing factor to drug resistance in cancer by expelling drugs in the opposite direction to which they are absorbed (Augustijns *et al*., 1993). Polarised Caco-2 monolayers are known to apically express P-glycoprotein (Anderle *et al*., 1998; Pang, 2003) and are useful for investigating this phenomenon. Studies have found that conjugation of chemotherapeutic agents to peptides for receptor-mediated delivery can overcome drug resistance induced in this manner (Ai *et al*., 2013).

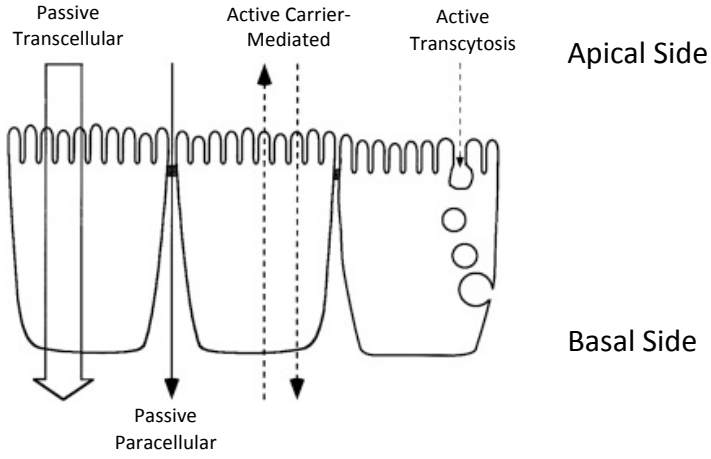

Figure 6.1: Adapted from Artursson *et al*., (2012). Documents the four routes of drug transport in intestinal epithelial monolayers

The active transcytosis route of transport from the apical to basal side of the monolayer has proven to be the least attractive route of transport in terms of drug delivery, due to its small capacity. However, more potent drugs, such as high affinity peptides, are transported much more efficiently through their respective receptors. Transport via receptor-mediated internalisation can occur in proteolytic enzyme-containing vesicles, as a result, exogenous proteins can be degraded during transport (Heyman *et al*., 1982).

One of the principal limiting factors of the design and development of peptide-based therapies is poor transport of the drug across the intestinal mucosa. Shimizu *et al*., (1997) suggested that the transcytosis of peptides into Caco-2 monolayers is dependent on the hydrophobic properties of the peptide itself and susceptibility to brush-border and intracellular peptidases. Furthermore, differences in transport activity, permeability and TEER readings of Caco-2 monolayers have been documented and are thought to be due to heterogeneity between Caco-2 cell lines in different laboratories. It has been suggested that variability between Caco-2 cell lines is induced as a result of differing culture conditions, yielding varying compositions of sub-populations (Walter and Kissel, 1995).

6.2: Results

6.2.1: Quantification of Uptake of Fluorophore-Conjugated NT in Polarised Caco-2 Monolayers

The figures in this section (figures 6.2-6.9) describe internalisation of GFP-NT and F-NT into polarised Caco-2 monolayers at 30-minute intervals for a total of 150 minutes. Sample solutions were made using serum-free media as a diluent. Refer to section 2.2.30 for detail of the methods used in this section. Briefly, samples of fluorophore at known concentrations (which are specified in each figure) were applied to the apical surface of each Caco-2 monolayer and incubated for a set period of time (30, 60, 90, 120 or 150 minutes). After incubation, the monolayer was thoroughly washed with cold PBS and lysed with lysis buffer (composition of the lysis buffer is stated in section 2.2.30). Cellular debris was then removed and the remaining solution was analysed for fluorescence intensity. The intensity reading was then converted into intracellular molar concentration using the same method stated in section 5.2.1. TEER measurements were also taken prior to use of each Caco-2 monolayer to ensure monolayer integrity. Figure 6.2 shows internalisation of NT-GFP vs GFP over time in a polarised Caco-2 monolayer to assess whether conjugation to NT affects uptake of the fluorophore. This experiment was also conducted to assess how internal amounts of fluorophore differs over time.

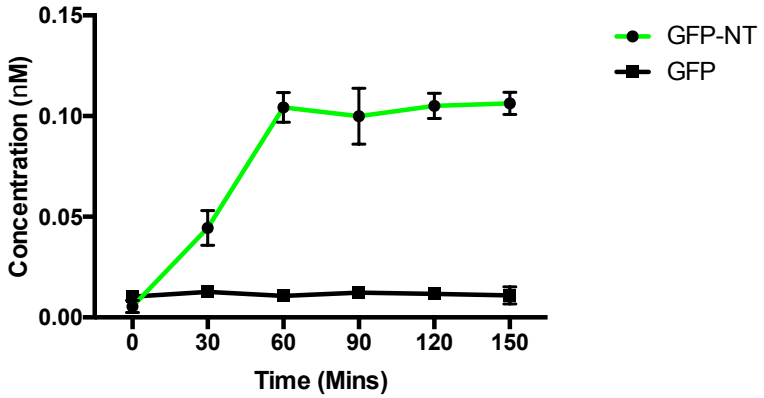

Figure 6.2: Quantified uptake of GFP-NT in Polarised Caco-2 monolayers over time. Error bars are representative of ± SD. Data points are representative of the mean of n=3. The y-axis represents the intracellular concentration of each fluorophore (GFP-NT or GFP) after incubation with 100 nM solutions on the apical side of the monolayer. Fluorescence was detected as stated in section 2.2.30 and converted into a molar concentration as stated in section 5.2.1.

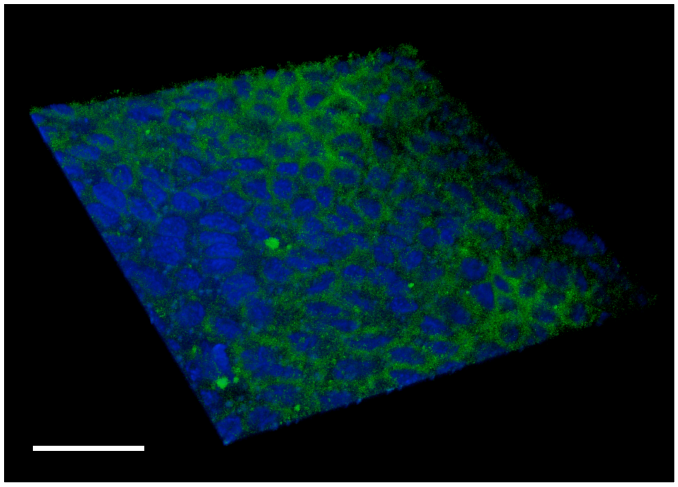

Figure 6.3: 3D confocal microscope image of internalised GFP-NT in a section of polarised Caco-2 monolayer after 3 hours of incubation with 100 nM GFP-NT. The white bar is representative of 50 µm.

Figure 6.3 shows the presence of intracellular GFP-NT in a section of Caco-2 monolayer following incubation with a 100 nM solution of GFP-NT in HBSS. This image was constructed using the z-stack function of the Leica confocal microscope described in section 2.2.26, from 25 individual images at set increments between the apical and basal side of the monolayer. Figures 6.7 and 6.9 in this section were constructed in that same manner. GFP-NT does not appear to concentrate in any one area of the cell, but is scattered throughout. Figure 6.4 shows internalisation of F-NT vs F alone into a polarised Caco-2 monolayer over time – comparing this experiment to internalisation of GFP-NT (see figure 6.2) in the same conditions allows for comparison of how fluorophore size affects internalisation.

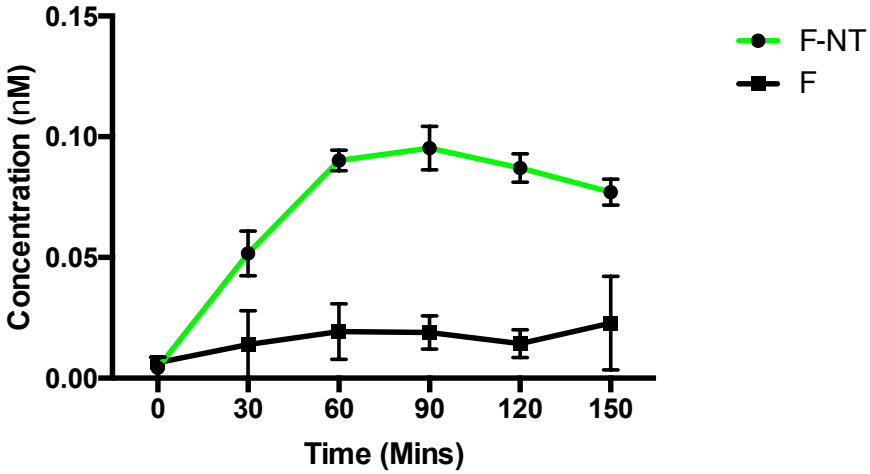

Figure 6.4: Quantified uptake of F-NT in Polarised Caco-2 monolayers over time. Error bars are representative of ± SD. Data points are representative of the mean of n=3. The y-axis represents the intracellular concentration of each fluorophore (F-NT or F) after incubation with 100 nM solutions on the apical side of the monolayer. Fluorescence was detected as stated in section 2.2.30 and converted into a molar concentration as stated in section 5.2.1.

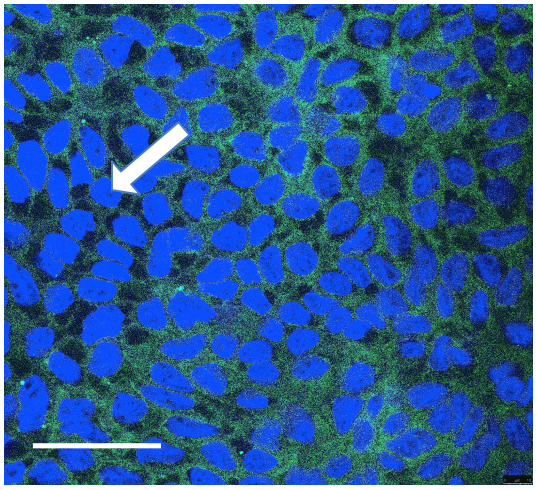

Figure 6.5: Confocal microscope image of internalised F-NT in a section of polarised Caco-2 monolayer after 3 hours of incubation with 100 nM F-NT. The white arrow indicates areas when F-NT has collected around the cell membrane instead of internally. The white bar is representative of 50 µm.

Figure 6.5 above shows a 2D image of a polarised Caco-2 monolayer after incubation with 100 nm F-NT for three hours. The image shows F-NT to be scattered throughout the cytoplasm with no obvious areas of concentration of the fluorophore. Some areas (indicated by a white arrow) appear to have low levels of the fluorophore within the cytoplasm, but collections of it around the membrane itself. This could be an indication of paracellular transport of F-NT. A 2D image was selected for this figure as it best displays collections of F-NT around the outside of the cell. Figure 6.6 shows internalisation of NT-GFP in uninhibited and inhibited conditions. This experiment was conducted to ascertain whether inhibition of NT receptors (all NT receptors in this case) would also inhibit uptake of the NT-bound fluorophore.

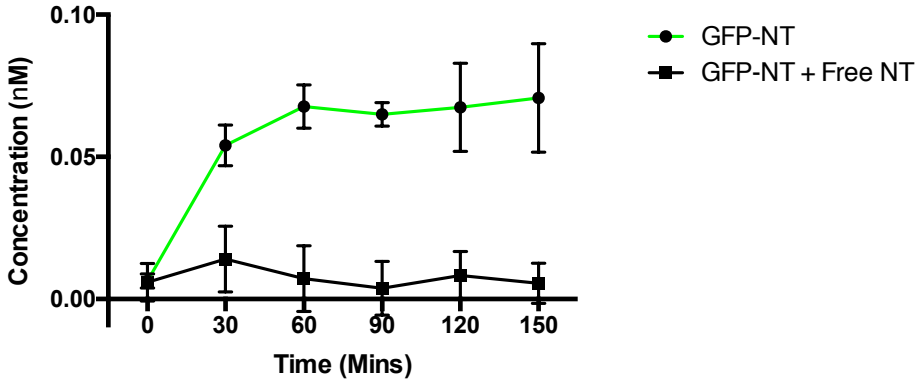

Figure 6.6: Quantified uptake of GFP-NT vs GFP-NT inhibited by 100x free NT in Polarised Caco-2 monolayers over time. Error bars are representative of ± SD. Data points are representative of the mean of n=3. The y-axis represents the intracellular concentration of GFP-NT after incubation with 100 nM solutions of either GFP-NT or GFP-NT with 100x free NT on the apical side of the monolayer. Fluorescence was detected as stated in section 2.2.30 and converted into a molar concentration as stated in section 5.2.1.

Figure 6.7 shows an image obtained by confocal microscopy of a polarised monolayer of differentiated Caco-2 cells following incubation with GFP-NT whilst in the presence of excess NT receptor inhibitor (100x free NT). This image was taken to display GFP-NT localisation/relative amount of GFP-NT present within the cell. This experiment was conducted to determine whether uptake was reduced compared to figure 6.3 (uninhibited conditions) due to inhibition of neurotensin receptors.

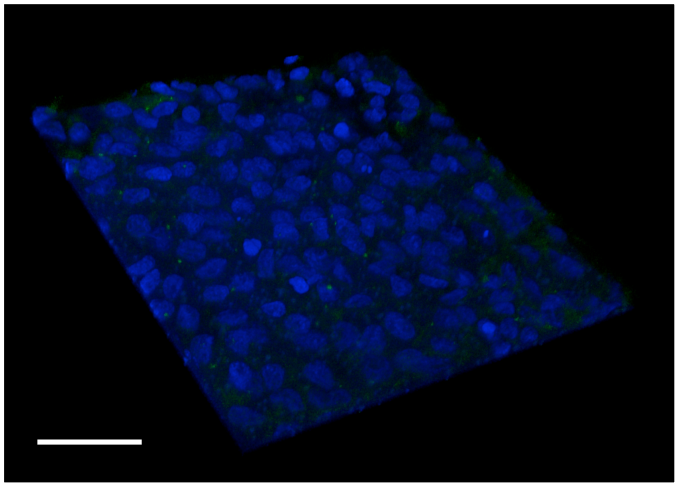

Figure 6.7: 3D confocal microscope image of internalised GFP-NT in a section of polarised Caco-2 monolayer when incubated with a solution of 100 nM GFP-NT and 100x excess free NT (10 µM) for 3 hours. The white bar is representative of 50 µm.

Figure 6.8 shows F-NT uptake in uninhibited and inhibited (excess free NT) conditions. This experiment was conducted to determine whether inhibition of NT receptors would also inhibit uptake of the NT-bound fluorophore.

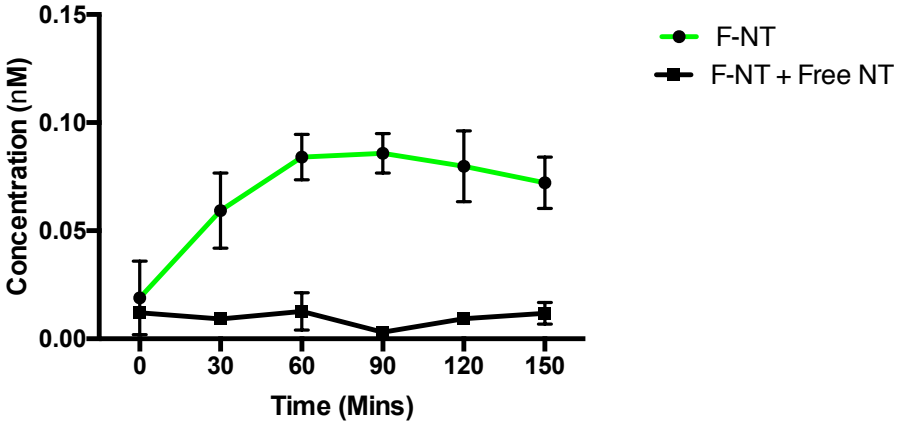

Figure 6.8: Quantified uptake of F-NT vs F-NT inhibited by 100x free NT in Polarised Caco-2 monolayers over time. Error bars are representative of ± SD. Data points are representative of the mean of n=3. The y-axis represents the intracellular concentration of F-NT after incubation with a 100 nM solution of F-NT or 100 nM solution of F-NT with 100x free NT on the apical side of the monolayer. Fluorescence was detected as stated in section 2.2.30 and converted into a molar concentration as stated in section 5.2.1.

Figure 6.9 shows an image obtained by confocal microscopy of a polarised monolayer of differentiated Caco-2 cells following incubation with F-NT whilst in the presence of excess NT receptor inhibitor (100x free NT). This image was taken to display F-NT localisation/relative amount of F-NT present within the cell. This experiment was conducted to determine whether uptake was reduced compared to figure 6.5 (uninhibited conditions) due to inhibition of neurotensin receptors. Imaging of F-NT uptake in inhibited and uninhibited comditions also allows for comparison of GFP-NT under the same conditions to see if fluorophore size affects localisation of uptaken fluorophore (see figures 6.3 and 6.7).

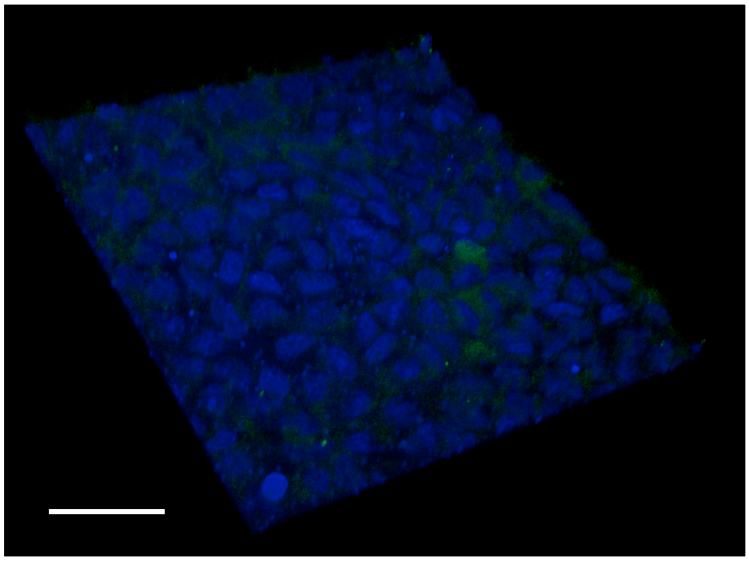

Figure 6.9: 3D confocal microscope image of internalised GFP-NT in a section of polarised Caco-2 monolayer when incubated with a solution of 100 nM F-NT and 100x excess free NT (10 µM) for 3 hours. The white bar is representative of 50 µm.

6.2.2: Quantification of Transport of Fluorophore-Conjugated NT Across Polarised Caco-2 Monolayers

The figures in this section (figures 6.10-6.14) describe transport of GFP-NT and F-NT across polarised Caco-2 monolayers (apical → basal side) at 30-minute intervals for a total of 180 minutes. Sample solutions were made using serum-free media as a diluent. Refer to section 2.2.29 for detail of the methods used in this section. Briefly, samples of NT-fluorophore at known concentrations (which are specified in each figure) were applied to the apical surface of each Caco-2 monolayer and incubated for 180 minutes. 100 µl samples were taken from the media on the basal side of the monolayer every 30 minutes for each well/monolayer and the fluorescence intensity

of the sample was read as described in section 2.2.29. This reading was then converted into a molar concentration using a calibration curve constructed from known dilutions of each fluorophore in HBSS. Samples were taken at time 0 for all data sets in this chapter to ensure the integrity of the cell monolayer and ensure that any transport was mediated by the cells themselves and not through gaps in the monolayer. TEER measurements were also taken prior to use of each Caco-2 monolayer to ensure monolayer integrity. Figures 6.10 and 6.11 shows transport of GFP-NT at differing concentrations to assess whether transport is concentration dependent. GFP alone was used as a control.

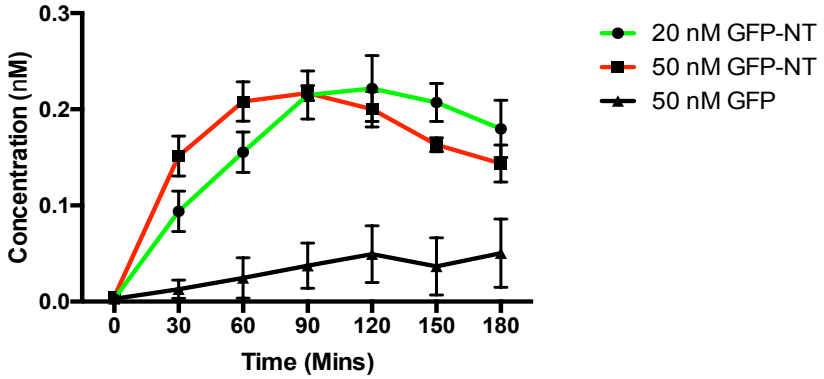

Figure 6.10: Comparison of transport of GFP-NT across polarised Caco-2 monolayers read every 30 minutes after application of either 20 nM or 50 nM GFP-NT solutions to the apical side of monolayer. The data points are representative of the concentration of GFP-NT in the 1.5 ml volume of media on the basal side of the monolayer. 50 nM GFP alone was used as a negative control. Data points are representative of the mean of n = 3 and error bars are representative of ± SD.

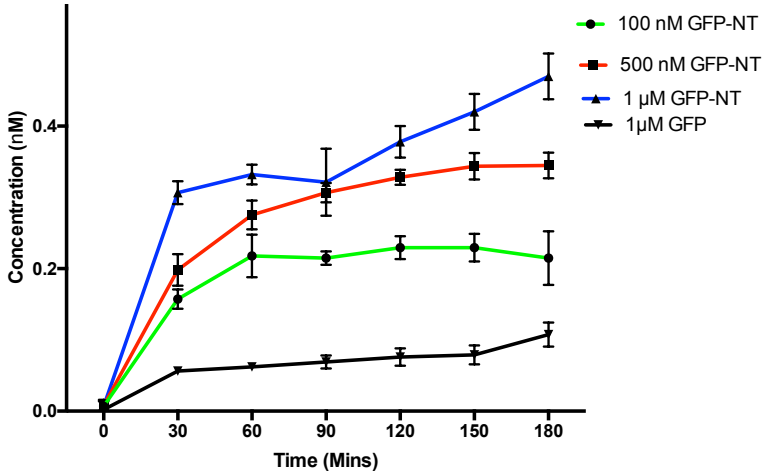

Figure 6.11: Comparison of transport of GFP-NT across polarised Caco-2 monolayers read every 30 minutes after application of either 100 nM, 500 nM or 1 µM GFP-NT solutions to the apical side of monolayer. The data points are representative of the concentration of GFP-NT in the 1.5 ml volume of media on the basal side of the monolayer. 1 µM GFP alone was used as a negative control. Data points are representative of the mean of n = 3 and error bars are representative of ± SD.

Figure 6.12 shows transport of F-NT at differing concentrations, with F alone as a control. This was done to assess whether transport of F-NT through a model epithelial monolayer is concentration dependent and compare transport to the fluorophore alone.

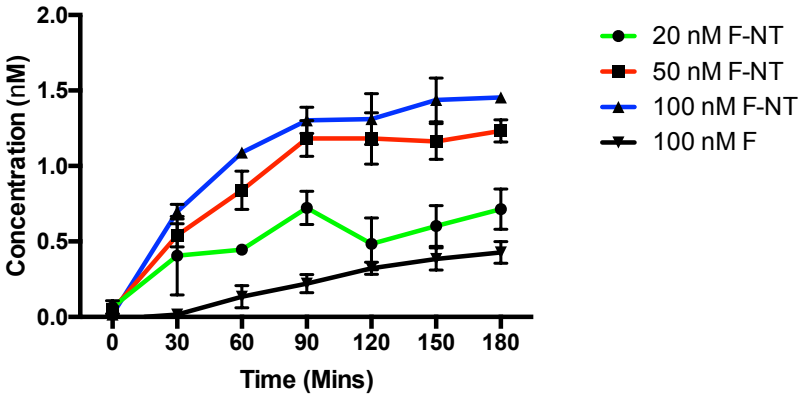

Figure 6.12: Comparison of transport of F-NT across polarised Caco-2 monolayers read every 30 minutes after application of either 20 nM, 50 nM or 100 nM F-NT solutions to the apical side of monolayer. The data points are representative of the concentration of F-NT in the 1.5 ml volume of media on the basal side of the monolayer. 100 nM F alone was used as a negative control. Data points are representative of the mean of n = 3 and error bars are representative of ± SD.

Figure 6.13 shows transport of GFP-NT under uninhibited and inhibited (100x excess free NT) conditions to determine whether transport can be inhibited through inhibition of neurotensin receptors. GFP alone was used as a control.

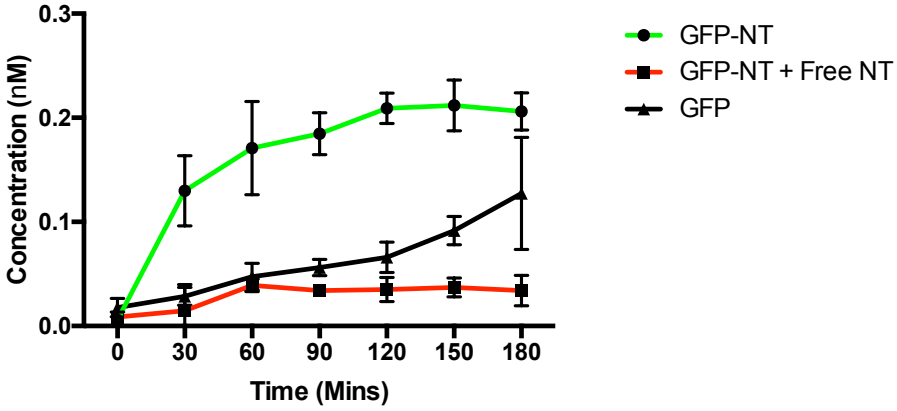

Figure 6.13: Comparison of transport of GFP-NT across polarised Caco-2 monolayers read every 30 minutes after application of either 100 nM GFP-NT or 100 nM GFP-NT + 100x excess free NT solution to the apical side of monolayer. The data points are representative of the concentration of GFP-NT in the 1.5 ml volume of media on the basal side of the monolayer. 100 nM GFP alone was used as a negative control. Data points are representative of the mean of n = 3 and error bars are representative of ± SD.

Figure 6.14 shows transport of F-NT in inhibited (100x excess free NT) and uninhibited conditions with F-NT at differing concentrations. This experiment was conducted to evaluate whether transport of F-NT can be inhibited by inhibiting NT receptors and whether this effect can be overcome by increasing the concentration of F-NT (keeping the ratio of F-NT to inhibitor the same).

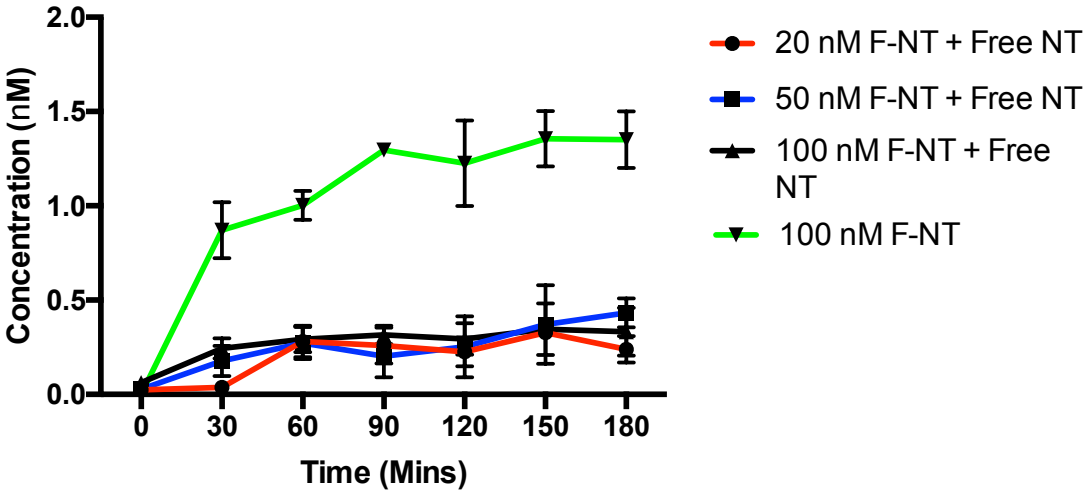

Figure 6.14: Comparison of transport of F-NT across polarised Caco-2 monolayers read every 30 minutes after application of solutions of F-NT + 100x free NT (20 nM, 50 nM and 100 nM) to the apical side of monolayer. The data points are representative of the concentration of F-NT in the 1.5 ml volume of media on the basal side of the monolayer. 100 nM F-NT alone was used as a positive control. Data points are representative of the mean of n = 3 and error bars are representative of ± SD.

Figures 6.10 and 6.11 show GFP-NT to be transported in a receptor-mediated manner due to observably greater transport than GFP alone, representing non-specific transport. Furthermore, increasing levels of transport can be seen in proportion with concentration of GFP-NT solutions applied to the apical side of the monolayer. For example, the transport observed with 1 µM GFP-NT solutions with greater than that observed with 100 nM GFP-NT solutions. The same trend is seen with internalisation of F-NT, however a greater amount of F-NT appears to be transported compared to the corresponding concentrations of GFP-NT.

GFP-NT and F-NT transport is further confirmed as receptor-mediated by the apparent inhibition of transport caused by addition of 100x free NT in each sample concentration. This is observable in both GFP-NT and F-NT samples detailed in figures 6.13 and 6.14 respectively. In these inhibitory assays, transport of GFP-NT

and F-NT is comparable to (if not less) the amount of non-specific transport demonstrated by each unconjugated fluorophore.

6.3: Discussion

The main aim of this chapter is to evaluate the potential for NT conjugation to bio-therapeutics (comparable in size to that of GFP) to allow for receptor-targeted internalisation and transport of the bio-therapeutic itself. The ability for bio-theraputics to be targeted to NT-R overexpressing cancerous cells would reduce the need for quantities of bio-therapeutics that elicit unnecessary toxicities for non-cancerous cells, as neurotensin has a very high affinity for its receptor (~0.3 nM affinity for NTS1). As previously mentioned, Caco-2 cells closely resemble the morphological characteristics of mature enterocytes once differentiated and thus present an *in vitro* model closer to *in vivo* conditions that conventional tissue culture of Caco-2 cells allows for. This model serves as an effective tool to mimic the uptake and transport of NT-conjugated fluorophores in mature enterocytes. Polarised Caco-2 cells have been previously characterised to almost homogenously express high levels of NTS1 (see chapter 3).

Referring to figures 6.6 and 6.8, inhibition of internalisation of NT with an excess of NT suggests that uptake of NT in polarised Caco-2 monolayers is receptor mediated. Uptake of GFP-NT (figures 6.2 and 6.6) and F-NT (figures 6.4 and 6.8) appears to plateau, starting at around minute 60. The plateau of GFP-NT uptake remains constant, whereas F-NT levels begin to decrease towards the end of the 150-minute incubation. As large cargo size is known to have a negative influence on the rate of transport through caco-2 monolayers and the hydrophilic nature of the molecule determines that it cannot diffuse through the cell membrane. As previously discussed in chapter 5, it is unclear with the data obtained in this study whether NT is degraded once it internalises into the cells. Therefore, it is unclear whether the fluorophore detected within the cell has followed the same trafficking pattern that would be elicited with NT alone. For future work, it is advised that stable

neurotensin analogues be used to repeat these findings and the trafficking mechanisms of NT in polarised Caco-2 be elucidated.

Figures 6.3, 6.5, 6.7 and 6.9 can be used to speculate the locality of NT-bound fluorophores following internalisation. It should be noted that these images were taken three hours after initial exposure to 100 nM solutions of both NT-conjugates (as they were taken following on from transport studies) and so are not directly comparable to the images included in chapter 5. Figure 6.3 displays the position of GFP-NT after incubation and does not appear to be as localised to the nucleus as seen in figure 5.6. This may be due to polarised Caco-2 cells having a greater proteolytic activity than HEK293 cells, resulting in a greater amount of free GFP able to readily diffuse throughout the cell cytoplasm. However, the monolayer imaged in figure 5.6 was subjected to a much lower concentration of GFP-NT than that seen in figure 6.3, perhaps leading to increased uptake and increased scattering of the fluorophore.

Since the discovery of neurotensin in 1973, many studies that document cellular responses to the neuropeptide report rapid desensitisation following exposure. This is characterised by a decrease in responsiveness to the peptide following long periods of exposure or lack of response to repeated exposure (Carraway and Leeman, 1973; Hermans and Maloteaux, 1998). In studies concerning the effects of neurotensin on the gastrointestinal system of rats, exposure to concentrations of neurotensin as low as 5 nM for prolonged periods of time induced a decrease in maximum response (compared to at time = 0 mins) and shifted the dose-response curve to the right. However, thorough washing of neurotensin from the tissue allowed for time-dependant recovery (Mulè *et al*., 1995). It is clear form the data presented in this chapter that the internalisation and transport of both GFP-NT and F-NT reaches a plateau after around 60 minutes (figures 6.2, 6.4, 6.6, 6.8-14) and in some cases begins to decrease toward the end of the three-hour exposure (figure 6.10). This could be attributable to desensitisation of neurotensin receptors.

The regulation of neurotransmitter desensitisation is thought to be entirely dependent on the individual receptor and a common property of neurotransmitter receptors (Huganir and Greengardt, 1990). The influence of receptor phosphorylation on desensitisation has been investigated into using the β-adrenergic receptor; concluding that it is possible for receptor activated kinases, such as protein kinase A and C, to control desensitisation through receptor inactivation and uncoupling from intracellular second messengers (Premont *et al*., 1995). Desensitisation of the neurotensin receptor may be regulated in the same manner. Turner *et al*., (1990) used the HT-29 human colonic adenocarcinoma cell line to question whether desensitisation of neurotensin receptors is mediated from this early uncoupling of receptor from second messenger, or from later phases of internalisation. The study highlighted that protein kinases were not responsible for the regulation of receptors induced by exposure to neurotensin like it does in other receptor systems.

It has been proposed recently that the structure and composition of neurotensin itself plays a part in regulation of its corresponding cell surface receptors. Lee *et al*., (2015) documented the comparison of contulakin-G (a marine glycopeptide with a similar C-terminal structure to NT, and therefore with an ability to act as an agonist to neurotensin receptors) to NT in their ability to desensitise receptors. The two molecules differ in the presence of the conserved Lys6 residue in NT and an extended N-terminus in contulakin-G. Due to these structural differences, contulakin-G is known to have a much lower affinity to neurotensin receptors and, interestingly, not exert as greater a desensitising effect on cell surface receptors (Craig *et al*., 1999). The study by Lee *et al*., (2015) employed structure related desensitisation assays with several NT analogues to ascertain the structural component contributing to increased desensitisation – they concluded that removal of the negatively charged residue at position 4 did not affect affinity of NT to NT-R, but did reduce desensitisation potency five-fold.

Figures 6.11 and 6.12 show the comparison of maximum transport of each NT-conjugate. Using 100 nM samples for comparison, GFP-NT transport plateaus at around 0.4 nM, as opposed to 1.5 nM for F-NT. This may be due to the small size of fluorescein allowing for a greater extent of transport. Inhibition of transport by excess NT (as can be seen in figures 6.13 and 6.14) suggests that receptor mediated-transport rather than diffusion is predominantly responsible for F-NT translocation across the monolayers. Another factor responsible for this discrepancy between GFP-NT and F-NT transport is the macromolecular nature of GFP attenuating the efficiency of NT receptor mediated transport. The extent of transport of each NT-conjugated fluorophore also appears to be concentration-dependant. Figure 6.11 displays transport of GFP-NT at concentrations of 100 nM, 500 nM and 1 µM, showing a correlation between the concentrations of fluorophore applied to the monolayer and the maximum rate of transport of GFP-NT taking place between 0 and 30 minutes. As the majority of transport is documented to occur within the first 30 minutes of incubation, further work to elucidate the dynamics of transport within this time range is recommended.

Although uptake of GFP-NT and F-NT (100 nM each) is relatively similar at ~0.1 nM (see Figures 6.4 and 6.2), transport varies. It is not possible to compare the figure for cellular uptake against the number of cells per Transwell® well as this was not characterised after 21 days of growth, but the data sets are comparable against one another as each well was cultured and seeded identically. Transport of GFP-NT after incubation with a concentration of 100 nM plateaus at around 0.2 nM (this value is variable in proportion with the incubation concentration). F-NT however, reaches a transport maximum of around 1.25 nM at a concentration of 100 nM (this value is also variable with incubation concentration). Again, this could be due to an increased transport efficiency with the smaller fluorophore.

6.4: Conclusion

Both GFP-NT and F-NT have shown to be internalised and transported in a receptor-mediated fashion in polarised Caco-2 monolayers. A relationship between the nature

of the cargo conjugated to NT, in this case fluorescein versus GFP, is also apparent, influencing the efficiency of transport, with the amount F-NT transported being over 3x greater than that of GFP-NT over 3 hours. As described in chapter 5, only NTS1 expression was characterised in this cell line so it is unclear which receptor is responsible for any transport or uptake observed. Further work is needed to elucidate whether NT is degraded within the cell following internalisation. As a response is observed in concentrations as low as 20 nM for transport and internalisation, neurotensin receptor-targeted delivery has been shown to be a promising candidate for delivery of bio-therapeutics to NT receptor over-expressing tumours.

General Conclusion

Firstly, NTS1 expression was characterised by immunostaining in two separate cell lines – Caco-2 and HEK293. Concluding a lack of expression on unpolarised Caco-2, but moderate expression on wild type HEK293. In an attempt to mimic NTS1 expression in NTS1 over-expressing tumour cells, HEK293 were transfected with NTS1. This procedure was optimised and found to induce a much higher level of expression of NTS1 than that seen on wild type HEK293. Caco-2 cells can be grown on polycarbonate membranes for an extended period of time after confluency is reached (21 days), which causes them to differentiate into 'polarised' Caco-2 monolayers and acquire a similar structure to that of mature enterocytes. Characterisation of polarised Caco-2 showed NTS1 expression to be highly up regulated and membrane-localised compared to that of wild-type Caco-2.

In chapter 4, the optimised production of GFP-NT and GFP alone by recombinant protein expression is also documented in this study. Quikchange mutagenesis of the original his-tagged GFP-NT (His-GFP-NT) containing plasmid was shown to successfully introduce an stop codon (TAA) before the sequence for NT, making a plasmid that recombinantly expresses GFP alone. Expression of each plasmid in BL21 *E.coli* was optimised and the purification of the respective proteins was shown to be successful with UV-Vis spectrophotometry and SDS-PAGE.

In chapters 5 and 6, the production, internalisation and transport of GFP-NT is documented and discussed, and compared against the elicited internalisation of F-NT , a smaller fluorophore. Both GFP-NT and F-NT were shown to be internalised in a receptor-mediated fashion in undifferentiated Caco-2 and HEK293. Chapter 6 documented the interaction of GFP-NT and F-NT with differentiated Caco-2 monolayers, showing cellular uptake to also be receptor mediated, as well as concentration and time dependent. A ubiquitous plateau in cellular uptake after ~ 60 minutes suggests desensitisation of the receptor. Localisation of each fluorophore within transfected HEK293 cells shows localisation around the nucleus, suggesting eventual and general trafficking to the trans-golgi network within the cell.

Future Work

NTS1 expression was characterised on the cell lines used in this study, however, characterisation of NTS2 and NTS3 (the other membrane-bound receptors shown to internalise upon interaction with NT) expression on the same cell lines was not performed. Although literature suggests that the majority of the effects of NT are exhibited through interactions with NTS1, as this study documents internalisation rather than exhibited effects, the presence of these other receptors should be evaluated. Furthermore, the characterisation of NTS1 expression in this study is purely qualitative. It is suggested that evaluation of expression be repeated in a quantitative manner with techniques such as flow cytometry or quantitative image evaluation software. Also, as transfection with lipofectamine yielded non-homogenous expression of NTS1, further optimisation or a different method of transfection is advised to eliminate this.

The precise mechanism of internalisation of NT is variable among cell lines and tissue types, as previously discussed in this document. This study visually documents the location of NT-conjugated fluorophores, but does not elucidate the step-wise dynamics of NT internalisation into the cells. It is suggested that the specific mechanism of internalisation in HEK293 and Caco-2 be investigated with endosome staining techniques. Usually, in studies such as this that document cellular uptake of a protein conjugated to NT, stable mutants analogues of NT are used to prevent internal degradation by peptidases. An analogue of NT was not used in this study and therefore the structural integrity of the NT portion of GFP-NT or F-NT cannot be confirmed. It is suggested that this study be repeated with the use of a stable NT analogue.

References

Ai, S., Jia, T., Ai, W., Duan, J., Liu, Y., Chen, J., Liu, X., Yang, F., Tian, Y., and Huang, Z. (2013). Targeted delivery of doxorubicin through conjugation with EGF receptor–binding peptide overcomes drug resistance in human colon cancer cells. Br J Pharmacol *168*, 1719–1735.

Alifano, M., Souazé, F., Dupouy, S., Camilleri-Broët, S., Younes, M., Ahmed-Zaïd, S.-M., Takahashi, T., Cancellieri, A., Damiani, S., Boaron, M., et al. (2010a). Neurotensin Receptor 1 Determines the Outcome of Non–Small Cell Lung Cancer. Clin. Cancer Res. *16*, 4401–4410.

Alifano, M., Loi, M., Camilleri-Broet, S., Dupouy, S., Régnard, J.F., and Forgez, P. (2010b). Neurotensin expression and outcome of malignant pleural mesothelioma. Biochimie *92*, 164–170.

Altman, S.A., Randers, L., and Rao, G. (1993). Comparison of trypan blue dye exclusion and fluorometric assays for mammalian cell viability determinations. Biotechnol. Prog. *9*, 671–674.

Anderle, P., Niederer, E., Rubas, W., Hilgendorf, C., Spahn-Langguth, H., Wunderli-Allenspach, H., Merkle, H.P., and Langguth, P. (1998). P-glycoprotein (P-gp) mediated efflux in Caco-2 cell monolayers: The influence of culturing conditions and drug exposure on P-gp expression levels. J. Pharm. Sci. *87*, 757–762.

Anderle, P., Rakhmanova, V., Woodford, K., Zerangue, N., and Sadée, W. (2003). Messenger RNA Expression of Transporter and Ion Channel Genes in Undifferentiated and Differentiated Caco-2 Cells Compared to Human Intestines. Pharm. Res. *20*, 3–15.

Antunes, F., Andrade, F., Ferreira, D., Morck Nielsen, H., and Sarmento, B. (2013). Models to Predict Intestinal Absorption of Therapeutic Peptides and Proteins. Curr. Drug Metab. *14*, 4–20.

Antunes, P., Ginj, M., Walter, M.A., Chen, J., Reubi, J.-C., and Maecke, H.R. (2007). Influence of different spacers on the biological profile of a DOTA-somatostatin analogue. Bioconjug. Chem. *18*, 84–92.

Artursson, P., Palm, K., and Luthman, K. (2012). Caco-2 monolayers in experimental and theoretical predictions of drug transport. Adv. Drug Deliv. Rev. *64, Supplement*, 280–289.

Atamas, S.P. (2012). Relief from Within: A Peptide Therapy for Fibrosis. Sci. Transl. Med. *4*, 16.

August, T.J. (2013). Biological Response Mediators and Modulators: John Jacob Abel Symposia on Drug Development (Elsevier).

Augustijns, P.F., Bradshaw, T.P., Gan, L.S.L., Hendren, R.W., and Thakker, D.R. (1993). Evidence for a Polarized Efflux System in Caco-2 Cells Capable of Modulating Cyclosporine A Transport. Biochem. Biophys. Res. Commun. *197*, 360–365.

Backer, J.M., Kahn, C.R., and White, M.F. (1990). The dissociation and degradation of internalized insulin occur in the endosomes of rat hepatoma cells. J. Biol. Chem. *265*, 14828–14835.

Baldwin, R.W. (1985). Monoclonal antibody targeting of anti-cancer agents: Mühlbock memorial lecture. Eur. J. Cancer and Clin. Onc. *21*, 1281–1285.

Baneyx, F. (1999). Recombinant protein expression in Escherichia coli. Curr. Opin. Biotech. *10*, 411–421.

Barbieri, F., Bajetto, A., Pattarozzi, A., Gatti, M., W&#xfc, Rth, R., Thellung, S., Corsaro, A., Villa, V., Nizzari, M., et al. (2013). Peptide Receptor Targeting in Cancer: The Somatostatin Paradigm. International Journal of Peptides [online] Available from: [http://www.hindawi.com/journals/ijpep/2013/926295/].

Bareford, L.M., and Swaan, P.W. (2007). Endocytic mechanisms for targeted drug delivery. Adv. Drug Deliv. Rev. *59*, 748–758.

Baum, R.P., and Kulkarni, H.R. (2012). THERANOSTICS: From Molecular Imaging Using Ga-68 Labeled Tracers and PET/CT to Personalized Radionuclide Therapy - The Bad Berka Experience. Theranostics *2*, 437–447.

Bison, S.M., Konijnenberg, M.W., Melis, M., Pool, S.E., Bernsen, M.R., Teunissen, J.J.M., Kwekkeboom, D.J., and Jong, M. de (2014). Peptide receptor radionuclide therapy using radiolabeled somatostatin analogs: focus on future developments. Clin. Trans. Imaging *2*, 55–66.

Botto, J.-M., Chabry, J., Sarret, P., Vincent, J.-P., and Mazella, J. (1998). Stable Expression of the Mouse Levocabastine-Sensitive Neurotensin Receptor in HEK 293 Cell Line: Binding Properties, Photoaffinity Labeling, and Internalization Mechanism. Biochem. Biophys. Res. Commun. *243*, 585–590.

Boulet, L.-P. (2004). Allergen-derived T Cell Peptides and Late Asthmatic Responses. Am. J. Respir. Crit. Care Med. *169*, 2–3.

Brannon-Peppas, L., and Blanchette, J.O. (2012). Nanoparticle and targeted systems for cancer therapy. Adv. Drug Deliv. Rev. *64, Supplement*, 206–212.

Brautaset, T., Lale, R., and Valla, S. (2009). Positively regulated bacterial expression systems. Micro. Biotech. *2*, 15–30.

Bravo, S.A., Nielsen, C.U., Amstrup, J., Frokjaer, S., and Brodin, B. (2004). In-depth evaluation of Gly-Sar transport parameters as a function of culture time in the Caco-2 cell model. Eur. J. Pharm. Sci. *21*, 77–86.

Briske-Anderson, M.J., Finley, J.W., and Newman, S.M. (1997). The Influence of Culture Time and Passage Number on the Morphological and Physiological Development of Caco-2 Cells. Exp. Biol. Med. (Maywood) *214*, 248–257.

Buchegger, F., Bonvin, F., Kosinski, M., Schaffland, A.O., Prior, J., Reubi, J.C., Bläuenstein, P., Tourwé, D., Garayoa, E.G., and Delaloye, A.B. (2003). Radiolabeled Neurotensin Analog, 99mTc-NT-XI, Evaluated in Ductal Pancreatic Adenocarcinoma Patients. J. Nucl. Med. *44*, 1649–1654.

Carraway, R.E., and Plona, A.M. (2006). Involvement of neurotensin in cancer growth: Evidence, mechanisms and development of diagnostic tools. Peptides *27*, 2445–2460.

Carraway, R., and Leeman, S.E. (1973). The Isolation of a New Hypotensive Peptide, Neurotensin, from Bovine Hypothalami. J. Biol. Chem. *248*, 6854–6861.

Carter, P.J. (2011). Introduction to current and future protein therapeutics: A protein engineering perspective. Exper. Cell Res. *317*, 1261–1269.

Chabner, B.A., and Roberts, T.G. (2005). Timeline: Chemotherapy and the war on cancer. Nat. Rev. Cancer *5*, 65–72.

Chabry, J., Gaudriault, G., Vincent, J.P., and Mazella, J. (1993). Implication of various forms of neurotensin receptors in the mechanism of internalization of neurotensin in cerebral neurons. J. Biol. Chem. *268*, 17138–17144.

Chabry, J., Labbé-Jullié, C., Gully, D., Kitabgi, P., Vincent, J.P., and Mazella, J. (1994). Stable expression of the cloned rat brain neurotensin receptor into fibroblasts: binding properties, photoaffinity labeling, transduction mechanisms, and internalization. J. Neurochem. *63*, 19–27.

Cody, C.W., Prasher, D.C., Westler, W.M., Prendergast, F.G., and Ward, W.W. (1993). Chemical structure of the hexapeptide chromophore of the Aequorea green-fluorescent protein. Biochemistry *32*, 1212–1218.

Conner, S.D., and Schmid, S.L. (2003). Regulated portals of entry into the cell. Nature *422*, 37–44.

Cook, J.A., and Mitchell, J.B. (1989). Viability measurements in mammalian cell systems. Anal. Biochem. *179*, 1–7.

Coons, A.H., and Kaplan, M.H. (1950). Localization of antigen in tissue cells; improvements in a method for the detection of antigen by means of fluorescent antibody. J. Exp. Med. *91*, 1–13.

Corchero, J.L., and Villaverde, A. (1998). Plasmid maintenance in Escherichia coli recombinant cultures is dramatically, steadily, and specifically influenced by features of the encoded proteins. Biotechnol. Bioeng. *58*, 625–632.

Craig, A.G., Norberg, T., Griffin, D., Hoeger, C., Akhtar, M., Schmidt, K., Low, W., Dykert, J., Richelson, E., Navarro, V., et al. (1999). Contulakin-G, an O-glycosylated invertebrate neurotensin. J. Biol. Chem. *274*, 13752–13759.

Cubitt, A.B., Heim, R., Adams, S.R., Boyd, A.E., Gross, L.A., and Tsien, R.Y. (1995). Understanding, improving and using green fluorescent proteins. Trends Biochem. Sci. *20*, 448–455.

Cui, S., Zhang, S., Chen, H., Wang, B., Zhao, Y., and Zhi, D. (2012). The Mechanism of Lipofectamine 2000 Mediated Transmembrane Gene Delivery. Engineering *04*, 172–175.

Das, S., Jagan, L., Isiah, R., Rajesh, B., Backianathan, S., and Subhashini, J. (2011). Nanotechnology in oncology: Characterization and in vitro release kinetics of cisplatin-loaded albumin nanoparticles: Implications in anticancer drug delivery. Indian J. Pharmacol. *43*, 409–413.

De Jong, M., Bernard, B.F., De Bruin, E., Van Gameren, A., Bakker, W.H., Visser, T.J., Mäcke, H.R., and Krenning, E.P. (1998). Internalization of radiolabelled [DTPA0]octreotide and [DOTA0,Tyr3]octreotide: peptides for somatostatin receptor-targeted scintigraphy and radionuclide therapy. Nucl. Med. Commun. *19*, 283–288.

Delom, F., and Fessart, D. (2011). Role of Phosphorylation in the Control of Clathrin-Mediated Internalization of GPCR. Inter. J. Cell Bio. *2011*, e246954.

Ehlers, R.A., Kim, S., Zhang, Y., Ethridge, R.T., Murrilo, C., Hellmich, M.R., Evans, D.B., Townsend, C.M., and Mark Evers, B. (2000). Gut Peptide Receptor Expression in Human Pancreatic Cancers. Ann. Surg. *231*, 838–848.

Ehrlich, P. (1956). The relationship existing between chemical constitution, distribution, and pharmacological action. The Collected Papers of Paul Ehrlich *1*, 596–618.

Elbashir, S.M., Harborth, J., Weber, K., and Tuschl, T. (2002). Analysis of gene function in somatic mammalian cells using small interfering RNAs. Methods *26*, 199–213.

Endres, C.J., Hsiao, P., Chung, F.S., and Unadkat, J.D. (2006). The role of transporters in drug interactions. Eur. J. Pharm. Sci. *27*, 501–517.

Evers, B.M., Rajaraman, S., Chung, D.H., Townsend, C.M., Wang, X., Graves, K., and Thompson, J.C. (1993). Differential expression of the neurotensin gene in the developing rat and human gastrointestinal tract. Am. J. Phys. - Gastro. Liver Phys. *265*, G482–G490.

Fan, M., Yang, D., Liang, X., Ao, J., Li, Z., Wang, H., and Shi, B. (2015). Design and biological activity of epidermal growth factor receptor-targeted peptide doxorubicin conjugate. Biomed. Pharmacother. *70*, 268–273.

Faure, M.-P., Labbé-Jullié, C., Cashman, N., Kitabgi, P., and Beaudet, A. (1995). Binding and internalization of neurotensin in hybrid cells derived from septa1 cholinergic neurons. Synapse *20*, 106–116.

Felgner, P.L., Gadek, T.R., Holm, M., Roman, R., Chan, H.W., Wenz, M., Northrop, J.P., Ringold, G.M., and Danielsen, M. (1987). Lipofection: a highly efficient, lipid-mediated DNA-transfection procedure. Proc. Natl. Acad. Sci. *84*, 7413–7417.

Ferguson, S.S.G. (2001). Evolving Concepts in G Protein-Coupled Receptor Endocytosis: The Role in Receptor Desensitization and Signaling. Pharmacol. Rev. *53*, 1–24.

Ferguson, S.S.G., Ménard, L., Barak, L.S., Koch, W.J., Colapietro, A.-M., and Caron, M.G. (1995). Role of Phosphorylation in Agonist-promoted β2-Adrenergic Receptor Sequestration RESCUE OF A SEQUESTRATION-DEFECTIVE MUTANT RECEPTOR BY βARK1. J. Biol. Chem. *270*, 24782–24789.

Ferguson, S.S.G., Downey, W.E., Colapietro, A.-M., Barak, L.S., Ménard, L., and Caron, M.G. (1996). Role of β-Arrestin in Mediating Agonist-Promoted G Protein-Coupled Receptor Internalization. Science *271*, 363–366.

Ferrer-Miralles, N., Domingo-Espín, J., Corchero, J.L., Vázquez, E., and Villaverde, A. (2009). Microbial factories for recombinant pharmaceuticals. Microb. Cell Fact. *8*, 17.

Ferris, C.F. (2010). Neurotensin. *Comprehensive Physiology*, (John Wiley & Sons, Inc.) pp 559-586 [online] available from: [http://onlinelibrary.wiley.com/doi/10.1002/cphy.cp060223/full]

Freedman, N.J., and Lefkowitz, R.J. (1996). Desensitization of G protein-coupled receptors. Recent Prog. Horm. Res. *51*, 319–351; discussion 352–353.

Garland, A.M., Grady, E.F., Lovett, M., Vigna, S.R., Frucht, M.M., Krause, J.E., and Bunnett, N.W. (1996). Mechanisms of desensitization and resensitization of G protein-coupled neurokinin1 and neurokinin2 receptors. Mol. Pharmacol. *49*, 438–446.

Goeddel, D.V., Kleid, D.G., Bolivar, F., Heyneker, H.L., Yansura, D.G., Crea, R., Hirose, T., Kraszewski, A., Itakura, K., and Riggs, A.D. (1979). Expression in Escherichia coli of chemically synthesized genes for human insulin. PNAS *76*, 106–110.

Grady, E.F., Gamp, P.D., Jones, E., Baluk, P., McDonald, D.M., Payan, D.G., and Bunnett, N.W. (1996). Endocytosis and recycling of neurokinin 1 receptors in enteric neurons. Neurosci. *75*, 1239–1254.

Graham, F.L., Smiley, J., Russell, W.C., and Nairn, R. (1977). Characteristics of a Human Cell Line Transformed by DNA from Human Adenovirus Type 5. J. Gen. Virol. *36*, 59–72.

Gugger, M., and Reubi, J.C. (1999). Gastrin-Releasing Peptide Receptors in Non-Neoplastic and Neoplastic Human Breast. Am. J. Path. *155*, 2067–2076.

Gui, X., Guzman, G., Dobner, P.R., and Kadkol, S.S. (2008). Increased neurotensin receptor-1 expression during progression of colonic adenocarcinoma. Peptides *29*, 1609–1615.

Gulenchyn, K.Y., Yao, X., Asa, S.L., Singh, S., and Law, C. (2012). Radionuclide Therapy in Neuroendocrine Tumours: A Systematic Review. Clin. Onc. *24*, 294–308.

Gully, D., Canton, M., Boigegrain, R., Jeanjean, F., Molimard, J.C., Poncelet, M., Gueudet, C., Heaulme, M., Leyris, R., and Brouard, A. (1993). Biochemical and pharmacological profile of a potent and selective nonpeptide antagonist of the neurotensin receptor. PNAS *90*, 65–69.

Haldemann, A.., Rösler, H., Barth, A., B, W., Geiger, L., Godoy, N., Markwalder, R.., Seiler, R.., Sulzer, M., and Reubi, J.. (1995). Somatostatin receptor scintigraphy in central nervous system tumors: role of blood-brain barrier permeability. J. Nucl. Med. *36*, 403–410.

Hanahan, D., and Weinberg, R.A. (2011). Hallmarks of Cancer: The Next Generation. Cell *144*, 646–674.

Heasley, L.E. (2001). Autocrine and paracrine signaling through neuropeptide receptors in human cancer. Oncogene *20*, 1563.

Heppeler, A., Froidevaux, S., Eberle, A.N., and Maecke, H.R. (2000). Receptor targeting for tumor localisation and therapy with radiopeptides. Curr. Med. Chem. *7*, 971–994.

Hermans, E., and Maloteaux, J.-M. (1998). Mechanisms of Regulation of Neurotensin Receptors. Pharmacol. Therap. *79*, 89–104.

Heuser, J. (1980). Three-dimensional visualization of coated vesicle formation in fibroblasts. J. Cell. Biol. *84*, 560–583.

Heyman, M., Ducroc, R., Desjeux, J.F., and Morgat, J.L. (1982). Horseradish peroxidase transport across adult rabbit jejunum in vitro. Am. J. Phys. - Gastro. Liver Phys. *242*, G558–G564.

Hidalgo, I.J., Raub, T.J., and Borchardt, R.T. (1989). Characterization of the human colon carcinoma cell line (Caco-2) as a model system for intestinal epithelial permeability. Gastroenterology *96*, 736–749.

Hoosain, F.G., Choonara, Y.E., Tomar, L.K., Kumar, P., Tyagi, C., du Toit, L.C., and Pillay, V. (2015). Bypassing P-Glycoprotein Drug Efflux Mechanisms: Possible Applications in Pharmacoresistant Schizophrenia Therapy. BioMed Research International [online] available from: [http://www.hindawi.com/journals/bmri/2015/484963/]

Huganir, R.L., and Greengardt, P. (1990). Regulation of neurotransmitter receptor desensitization by protein phosphorylation. Neuron *5*, 555–567.

Jia, Y., Shi, W., Zhou, Z., Wagh, N., Brusnahan, S., and Garrison, J. (2015). Evaluation of DOTA-chelated neurotensin analogs with a spacer for targeting of neurotensin receptor 1 positive tumors. J. Nucl. Med. *56*, 1159–1159.

Johnson, I.S. (1983). Human insulin from recombinant DNA technology. Science *219*, 632–637.

Kaemmerer, D., Athelogou, M., Lupp, A., I, L., Schulz, S., Peter, L., Hommann, M., Prasad, V., Binnig, G., and Baum Richard, P. (2014). Somatostatin receptor immunohistochemistry in neuroendocrine tumors: comparison between manual and automated evaluation. Int. J. Clin. Exp. Pathol. *7*, 4971–4980.

Kalgaonkar, S., and Lönnerdal, B. (2009). Receptor-mediated uptake of ferritin-bound iron by human intestinal Caco-2 cells. J. Nutr. Biochem. *20*, 304–311.

Kim, T.K., and Eberwine, J.H. (2010). Mammalian cell transfection: the present and the future. Anal. Bioanal. Chem. *397*, 3173–3178.

Kimchi-Sarfaty, C., Schiller, T., Hamasaki-Katagiri, N., Khan, M.A., Yanover, C., and Sauna, Z.E. (2013). Building better drugs: developing and regulating engineered therapeutic proteins. Tr. Pharma. Sci. *34*, 534–548.

Kislauskis, E., Bullock, B., McNeil, S., and Dobner, P.R. (1988). The rat gene encoding neurotensin and neuromedin N. Structure, tissue-specific expression, and evolution of exon sequences. J. Biol. Chem. *263*, 4963–4968.

Köhler, G., and Milstein, C. (1975). Continuous cultures of fused cells secreting antibody of predefined specificity. Nature *256*, 495–497.

Körner, M., Waser, B., Strobel, O., Büchler, M., and Reubi, J.C. (2015). Neurotensin receptors in pancreatic ductal carcinomas. EJNMMI Res *5*, 17.

Krenning, E.P., Bakker, W.H., Breeman, W.A., Koper, J.W., Kooij, P.P., Ausema, L., Lameris, J.S., Reubi, J.C., and Lamberts, S.W. (1989). Localisation of endocrine-related tumours with radioiodinated analogue of somatostatin. Lancet *1*, 242–244.

Kwekkeboom, D., Krenning, E.P., and de Jong, M. (2000). Peptide receptor imaging and therapy. J. Nucl. Med. *41*, 1704–1713.

Kwekkeboom, D.J., Bakker, W.H., Kam, B.L., Teunissen, J.J.M., Kooij, P.P.M., Herder, W.W. de, Feelders, R.A., Eijck, C.H.J. van, Jong, M. de, Srinivasan, A., et al. (2003). Treatment of patients with gastro-entero-pancreatic (GEP) tumours with the novel radiolabelled somatostatin analogue [177Lu-DOTA0,Tyr3]octreotate. Eur. J. Nucl. Med. *30*, 417–422.

Lamberts, S.W.J., van der Lely, A.-J., de Herder, W.W., and Hofland, L.J. (1996). Octreotide. New Eng. J. Med. *334*, 246–254.

Larché, M. (2005). Peptide therapy for allergic diseases: basic mechanisms and new clinical approaches. Pharmacol. Ther. *108*, 353–361.

Law, I.K.M., Murphy, J.E., Bakirtzi, K., Bunnett, N.W., and Pothoulakis, C. (2012). Neurotensin-induced Proinflammatory Signaling in Human Colonocytes Is Regulated by β-Arrestins and Endothelin-converting Enzyme-1-dependent Endocytosis and Resensitization of Neurotensin Receptor 1. J. Biol. Chem. *287*, 15066–15075.

Lee, H.-K., Zhang, L., Smith, M.D., Walewska, A., Vellore, N.A., Baron, R., McIntosh, J.M., White, H.S., Olivera, B.M., and Bulaj, G. (2015). A marine analgesic peptide, Contulakin-G, and neurotensin are distinct agonists for neurotensin receptors: uncovering structural determinants of desensitization properties. Front. Pharmacol. *6*.

Leffel, S.M., Mabon, S.A., and Stewart, C.N. (1997). Applications of green fluorescent protein in plants. BioTechniques *23*, 912–918.

Le Guludec, D., Cadiot, G., Lebtahi, R., and Mignon, M. (1996). [Detection of endocrine tumors of the digestive tract. Value and limitations of scintigraphy of somatostatin receptors]. Presse. Med. *25*, 677–682.

Lin, Y.-C., Boone, M., Meuris, L., Lemmens, I., Van Roy, N., Soete, A., Reumers, J., Moisse, M., Plaisance, S., Drmanac, R., et al. (2014). Genome dynamics of the human embryonic kidney 293 lineage in response to cell biology manipulations. Nat. Commun. *5*.

Liu, H.-S., Jan, M.-S., Chou, C.-K., Chen, P.-H., and Ke, N.-J. (1999). Is Green Fluorescent Protein Toxic to the Living Cells? Biochem. Biophys. Res. Commun. *260*, 712–717.

Liu, J., Sun, Y., Drubin, D.G., and Oster, G.F. (2001). Clathrin-mediated endocytosis. In In Endocytosis. Mark Marsh, Edit., Oxford U.P, pp. 1–25.

Louis, N., Evelegh, C., and Graham, F.L. (1997). Cloning and Sequencing of the Cellular–Viral Junctions from the Human Adenovirus Type 5 Transformed 293 Cell Line. Virology *233*, 423–429.

Lu, S., Gough, A.W., Bobrowski, W.F., and Stewart, B.H. (1996). Transport properties are not altered across Caco-2 cells with heightened TEER despite underlying physiological and ultrastructural changes. J. Pharm. Sci. *85*, 270–273.

Luo, J., Solimini, N.L., and Elledge, S.J. (2009). Principles of cancer therapy: oncogene and non-oncogene addiction. Cell *136*, 823–837.

Mäde, V., Babilon, S., Jolly, N., Wanka, L., Bellmann-Sickert, K., Diaz Gimenez, L.E., Mörl, K., Cox, H.M., Gurevich, V.V., and Beck-Sickinger, A.G. (2014). Peptide Modifications Differentially Alter G Protein-Coupled Receptor Internalization and Signaling Bias. Angew. Chem. *126*, 10231–10235.

Majumdar, S., and Siahaan, T.J. (2012). Peptide-mediated targeted drug delivery. Med. Res. Rev. *32*, 637–658.

Margaritis, A., and Bassi, A.S. (1991). Plasmid stability of recombinant DNA microorganisms (McGraw-Hill, New York, NY).

Maurer, R., and Reubi, J.C. (1986). Somatostatin receptors in the adrenal. Mol. Cell. Endocrinol. *45*, 81–90.

Mazella, J., Leonard, K., Chabry, J., Kitabgi, P., Vincent, J.-P., and Beaudet, A. (1991). Binding and internalization of iodinated neurotensin in neuronal cultures from embryonic mouse brain. Brain Res. *564*, 249–255.

de los Milagros Bassani Molinas, M., Beer, C., Hesse, F., Wirth, M., and Wagner, R. (2014). Optimizing the transient transfection process of HEK-293 suspension cells for protein production by nucleotide ratio monitoring. Cytotech. *66*, 493–514.

Misset, J.L., Dieras, V., Gruia, G., Bourgeois, H., Cvitkovic, E., Kalla, S., Bozec, L., Beuzeboc, P., Jasmin, C., Aussel, J.P., et al. (1999). Dose-finding study of docetaxel and doxorubicin in first-line treatment of patients with metastatic breast cancer. Ann. Oncol. *10*, 553–560.

Moody, T.W., Chiles, J., Casibang, M., Moody, E., Chan, D., and Davis, T.P. (2001). SR48692 is a neurotensin receptor antagonist which inhibits the growth of small cell lung cancer cells. Peptides *22*, 109–115.

Moody, T.W., Chan, D., Fahrenkrug, J., and Jensen, R.T. (2003). Neuropeptides as autocrine growth factors in cancer cells. Curr. Pharm. Des. *9*, 495–509.

Moore, R.H., Sadovnikoff, N., Hoffenberg, S., Liu, S., Woodford, P., Angelides, K., Trial, J.A., Carsrud, N.D., Dickey, B.F., and Knoll, B.J. (1995). Ligand-stimulated beta 2-adrenergic receptor internalization via the constitutive endocytic pathway into rab5-containing endosomes. J. Cell. Sci. *108*, 2983–2991.

Morgat, C., Mishra, A.K., Varshney, R., Allard, M., Fernandez, P., and Hindié, E. (2014). Targeting neuropeptide receptors for cancer imaging and therapy: perspectives with bombesin, neurotensin, and neuropeptide-Y receptors. J. Nucl. Med. *55*, 1650–1657.

Mulè, F., Serio, R., and Postorino, A. (1995). Motility pattern of isolated rat proximal colon and excitatory action of neurotensin. European Journal of Pharmacology *275*, 131–137.

Niwa, H., Inouye, S., Hirano, T., Tsuji, F.I., Ohashi, M., Kubota, M., Kojima, S., Niwa, H., Inouye, S., Matsuno, T., et al. (1996). Chemical nature of the light emitter of the Aequorea green fluorescent protein. PNAS *93*, 13617–13622.

Nouel, D., Gaudriault, G., Houle, M., Reisine, T., Vincent, J.-P., Mazella, J., and Beaudet, A. (1997a). Differential Internalization of Somatostatin in COS-7 Cells

Transfected with SST1 and SST2 Receptor Subtypes: A Confocal Microscopic Study Using Novel Fluorescent Somatostatin Derivatives. Endocrin. *138*, 296–306.

Nouel, D., Faure, M.-P., Pierre, J.-A.S., Alonso, R., Quirion, R., and Beaudet, A. (1997b). Differential Binding Profile and Internalization Process of Neurotensin via Neuronal and Glial Receptors. J. Neurosci. *17*, 1795–1803.

Oakley, R.H., Laporte, S.A., Holt, J.A., Caron, M.G., and Barak, L.S. (2000). Differential Affinities of Visual Arrestin, βArrestin1, and βArrestin2 for G Protein-coupled Receptors Delineate Two Major Classes of Receptors. J. Biol. Chem. *275*, 17201–17210.

Oberstein, P.E., and Olive, K.P. (2013). Pancreatic cancer: why is it so hard to treat? Therap. Adv. Gastroenterol. *6*, 321–337.

O'Fágáin, C., Cummins, P.M., and O'Connor, B.F. (2011). Gel-filtration chromatography. Methods Mol. Biol. *681*, 25–33.

Olszewski, U., and Hamilton, G. (2009). Neurotensin signaling induces intracellular alkalinization and interleukin-8 expression in human pancreatic cancer cells. Mol. Oncol. *3*, 204–213.

Overton, T.W. (2014). Recombinant protein production in bacterial hosts. Drug Discov. Today *19*, 590–601.

Palomares, L.A., Estrada-Mondaca, S., and Ramírez, O.T. (2004). Production of recombinant proteins: challenges and solutions. Methods Mol. Biol. *267*, 15–52.

Pang, K.S. (2003). Modeling of Intestinal Drug Absorption: Roles of Transporters and Metabolic Enzymes (for the Gillette Review Series). Drug Metab. Dispos. *31*, 1507–1519.

Paulsson, J., and Ehrenberg, M. (2001). Noise in a minimal regulatory network: plasmid copy number control. Quart. Rev. Biophys. *34*, 1–59.

Pearse, B.M. (1982). Coated vesicles from human placenta carry ferritin, transferrin, and immunoglobulin G. PNAS *79*, 451–455.

Pheng, L.H., Dumont, Y., Fournier, A., Chabot, J.-G., Beaudet, A., and Quirion, R. (2003). Agonist- and antagonist-induced sequestration/internalization of neuropeptide Y Y1 receptors in HEK293 cells. Brit. J. Pharmacol. *139*, 695–704.

Pinto, M., Robine-Leon, S., Appay, M., Kedinger, M., Triadou, N., Dussaulx, E., Lacroix, B., Simon-Assmann, P., Haffen, K., Fogh, J., et al. (1983). Enterocyte-like differentiation and polarization of the human colon carcinoma cell line Caco-2 in culture. Biol. Cell *47*, 323–330.

Poinot-Chazel, C., Portier, M., Bouaboula, M., Vita, N., Pecceu, F., Gully, D., Monroe, J.G., Maffrand, J.P., Le Fur, G., and Casellas, P. (1996). Activation of mitogen-

activated protein kinase couples neurotensin receptor stimulation to induction of the primary response gene Krox-24. Biochem. J. *320 (Pt 1)*, 145–151.

Porath, J. (1975). Metal chelate affinity chromatography, a new approach to protein fraction. Nature *258*, 598–599.

Porath, J. (1992). Immobilized metal ion affinity chromatography. Protein Express. Purif. *3*, 263–281.

Premont, R.T., Inglese, J., and Lefkowitz, R.J. (1995). Protein kinases that phosphorylate activated G protein-coupled receptors. FASEB J *9*, 175–182.

Ranaldi, G., Consalvo, R., Sambuy, Y., and Scarino, M.L. (2003). Permeability characteristics of parental and clonal human intestinal Caco-2 cell lines differentiated in serum-supplemented and serum-free media. Toxicol. in Vitro *17*, 761–767.

Reubi, J.C. (2003). Peptide receptors as molecular targets for cancer diagnosis and therapy. Endocr. Rev. *24*, 389–427.

Reubi, J.C., Waser, B., Friess, H., Büchler, M., and Laissue, J. (1998). Neurotensin receptors: a new marker for human ductal pancreatic adenocarcinoma. Gut *42*, 546–550.

Reubi, J.C., Waser, B., Schmassmann, A., and Laissue, J.A. (1999). Receptor autoradiographic evaluation of cholecystokinin, neurotensin, somatostatin and vasoactive intestinal peptide receptors in gastro-intestinal adenocarcinoma samples: Where are they really located? Int. J. Cancer *81*, 376–386.

Reubi, J.C., Mäcke, H.R., and Krenning, E.P. (2005). Candidates for Peptide Receptor Radiotherapy Today and in the Future. J. Nucl. Med. *46*, 67S – 75S.

Reznikoff, W.S. (1992). The lactose operon-controlling elements: a complex paradigm. Mol. Micro. *6*, 2419–2422.

Robinson, M.S. (2004). Adaptable adaptors for coated vesicles. Trends Cell Biol. *14*, 167–174.

Sambuy, Y., Angelis, I.D., Ranaldi, G., Scarino, M.L., Stammati, A., and Zucco, F. (2005). The Caco-2 cell line as a model of the intestinal barrier: influence of cell and culture-related factors on Caco-2 cell functional characteristics. Cell. Biol. Toxicol. *21*, 1–26.

Sarret, P., Perron, A., Stroh, T., and Beaudet, A. (2003). Immunohistochemical distribution of NTS2 neurotensin receptors in the rat central nervous system. J. Comp. Neurol. *461*, 520–538.

Schally, A.V. (1988). Oncological applications of somatostatin analogues. Cancer Res. *48*, 6977–6985.

Schindler, M., Holloway, S., Humphrey, P.P., Waldvogel, H., Faull, R.L., Berger, W., and Emson, P.C. (1998). Localization of the somatostatin sst2(a) receptor in human cerebral cortex, hippocampus and cerebellum. Neuroreport *9*, 521–525.

Sehgal, I., Powers, S., Huntley, B., Powis, G., Pittelkow, M., and Maihle, N.J. (1994). Neurotensin is an autocrine trophic factor stimulated by androgen withdrawal in human prostate cancer. PNAS *91*, 4673–4677.

Serafini, A.N. (1993). From monoclonal antibodies to peptides and molecular recognition units: an overview. J. Nucl. Med. *34*, 533–536.

Sezonov, G., Joseleau-Petit, D., and D'Ari, R. (2007). Escherichia coli Physiology in Luria-Bertani Broth. J. Bacteriol. *189*, 8746–8749.

Shaw, G., Morse, S., Ararat, M., and Graham, F.L. (2002). Preferential transformation of human neuronal cells by human adenoviruses and the origin of HEK 293 cells. FASEB J. [online] available at: [http://www.fasebj.org/content/early/2002/06/02/fj.01-0995fje]

Shiloach, J., and Fass, R. (2005). Growing E. coli to high cell density—A historical perspective on method development. Biotech. Adv. *23*, 345–357.

Shimizu, M., Tsunogai, M., and Arai, S. (1997). Transepithelial Transport of Oligopeptides in the Human Intestinal Cell, Caco-2. Peptides *18*, 681–687.

Sjöback, R., Nygren, J., and Kubista, M. (1995). Absorption and fluorescence properties of fluorescein. Spectrochimica Acta Part A: Mol. Biomol. Spectros. *51*, L7–L21.

Souazé, F., Dupouy, S., Viardot-Foucault, V., Bruyneel, E., Attoub, S., Gespach, C., Gompel, A., and Forgez, P. (2006). Expression of Neurotensin and NT1 Receptor in Human Breast Cancer: A Potential Role in Tumor Progression. Cancer Res. *66*, 6243–6249.

Spadiut, O., Capone, S., Krainer, F., Glieder, A., and Herwig, C. (2014). Microbials for the production of monoclonal antibodies and antibody fragments. Trends Biotechnol. *32*, 54–60.

St-Gelais, F., Jomphe, C., and Trudeau, L.-É. (2006). The role of neurotensin in central nervous system pathophysiology: What is the evidence? J. Psychiatry Neurosci. *31*, 229–245.

Studier, F.W. (1991). Use of bacteriophage T7 lysozyme to improve an inducible T7 expression system. J. Mol. Biol. *219*, 37–44.

Summers, D. (1998). Timing, self-control and a sense of direction are the secrets of multicopy plasmid stability. Mol. Microbiol. *29*, 1137–1145.

Swift, S.L., Burns, J.E., and Maitland, N.J. (2010). Altered Expression of Neurotensin Receptors Is Associated with the Differentiation State of Prostate Cancer. Cancer Res. *70*, 347–356.

Tarasova, N.I., Stauber, R.H., Choi, J.K., Hudson, E.A., Czerwinski, G., Miller, J.L., Pavlakis, G.N., Michejda, C.J., and Wank, S.A. (1997). Visualization of G Protein-coupled Receptor Trafficking with the Aid of the Green Fluorescent Protein ENDOCYTOSIS AND RECYCLING OF CHOLECYSTOKININ RECEPTOR TYPE A. J. Biol. Chem. *272*, 14817–14824.

Tavelin, S., Gråsjö, J., Taipalensuu, J., Ocklind, G., and Artursson, P. (2002). Applications of epithelial cell culture in studies of drug transport. Methods Mol. Biol. *188*, 233–272.

Terai, T., and Nagano, T. (2013). Small-molecule fluorophores and fluorescent probes for bioimaging. Pflugers Arch. *465*, 347–359.

Theodorsson-Norheim, E., and Rosell, S. (1983). Characterization of human plasma neurotensin-like immunoreactivity after fat ingestion. Regul. Pept. *6*, 207–218.

Thomas, P., and Smart, T.G. (2005). HEK293 cell line: A vehicle for the expression of recombinant proteins. J. Pharmaco. Toxico. Methods *51*, 187–200.

Thomas, R.P., Hellmich, M.R., Townsend, C.M., and Evers, B.M. (2003). Role of Gastrointestinal Hormones in the Proliferation of Normal and Neoplastic Tissues. Endocr. Rev. *24*, 571–599.

Thoss, V.S., Pérez, J., Probst, A., and Hoyer, D. (1996). Expression of five somatostatin receptor mRNAs in the human brain and pituitary. Naunyn-Schmiedeberg's Arch. Pharmacol. *354*, 411–419.

Tian, L., Yang, Y., Wysocki, L.M., Arnold, A.C., Hu, A., Ravichandran, B., Sternson, S.M., Looger, L.L., and Lavis, L.D. (2012). Selective esterase-ester pair for targeting small molecules with cellular specificity. Proc. Natl. Acad. Sci. U.S.A. *109*, 4756–4761.

Toy-Miou-Leong, M., Cortes, C.L., Beaudet, A., Rostène, W., and Forgez, P. (2004). Receptor trafficking via the perinuclear recycling compartment accompanied by cell division is necessary for permanent neurotensin cell sensitization and leads to chronic mitogen-activated protein kinase activation. J. Biol. Chem. *279*, 12636–12646.

Turner, J.T., James-Kracke, M.R., and Camden, J.M. (1990). Regulation of the neurotensin receptor and intracellular calcium mobilization in HT29 cells. J. Pharmacol. Exp. Ther. *253*, 1049–1056.

Vachon, P.H., Perreault, N., Magny, P., and Beaulieu, J.-F. (1996). Uncoordinated, transient mosaic patterns of intestinal hydrolase expression in differentiating human enterocytes. J. Cell. Physiol. *166*, 198–207.

Valerie, N.C.K., Casarez, E.V., DaSilva, J.O., Dunlap-Brown, M.E., Parsons, S.J., Amorino, G.P., and Dziegielewski, J. (2011). Inhibition of Neurotensin Receptor 1 Selectively Sensitizes Prostate Cancer to Ionizing Radiation. Cancer Res. *71*, 6817–6826.

Vandenbulcke, F., Nouel, D., Vincent, J.P., Mazella, J., and Beaudet, A. (2000). Ligand-induced internalization of neurotensin in transfected COS-7 cells: differential intracellular trafficking of ligand and receptor. J. Cell. Sci. *113 (Pt 17)*, 2963–2975.

Vega-Avila, E., and Pugsley, M.K. (2011). An overview of colorimetric assay methods used to assess survival or proliferation of mammalian cells. Proc. West. Pharmacol. Soc. *54*, 10–14.

Vincent, J.-P. (1995). Neurotensin receptors: Binding properties, transduction pathways, and structure. Cell. Mol. Neurobiol. *15*, 501–512.

Vincent, J.-P., Mazella, J., and Kitabgi, P. (1999). Neurotensin and neurotensin receptors. Trends Pharmaco. Sci. *20*, 302–309.

Walter, E., and Kissel, T. (1995). Heterogeneity in the human intestinal cell line Caco-2 leads to differences in transepithelial transport. European J. Pharma. Sci. *3*, 215–230.

Weigel, A.V., Tamkun, M.M., Krapf, D., Tamkun, M.M., and Weigel, A.V. (2013). Quantifying the dynamic interactions between a clathrin-coated pit and cargo molecules. PNAS *110*, E4591–E4600.

White, J.F., Noinaj, N., Shibata, Y., Love, J., Kloss, B., Xu, F., Gvozdenovic-Jeremic, J., Shah, P., Shiloach, J., Tate, C.G., et al. (2012). Structure of the agonist-bound neurotensin receptor. Nature *490*, 508–513.

Wu, Z., Martinez-Fong, D., Trédaniel, J., and Forgez, P. (2013). Neurotensin and its high affinity receptor 1 as a potential pharmacological target in cancer therapy. Front. Endocrinol. *3*, (184) 1-9.

Yamada, M., Yamada, M., Lombet, A., Forgez, P., and Rostène, W. (1998). Distinct functional characteristics of levocabastine sensitive rat neurotensin NT2 receptor expressed in Chinese hamster ovary cells. Life Sci. *62*, 375–380.

Yao, J.C., Hassan, M., Phan, A., Dagohoy, C., Leary, C., Mares, J.E., Abdalla, E.K., Fleming, J.B., Vauthey, J.-N., Rashid, A., et al. (2008). One Hundred Years After "Carcinoid": Epidemiology of and Prognostic Factors for Neuroendocrine Tumors in 35,825 Cases in the United States. JCO *26*, 3063–3072.

Zastrow, M. von, and Kobilka, B.K. (1992). Ligand-regulated internalization and recycling of human beta 2-adrenergic receptors between the plasma membrane and endosomes containing transferrin receptors. J. Biol. Chem. *267*, 3530–3538.

Zhang, Y., Li, H., Sun, J., Gao, J., Liu, W., Li, B., Guo, Y., and Chen, J. (2010). DC-Chol/DOPE cationic liposomes: A comparative study of the influence factors on plasmid pDNA and siRNA gene delivery. Inter. J. Pharma. *390*, 198–207.

Zhao, D., and Pothoulakis, C. (2006). Effects of NT on gastrointestinal motility and secretion, and role in intestinal inflammation. Peptides *27*, 2434–2444.